THÈSE

En vue de l'obtention du

DOCTORAT DE L'UNIVERSITÉ DE TOULOUSE

Délivré par :
Institut National Polytechnique de Toulouse (INP Toulouse)

Discipline ou spécialité :

Systèmes Automatiques

Présentée et soutenue par :
Tan Viet Anh TRUONG

le : vendredi 2 juillet 2010

Titre :

Un modèle de locomotion humaine unifiant
comportements holonomes et nonholonomes
Unifying nonholonomic and holonomic behaviors in human locomotion

---

Ecole doctorale :
Systèmes (EDSYS)

Unité de recherche :
LAAS - CNRS

Directeur(s) de Thèse :
M. Jean-Paul LAUMOND
M. Philippe SOUERES

Rapporteurs :
M. Ronan BOULIC
M. Franck MULTON

Autre(s) membre(s) du jury

M. Julien PETTRÉ, Président
Mme. Katja MOMBAUR

INSTITUT NATIONAL POLYTECHNIQUE DE TOULOUSE
ÉCOLE DOCTORALE SYSTÈMES

THÈSE

en vue de l'obtention du

Doctorat de l'Université de Toulouse
délivré par Institut National Polytechnique de Toulouse

Spécialité: Systèmes Automatiques

Unifying nonholonomic and holonomic behaviors in human locomotion

Tan Viet Anh TRUONG

Préparée au Laboratoire d'Analyse et d'Architecture des Systèmes
sous la direction de M. Jean-Paul LAUMOND

Jury

M. Ronan BOULIC	Rapporteur
M. Franck MULTON	Rapporteur
Mme. Katja MOMBAUR	Examinateur
M. Julien PÉTTRÉ	Examinateur
M. Jean-Paul LAUMOND	Directeur de Thèse

Abstract

Our motivation is to understand human locomotion to better control locomotion of virtual systems (robots and mannequins). Human locomotion has been studied so far in different disciplines. We consider locomotion as the level of a body frame (in direction and orientation) instead of the complexity of many kinematic joints systems as other approaches.

Our approach concentrates on the computational foundation of human locomotion. The ultimate goal is to find a model that explains the shape of human locomotion in space. To do that, we first base on the behavior of trajectories on the ground during intentional locomotion.

When human walk, they put one foot in front of the other and consequently, the direction of motion is deduced by the body orientation. That's what we called the nonholonomic behavior hypothesis. However, in the case of a sideward step, the body orientation is not coupled to the tangential direction of the trajectory, and the hypothesis is no longer validated. The behavior of locomotion becomes holonomic. The aim of this thesis is to distinguish these two behaviors and to exploit them in neuroscience, robotics and computer animation.

The first part of the thesis is to determine the configurations of the holonomic behavior by an experimental protocol and an original analytical tool segmenting the nonholonomic and holonomic behaviors of any trajectory.

In the second part, we present a model unifying nonholonomic and holonomic behaviors. This model combines three velocities generating human locomotion: forward, angular and lateral. The experimental data in the first part are used in an inverse optimal control approach to find a multi-objective function which produces calculated trajectories as those of natural human locomotion.

The last part is the application that uses the two behaviors to synthesize human locomotion in computer animation. Each locomotion is characterized by three velocities and is therefore considered as a point in 3D control space (of three speeds). We collected a library that contains locomotions at different velocities - points in 3D space. These points are structured in a tetrahedra cloud. When a desired speed is given, it is projected into the 3D space and we find the corresponding tetrahedron that contains it. The new animation is interpolated by four locomotions corresponding to four vertices of the selected tetrahedron. We exhibit several animation scenarios on a virtual character.

Résumé

Notre motivation est de comprendre la locomotion humaine pour un meilleur contrôle des systèmes virtuels (robots et mannequins). La locomotion humaine a été étudiée depuis longtemps dans des domaines différents. Nous considérons la locomotion comme le déplacement d'un repère attaché au corps humain (direction et orientation) au lieu de la trajectoire articulaire du corps complet.

Notre approche est basée sur le fondement calculatoire de la locomotion humaine. Le but est de trouver un modèle qui explique la forme de la locomotion humaine dans l'espace. Pour ce faire, nous étudions tout d'abord le comportement des trajectoires au sol pendant la locomotion intentionnelle.

Quand un humain marche, il met un pied devant l'autre et par conséquence, l'orientation du corps suit la direction tangente de la trajectoire. C'est ce qu'on appelle l'hypothèse de comportement nonholonome. Cependant, dans le cas d'un pas de côté, l'orientation du corps n'est plus semblable à la direction de trajectoire, et l'hypothèse n'est plus valable. Le comportement de la locomotion devient holonome. Le but de la thèse est de distinguer ces deux comportements et de les exploiter en neuroscience, robotique et animation graphique.

La première partie de la thèse présente une étude qui permet de déterminer des configurations de comportement holonome par un protocole expérimental et par une fonction qui segmente les comportements nonholonomes et holonomes d'une trajectoire.

Dans la deuxième partie, nous établissons un modèle unifiant comportements nonholonomes et holonomes. Ce modèle combine trois vitesses générant la locomotion humaine : tangentielle, angulaire et latérale. Par une approche de commande optimale inverse nous proposons une fonction multi-objectifs qui optimise des trajectoires calculées pour les rendre proches des trajectoires humaines naturelles.

La dernière partie est l'application qui utilise les deux comportements pour synthétiser des locomotions humaines dans un environnement d'animation graphique. Chaque locomotion est caractérisée par trois vitesses et est donc considérée comme un point dans l'espace de commande 3D (de trois vitesses). Nous avons collecté une librairie qui contient des locomotions de vitesses différentes - des points dans l'espace 3D. Ces points sont structurés en un nuage de tétraèdres. Quand une vitesse désirée est donnée, elle est projetée dans l'espace 3D et on trouve le tétraèdre qui la contient. La nouvelle animation est interpolée par quatre locomotions correspondant aux quatre sommets du tétraèdre. On expose plusieurs scénarios d'animations sur un personnage virtuel.

Acknowledgements

Fist of all, I would like to express the deepest gratitude to my thesis advisor Jean-Paul Laumond. It is an honor for me to work, to discuss with him during past three years. I learned a lot from his way of thinking, of presenting, of solving difficult problems as well as his sense of humor. Annual Gepettiste's parties at his residence were so nice and familiar.

It is a pleasure to thank Katja Mombaur and Julien Pettré and Gustavo Arechavaleta for their collaborations in international conferences and journals.

I would like to thank Prof. Ronan Boulic and Franck Multon for the review of this thesis. Their precious comments and suggestions help me a lot in finishing the final version of the manuscript.

I'm grateful for participants in the experiments of the thesis: Ali, Juan-Pablo, Jens, Van, Duong ...

I am indebted to my many Gepettiste colleagues to support me in a number of ways during my thesis: Sebastien, David, Manish, Oussama, Ali, Minh, Mathieu, Thomas, Duong, Layale, Sovan, (especially, great thank to my French professor - real parisian Sebastien). More than that, we spent unforgettable time together:

- The housewarming loop: Sebastien (sausage, bread and wine as typical French meal) → Minh (sping rolls made by ourselves) → David (many Reunion food) → Anh-Pancho-Diego (vietnamese lotus rootstock and shrimp salad, guacamole, mole) → Manish (chicken curry) → Layale (hummus, lebanese food)
- Travel: short travel during one weekend such as: Toulouse-Carcasonne bicycle trip, kayaking and canoeing at Parc de Ceven; or the long trip to Prague, Vienne
- Sport activities: tennis, football → just for fun because I won them (Sebastien, Pancho, Manish) easily :))

Thank to vietnameses at LAAS: Mai, Hưng, Thành, Vân, Dương, Nam, Tùng ôtô, Tùng TM, Hùng, Đức. And thanks also to VNLAAS football team of which I was captain during one year that we didn't win the vietnamese tournement of football yet :)). Anyway, we won many matches at INSA stadium and had many nice goals.

Weekend nights with Xavier and two my roommates "latinos" Pancho and Diego were so exciting and enjoyable.

Nothing could be greater than the support from my beloved family: my parents Ngạn-Tý, my sister Mai Anh, my niece Bo at Nha Trang - Việt Nam, and my elder twin brother Đức And at Illinois - USA. They put all their faith in me and encourage me at all difficult moments.

Contents

1 Introduction

1.1 Problem statement

The goal of our research on human locomotion is to explain the shape of human locomotion in space by a computational model. The further application is to reproduce locomotions not only in terms of trajectory of human reference frame but also for the whole body movement of virtual characters. The question we always address is: In order to go from one configuration to another one, what trajectory human will follow? And how can we predict it? Such a problem is shown as a motion planning problem in the robotics community [Latombe 1991]. Our goal is to create a bridge between the life science community related to human locomotion studies and the engineering community. In our previous research, Arechavaleta et al. [Arechavaleta et al. 2008a] proposed a *nonholonomic* nature of human locomotion. They considered the trunk as a reference frame steering human body and motions of shoulders followed by a nonholonomic behavior during walking. According to the terminology used in mobile robotics [Laumond et al. 1998], we realize that a human walks with a nonholonomic behavior when his/her body direction supports the tangent to the trajectory. If (x,y) denotes the coordinates of the body driver (the midpoint of two shoulders in our case) and if θ denotes the body orientation, the nonholonomic behavior is characterized by the differential equation:

$$\dot{y}\cos\theta - \dot{x}\sin\theta = 0 \tag{1.1}$$

The hypothesis is that we can express information of human trajectory only by the above nonholonomic constraint.

In other words, the hypothesis represents a relation between body orientation and direction of motion, and it is a consequence of the fact that humans walk in the forward feet direction. Nevertheless, in

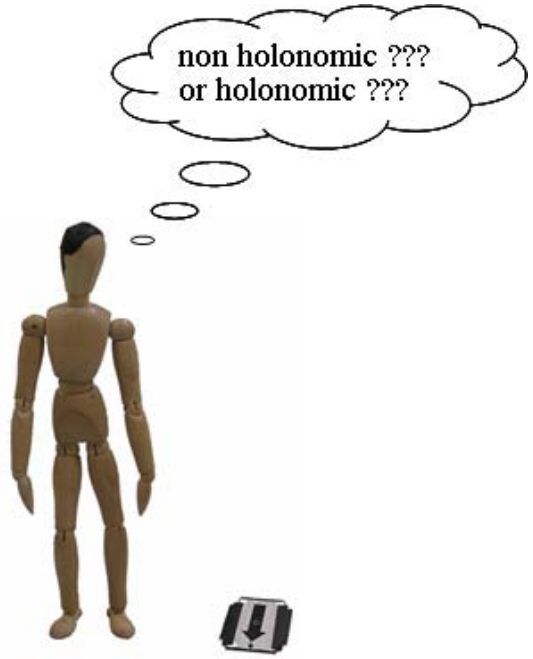

Figure 1.1: Nonholonomic or holonomic motion in nearby target?

.

very specific situations, sideward or diagonal steps called *holonomic* motions are performed. How to determine such configurations is also regarded as when (where) the hypothesis is no longer true? One of purposes of this thesis is to verify the hypothesis through studying the relation between body orientation and direction of human motion in the nearby space. But how humans change from holonomic to nonholonomic motion? Whether there exists a model unifying these two properties? And what are the criteria deciding when we walk by holonomic/nonholonomic behaviors? Are trajectories produced by these criteria similar to natural human trajectories? We address these questions by an inverse optimal control approach. A model taking into account the lateral velocity was used to explain the holonomic factor. A multi-attribute cost function from biomechanics knowledge and experimental statistic data reveals the combination of holonomic and nonholonomic behaviors. And finally, can we combine holonomic and nonholonomic properties to produce whole body movements? A synthesized technique using motion blending and holonomic/nonholonomic motions samples might solve this problem and interpolate new motions for the animation application.

1.2 Contributions

This work is first to refine the nonholonomic hypothesis by indicating the appearance of holonomic behaviors, then to unify holonomic and nonholonomic motions in a model, explain the transition between them and finally to combine them in an animation application. So there are three main contributions in the thesis:

- The first contribution is to propose a protocol that can allow subjects perform holonomic and

nonholonomic properties during intentional locomotions in neighboring space. We defined a function distinguishing these two characteristics. This function is associated with statistic analysis in recognizing a path behavior stereotypy: trajectories composed of holonomic-nonholonomic-holonomic behavior segmentations. We also found a dependency of holonomic parts on the distance to the origin/goal and a dependency of nonholonomic/holonomic parts on the velocity. But in the neighborhood of the origin, the implementation of this function indicates a disappearance of the stereotypy and reveals a holonomic behavior zone.

- The second contribution is to apply a model taking into account the lateral velocity in unifying holonomic and nonholonomic behaviors. Then, we used an inverse optimal control approach to identify a multi-attribute objectives function that can describe the optimal trajectories (natural or experimental trajectories).
- The third contribution is to present a locomotion controller combining holonomic and nonholonomic behaviors to synthesize whole body movements for the virtual character. This controller uses three components of velocity as the inputs. Thus, we collected a motion library varying these velocities for each locomotion. Then, new locomotions were synthesized by using the motion blending technique.

1.3 Document organization

This thesis consists of 7 chapters as follows:

Chapter 2 introduces multi-disciplinary approaches in human locomotion, from neuroscience, biomechanics, robotics to computer animations. We synthesize various work from many authors, and concentrate essentially on the control strategy, steering method and models interacting to environments, solving tasks for mechanical structures and integrating in the context of motions synthesizing.

Chapter 3 recalls briefly the nonholonomic hypothesis of our previous work on human locomotion, including the reference frame steering human locomotion, the kinematic and geometric stereotypy, and the family of words of human walking by using a numerical synthesis.

Chapter 4 presents the protocol and the data-recorded experiment. With an analytic tool decomposing trajectories into holonomic and nonholonomic parts, statistic analysis validates the existence of holonomic behaviors in the neighboring space. The relative results and discussions are very useful for predicting model and cost function in chapter 5.

In chapter 5, we adapt an inverse optimal control approach to choose the objective function in human walking. A model unifying holonomic and nonholonomic properties is presented. Then, we propose a multi-attribute objectives function essentially based on the experimental statistic results. The identification of this novel function is also discussed at the end of the chapter.

Chapter 6 shows an application of the holonomic/nonholonomic combination for producing whole body movements in animation field. Three velocities of human walking are used to build a motion library and they are the basis of controlling locomotions with the help of the motion blending technique.

Finally, chapter 7 concludes our work as well as suggesting some perspectives.

1.4 Publications

Publications and international conference:

1. TRUONG, T.-V.-A., FLAVIGNE, D., PETTRE, J., MOMBAUR, K. AND LAUMOND, J.-P. Reactive synthesizing of human locomotion combining nonholonomic and holonomic behaviors. *3rd IEEE RAS & EMBS International Conference on Biomedical Robotics and Biomechatronics*. Tokyo, Japan, 2010.
2. TRUONG, T.-V.-A., MOMBAUR, K., AND LAUMOND, J.-P. Holonomic and nonholonomic aspects of human locomotion: on the relationship between body orientation and motion. *Gait & Posture*. (submitted).
3. TRUONG, T.-V.-A., MOMBAUR, K., AND LAUMOND, J.-P. On the relationship between body orientation and direction of motion during human locomotion. *19th International Society for Posture and Gait Research (ISPGR)*. Bologna, Italy, 2009.
4. MOMBAUR, K., TRUONG, T.-V.-A., AND LAUMOND, J.-P. From human to humanoid locomotion an inverse optimal control approach. *Autonomous Robots, 28, 3*, April 2010, 369-383.
5. MOMBAUR, K., TRUONG, T.-V.-A., AND LAUMOND, J.-P.. Identifying the objectives of human path generation. *Computer Methods in Biomechanics and Biomedical Engineering, Vol. 12*, August 2009.
6. MOMBAUR, K., LAUMOND, J.-P., AND TRUONG, T.-V.-A. An inverse optimal control approach to human motion modeling. *STAR series. Proceedings of 15th International Symposium of Robotics Research (ISRR)*. Lucerne, Switzerland, 2009.
7. LAUMOND, J.-P., ARECHAVALETA, G., TRUONG, T.-V.-A., HICHEUR, H., PHAM, Q.-C., AND BERTHOZ, A. The words of the human locomotion. *STAR series. Proceedings of 13th International Symposium of Robotics Research (ISRR)*. Hiroshima, Japan, 2007.

National conference:

1. MOMBAUR, K., TRUONG, T.-V.-A., AND LAUMOND, J.-P. Identifying the objectives of human path generation. *34ème Congrès Annuel de la Société de Biomécanique (SB)*. Toulon, France, 2009.
2. TRUONG, T.-V.-A., LAUMOND, J.-P. AND MOMBAUR, K. Characteristics of human locomotion in neighboring space. *Groupe de Recherche Robotique: Robotique humanoïde*. Montpellier, France, 2008.

2

Natural human locomotion from multi-disciplinary approaches

2.1 Generation of coordinated movement

A locomotion is actually a change of coordinates of movements in time. In other word, it is a transition of successive postures from the beginning to the end. Although different classes of vertebrates move in different ways during locomotion (see figure 2.1), they have to deal with at least three tasks (followed a synthesized study in [Grillner 1975]):

- Perform the actual locomotor movements of the different limbs according to a stereotyped plan;
- Adapt these movements to external conditions in order to accomplish purposeful locomotion so as to achieve various goals;
- Maintain an equilibrium during the movements, i.e. the projection of the center of gravity must fall in an optimally stable point between the moving points of support and be maintained within narrow limits.

The second task including the feedback information is out of scope of our work which consider the open loop trajectory planning. The first task implies the *cycle* of locomotion. The cycle can be a tail wagging cycle of fish (figure 2.1 (a)), a flapping one of bird (figure 2.1 (b)), or a stepping one of mammals (figure 2.1 (d), (e), (f)). Above movements produce the locomotion. Third task is to distinguish human locomotion from other locomotions. Fish/bird floats in the water/air by a particular mechanism whereas land mammals keep balance by putting locomotive limbs on the ground. Movements of these subjects are actually the interlimb coordination, without concerning of they are tetrapod (or hexapod) or biped. How is the interlimb coordination achieved in tetrapod or biped? And how fishes and birds

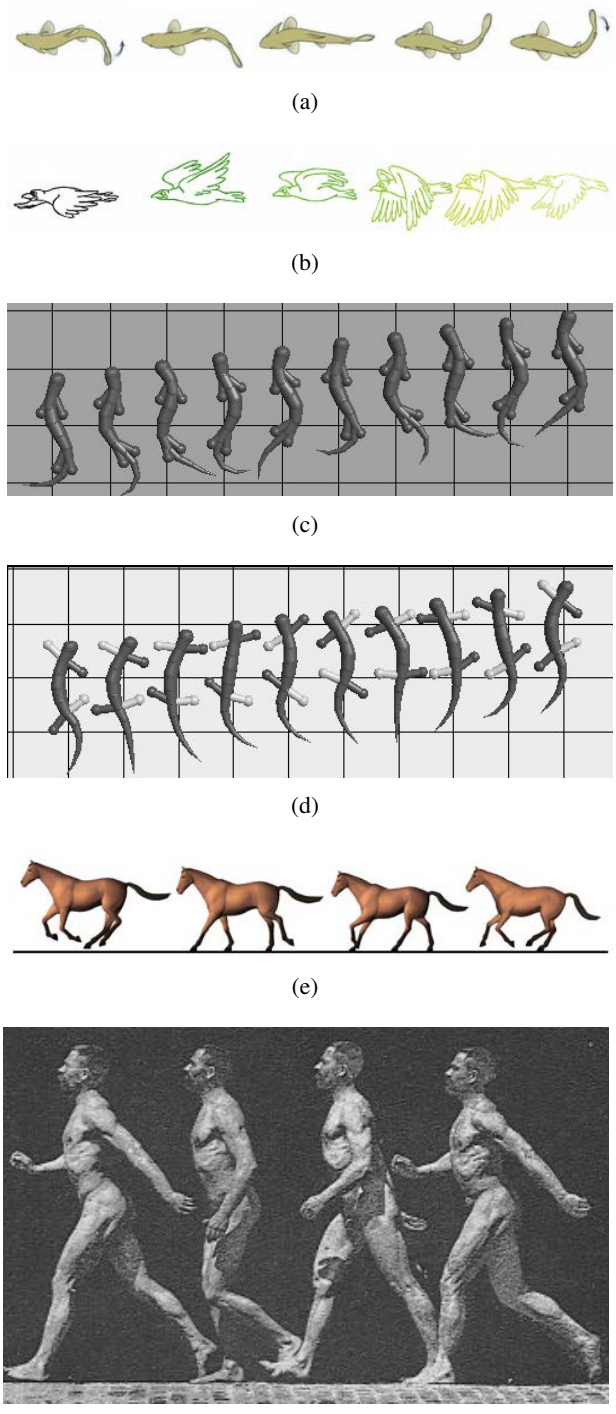

(a)

(b)

(c)

(d)

(e)

(f)

Figure 2.1: Vertebrate locomotions in instantaneous frames of fish (a) (from Michigan Science Art), bird (b) (www.flickr.com), horse (e) (from Visual Dictionary Online), and human (f) (borrowed from Etienne-Jules Marey in Le mouvement, 1894). Salamanders can perform two different types of locomotions corresponding to two different mechanisms (swimming (c) and stepping (d) [Ijspeert 1995]).

can also move without limbs? In the above study, the author supposed that there is a central pattern generator (*CPG*) for locomotion and that the spinal cord contains such a *CPG*. Human locomotion is a specific case of bipedal locomotion, and the *CPG* for human (or human-like systems) locomotion has been widely studied in multi-disciplinary approaches. The pioneer work of human locomotion was discovered by Bernstein [Bernstein 1967] in terms of movement coordination. One of his considerable ideas is the conception of *degrees of freedom* problem. The issue concerns the fact that the motor system has many different independent parts that move - too many for an individual to control separately at a conscious level. Roboticians adapted this kind of system in humanoid robotics called *redundant* system. Locomotor movements, according to Bernstein, display a synergy incorporating the whole musculatures and the entire moving skeleton. Whether or not these elements are combined in a dynamical locomotion task, they are controlled by a unique agent? And how to define this controller? Let's consider these questions in a synthesized study of Bernstein's research [Whiting and Bernstein 1984]:

... The structural elements of the dynamics of a locomotor act may certainly be deciphered by means of more or less complex mathematical and physiological alphabets which permit the revealing through them of underlying central nervous processes...

Our research has been inspired on this way. We tried to figure out a mathematical model of the central nervous controller through the understanding of the trajectories shape on the ground. In the following sections, we present various models describing how the central nervous system works in many disciplines.

2.2 Neuroscience: Control strategy of nervous system

Neuroscientists investigated the control strategy of nervous system via multisensory effects during walking. Additionally, the similarity of the arm reaching and the locomotion was also studied, some optimal control models used for arm movements were adapted in human locomotion.

2.2.1 Multisensory

Among various sensory receptor systems for movement (see [Abernethy et al. 2005] and [Berthoz and Viaud-Delmon 1999] for a review), visual and vestibular inputs were analyzed during human locomotion. For instance, figure 2.2 showed the vestibular influence on the human walking (first was presented in [Fitzpatrick et al. 1999], [Rossignol 1996], and then in [Soechting and Flanders 1994], [Kennedy et al. 2003], [Carlsen et al. 2005]).

Head, eyes and body iteration were also presented in [Imai et al. 2000]. The purpose was to know how head and eyes follow a trajectory in the space. Body parts reference frame were also investigated to know the human displacement and orientation in space, for example [Hicheur et al. 2005], and [Hollands et al. 2004].

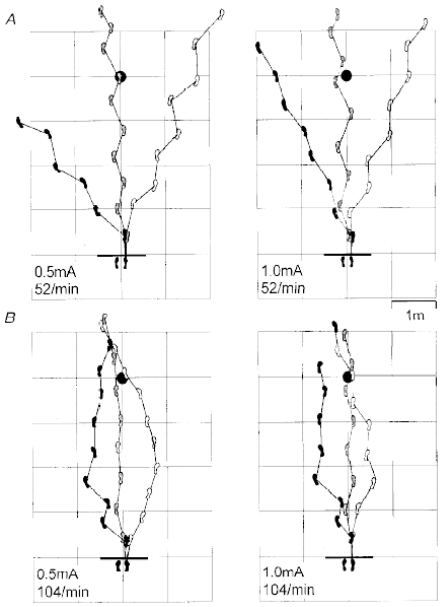

Figure 2.2: Changes of human walking caused by vestibular stimulation (cited from [Fitzpatrick et al. 1999]). Subjects walk from the starting line attempting to reach the target circle. Without a vestibular stimulus, subjects walk straight to the target (shaded footsteps). With the stimulus on the right, subject initially veered to the right. With the stimulus on the left, subject initially veered to the left.

2.2.2 Steering method

Which part of body plays a role of steering human walking and turning? This question brought many work for neuroscientists. Most of them regarded essentially on the head and eyes as the greatest effect on steering control [Pozzo et al. 1990], [Hicheur and Berthoz 2005], [Cinelli and Warren 2009]. The gaze was also studied as one of the multisensory controls of movement [Berthoz 1993].

Turning is an example which reveals the way of stepping when humans change the orientation during walking. In [Hase and Stein 1999], authors presented two turning strategies: spin turn and step turn (see figure 2.3). The shifting and rotating of body parts such as trunk, hip, legs were also implied to these strategies.

2.2.3 Human arm reaching and locomotion

There were many studies about the similarity of arms and legs movements during locomotion. In [Zehr and Duysens 2004], authors found that although the strength of coupling between the legs is stronger than that between the arms, arm and leg movements are similarly regulated by CPG activity and sensory feedback during locomotion (see figure 2.4)

The inter-limbs coordination was also considered. How we move the arms during a locomotion? It is hypothesized that during locomotion, upper limbs motoneurones are excited indirectly via propriospinal neurons in the cervical spinal cord. This allows a task-dependent neuronal linkage of cervical and thoraco-lumbar propriospinal circuits controlling leg and arm movements during human locomotor

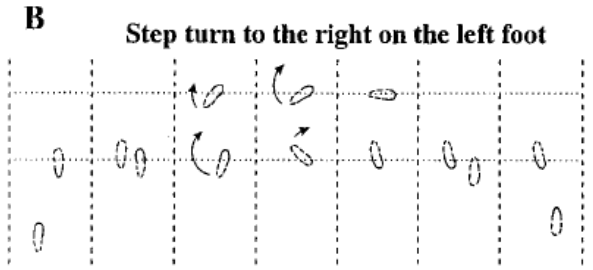

(a)

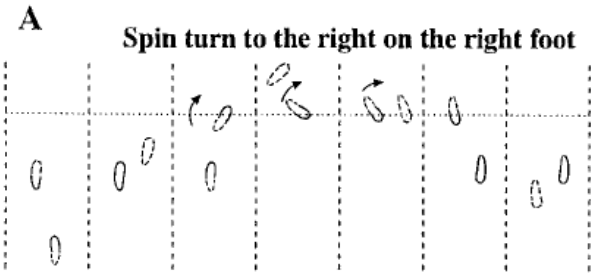

(b)

Figure 2.3: Two turning strategies during human walking: (a) Step turn and (b) Spin turn (cited from [Hase and Stein 1999])

activities [Dietz 2002].

In another way, the comparison of hand movements and locomotion was carried out by analyzing motion characteristics as the velocity and the curvature of trajectory ([Vieilledent et al. 2001], and afterwards by [Hicheur et al. 2005]). It is known that there is a relationship between velocity and curvature called Fitt's law [Fitts 1954]. This statement was verified for hand-writing movements. In those papers, authors proposed the hypothesis for human locomotion along different shaped trajectories on the ground. This result raised the intriguing possibility that some of the geometrical aspects of locomotor and hand-movement planning might be shared.

The similarity of arms movements and locomotion deduced a computational model for human locomotion adapted on the computational one developed before (see [Flash and Hogan 1985] for an example). This model based on the minimum jerk:

$$J = \int_0^{t_f} \left(\left(\frac{d^3x}{dt^3} \right)^2 + \left(\frac{d^3y}{dt^3} \right)^2 \right) dt \tag{2.1}$$

where (x, y) is the position of each instant from 0 to t_f. The optimized solution is analytically calculated as:

$$\begin{aligned} x(t) &= a_5t^5 + a_4t^4 + a_3t^3 + a_2t^2 + a_1t + a_0 \\ y(t) &= b_5t^5 + b_4t^4 + b_3t^3 + b_2t^2 + b_1t + b_0 \end{aligned} \tag{2.2}$$

Recently, this model was applied to predict the shape of human locomotion trajectories [Pham et al.

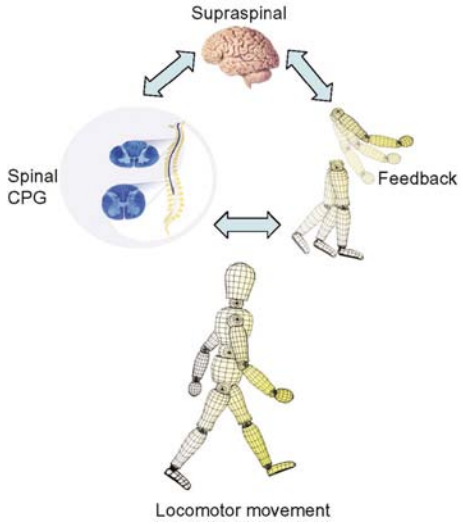

Figure 2.4: General outline of the interrelationships between spinal central pattern generators (CPG) activity (spinal cord sections shown), supraspinal input (brain shown), and sensory feedback arising during movement (moving arms and legs) in creating and sculpting human locomotion (shown at bottom). Cited from [Zehr and Duysens 2004]

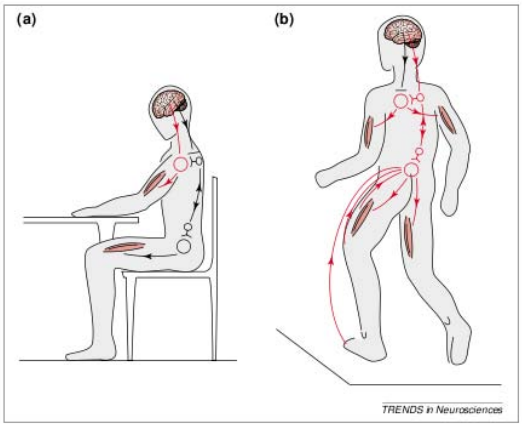

Figure 2.5: Movement control during different motor tasks. (a) During skilled hand movements, the direct cortical motoneuronal excitation is predominant (red lines) and the cervical propriospinal neuronal system is inhibited. (b) During locomotion, it is assumed that the brain command is predominantly mediated by interneurons. Cervical and thoraco-lumbar propriospinal systems become coupled and coordinate arm and leg movements (red lines). Cited from [Dietz 2002]

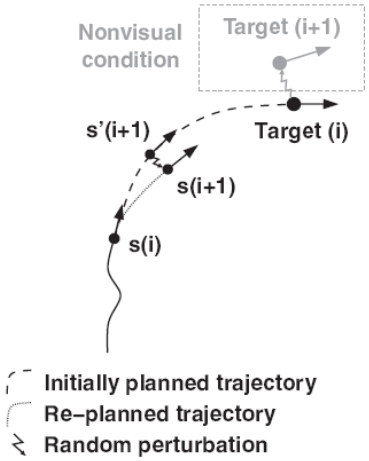

Figure 2.6: Illustration for the simplified optimal feedback control models. Cited from [Pham and Hicheur 2009]

2007]. The model proves the efficiency for highly curved trajectories. In [Pham and Hicheur 2009], authors modified the model (2.1) by adding a term which penalize a large variations of the velocity:

$$J = \int_0^{t_f} \left(\left(\frac{d^3x}{dt^3} \right)^2 + \left(\frac{d^3y}{dt^3} \right)^2 + y \left(\frac{d}{dt} \sqrt{\frac{d^2x}{dt^2} + \frac{d^2x}{dt^2}} \right)^2 \right) dt \tag{2.3}$$

Then, a stochastic model adapted form the simplified optimal feedback control scheme was also proposed. This model based on the open-loop model 2.3 complemented with an on-line feedback module (see figure 2.6)

2.2.4 Computational motor control models

In a recent study, [Schaal and Schweighofer 2005] synthesized a generic motor control diagram used in robotics that can be a guideline for biological motor control (see figure 2.7). Robotic motor controls then are used to explain the brain movement control mechanisms.

Beside the error-based learning, the Bayesian theory, the operational control space and redundancy resolutions, the brain is considered as a mixture model and as a stochastic optimal controller.

2.2.4.1 Internal model

It was proposed that the central nervous system internally simulates the dynamic behavior of the motor system in planning and control. That means the central nervous system has an internal model for sensorimotor integration (see [Wolpert 1995], [Jordan and Wolpert 1999] for a review). There are two varieties of the internal model: forward model and inverse model. Forward models mimic the causal flow of a process by predicting its next state (for example, position and velocity) given the current state and the motor command. Inverse models invert the causal flow by estimating the motor command that caused a particular state transition. Kawato et al. [Kawato 1999] proposed a computational model based

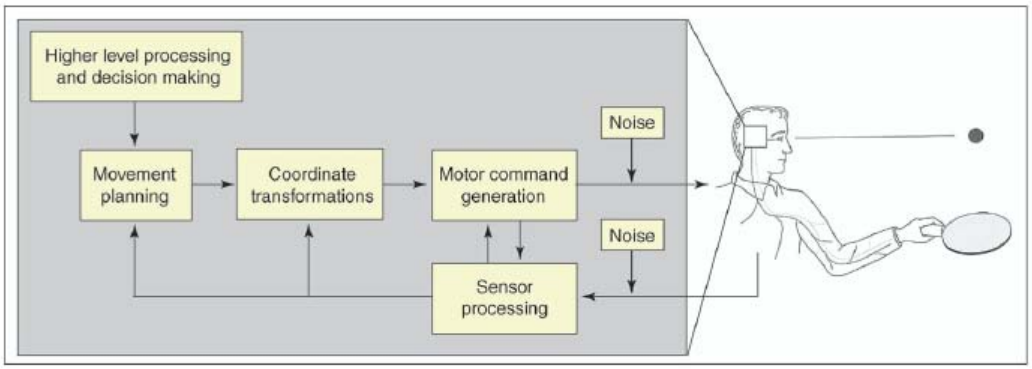

Figure 2.7: Sketch of a generic motor control diagram, typically used in robotics research, that can also function as a discussion guideline for biological motor control. Cited from [Schaal and Schweighofer 2005]

on internal forward and inverse models for the coordination of arms grip force and load force whereas Sabes et al. [Sabes 2000] dealt with the target-shift and multi-joint arm movements (see figure 2.8).

2.2.4.2 Optimal control model

Optimal control models of biological movements have explained behavioral observations on multiple levels of analysis (limb trajectories, joint torques, etc) and have arguably been more successful than any other class of models (see a synthesized study of this theme in [Todorov 2004], and [Todorov and Jordan 2002]). Any optimal control model is composed of: a family of control laws corresponding to the musculo-skeletal model and a quantitative definition of task performance. Performance is measured as the time-integral of some instantaneously defined quantity called a cost function. In fact, optimality models are often named Minimum X where the cost X can be jerk, torque change, energy, time, variance. However, traditional optimal control models emphasized on optimizing average trajectories while ignoring sensory feedback. Sensorimotor information can be considered to modify types of control law: feedback optimal control.

Open-loop optimization. Open-loop optimal control models predict average movement trajectories by optimizing a variety of cost functions. They are models of average behavior, and the cost of these models can be energy, smoothness, accuracy and multi-attribute. We present here some energy criteria developed longtime ago, from [Hatze and Buys 1977] for the mammalian neuromuscular system to various types of control theory (see [Kirk 2004] for a review). Recently, Berret et al. [Berret et al. 2008] proposed an inactivation principle (mathematical solutions) minimizing absolute work and biological terms for arm movements.

$$J(u) = \int_0^T \widetilde{f}(x,y,u)dt + Aw \tag{2.4}$$

where Aw is the *absolute work*, and $\widetilde{f}$ is the function of other *comfort terms*.

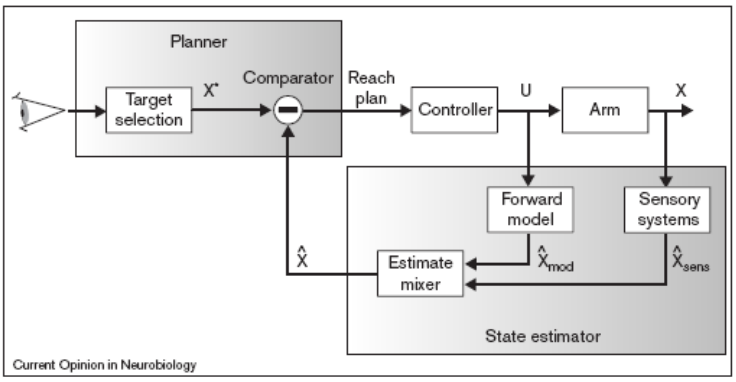

(a)

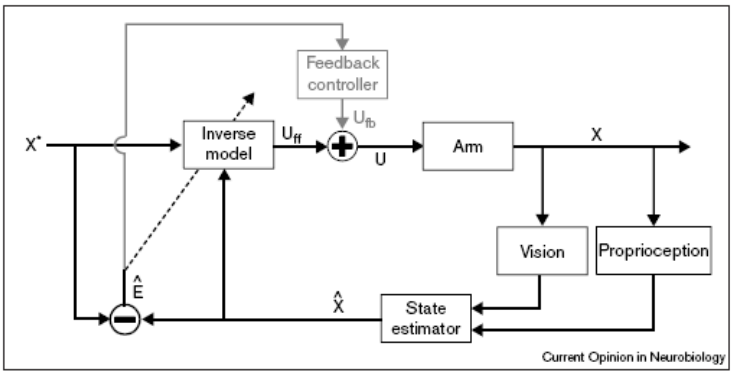

(b)

Figure 2.8: Schematic diagram of the internal models used in the target-shift task (a), and in controlling multi-joint arm movements (b). Cited from [Sabes 2000]

Tuan et al. [Tuan et al. 2008] later applied efficiently the optimal control model of Guigon [Guigon et al. 2007] minimizing motoneuron energies to obtain the human-like reaching for humanoid robot HRP2:

$$E = \sum_{i=1}^{2n} \int_{t_0}^{t_f} u_i^2(t)dt \tag{2.5}$$

where u_i is the motoneuron stimulating the i-th actuator (muscle) out of $2n$ actuators, and t_0, t_f are the initial and final movement times respectively. The typical type of the smoothness criteria is minimum-jerk (time derivative of the acceleration) showed in section 2.2.4 ([Flash and Hogan 1985] for arm movements, then applied for human locomotion [Pham et al. 2007]). There is also the minimum torque-change model [Uno et al. 1989] for the smoothness classification.

$$C = \int_0^{t_f} \sum_{i=1}^{n} \left(\frac{dz_i}{dt} \right)^2 dt \tag{2.6}$$

where z_i is the torque generated by the i-th actuator (muscle) out of n actuators, and t_f is the movement time.

These criteria were mainly calculated for the arm movement. For the more sophisticated human

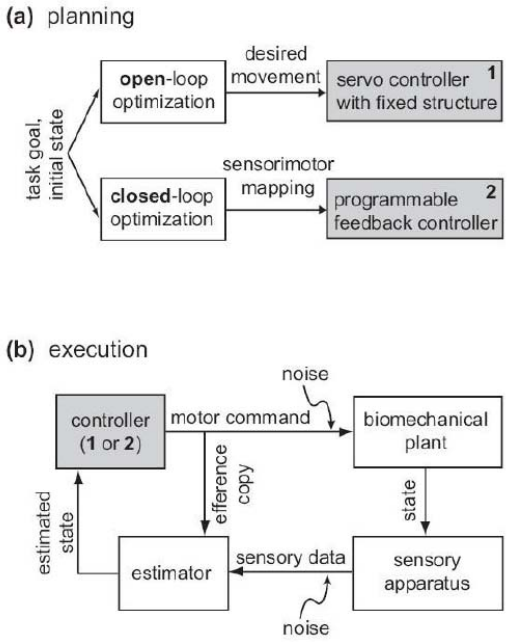

Figure 2.9: Schematic illustration of open- and closed-loop optimization. (a) The optimization phase, two procedures start with a specification of the task goal and the initial state. Both approaches yield a feedback control law, but in the case of open-loop optimization the feedback portion of the control law is predefined and not adapted to the task. (b) Either feedback controller can be used online to execute movements, although controller 2 will generally yield better performance. Noise is typically modeled as a property of the sensorimotor periphery, although a significant portion of it may originate in the nervous system. Cited from [Todorov 2004]

motions, the true performance criterion is likely to involve a mix of cost terms [Rosenbaum 2009]. The multi-attribute objectives function in chapter 5 also expresses this statement.

Closed-loop optimization: Models of sensorimotor integration. Instead of focusing on average behavior, sensorimotor integration can be modeled much more directly via closed-loop optimization. In figure 2.9, we can see two optimization procedures. Open loop optimization makes a desired movement. The closed loop optimization takes into account the presence of noise, thus the movement plan is usually executed by a feedback controller. That means it uses some servo mechanisms to eliminate the deviations between the desired and actual state of the plant (see such a closed loop controller in [Harris and Wolpert 1998]).

2.3 Biomechanics: locomotion models interact to the environment

The biomechanics of human movement can be defined as the interdiscipline that describes, analyzes and accesses human movement ([Winter 2009]). Researchers concentrated on the characteristics of configuration geometry than trajectory geometry. Human walking has been studied from the point of view of understanding the control mechanisms of pathological gait [Saunders et al. 1953], joint

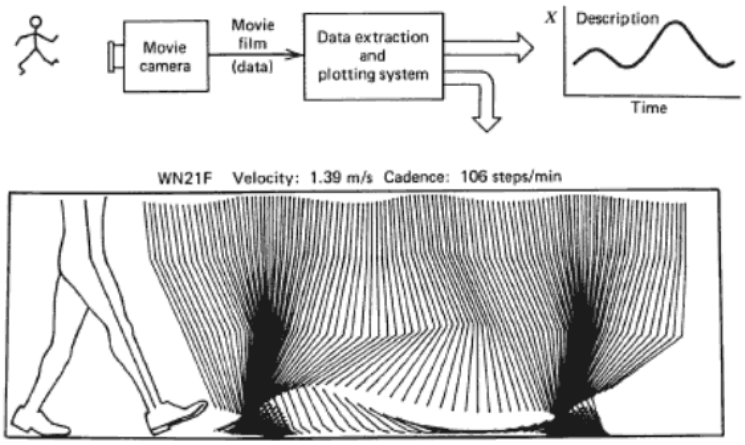

Figure 2.10: Flow of data from a camera system and plotting of data in two different forms, each yielding a different description of the same event. Cited from [Winter 2009]

kinematics, forces, torques [Anderson and Pandy 2001] and muscle coordination [Zajac et al. 2002], [Zajac et al. 2003]. In figure 2.10, Winter [Winter 2009] presented two way of studying human movement: by straight lines or stick plot and by a reference plot. Most biomechanical modeling involve the prediction of variables such as reaction forces, moments and mechanical energy. However, these studies were essentially conducted on the treadmill, and were quite far from daily human walking. We present here some studies which considered human walking in surrounding environments with or without obstacles. These works divide into two groups.

The first one deals with creating a locomotion model taking into account the priority of environments [Brogan and Johnson 2003]. In this paper, authors presented a novel behavioral of path planning based on pedestrian performance statistics during experiments. The pedestrian model was:

$$head(t+1) = c_{inertia}.head(t) + (1 - c_{inertia}).nav(t)$$

where $nav(t)$ is the navigation function, $c_{inertia}$ is the inertial weighting factor and $head(t)$ is the head state in the head chart (see figure 2.11).

The second one studies the locomotion strategies under different constraints, especially with obstacles. Fajen and Warren [Fajen and Warren 2003] considered a goal-directed locomotion with the appearance of obstacles (see figure 2.12). They found that goals and obstacles behave as attractors and repellers of heading, respectively, whose strengths depend on distance. The observed behavior was modeled as a dynamical system in which angular acceleration is a function of the goal angle, the obstacle angle and the distance to goal/obstacle:

$$\ddot{\phi} = -b\dot{\phi} - k_g(\phi - \psi_g) + k_o(\phi - \psi_o)e^{|\phi - \psi_o|} \tag{2.7}$$

where the goal ψ_g and obstacles ψ_0 shift along the ϕ axis, b and k are parameters expressing the ratios of damping and stiffness to the bodys moment of inertia. This model then was applied in [Fink et al. 2007] for both real and virtual environments.

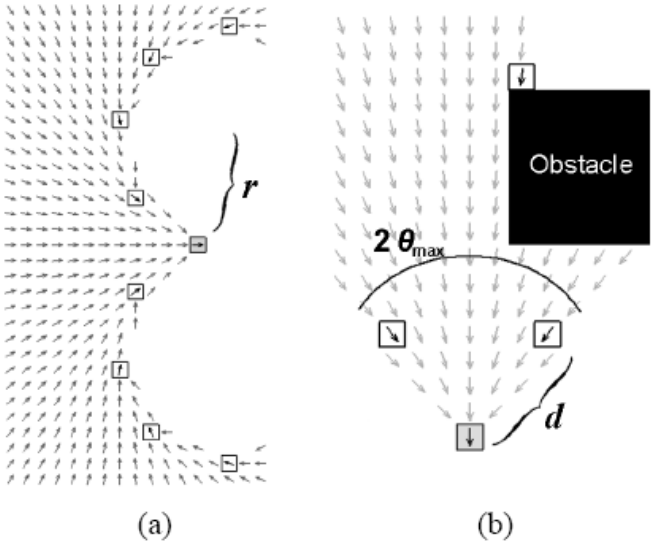

Figure 2.11: Constructing heading charts: subgoals shown with black outlines and goal with grey fill. (a) Vectors point toward the goal and never have a turning radius less than r. (b)After the first iteration, vectors in the arc of $2\theta_{max}$ point toward the goal, unless obscured by an obstacle (where $d = r\theta_{max}$). Cited from [Brogan and Johnson 2003]

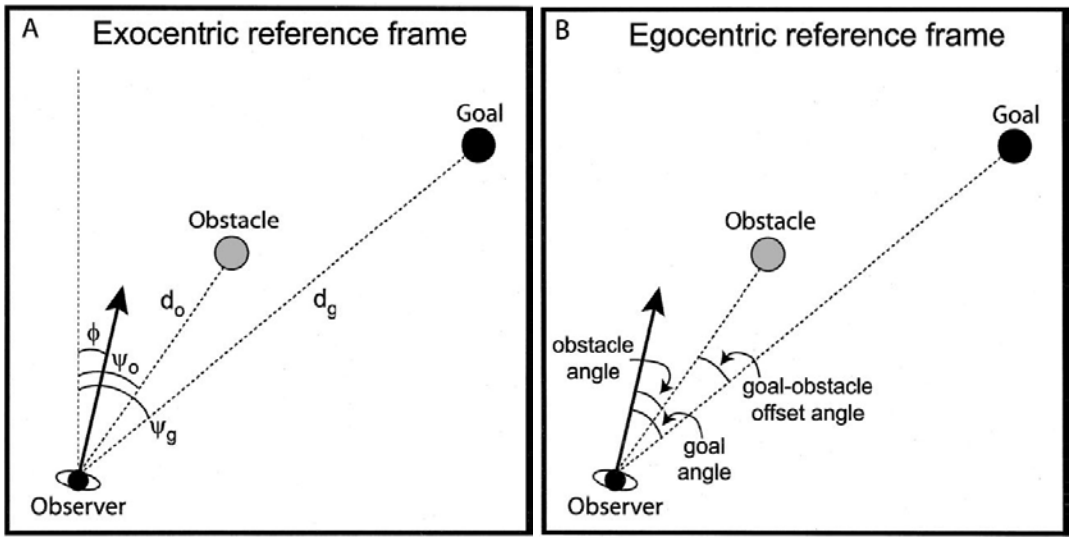

Figure 2.12: Plan view of an observer moving through an environment containing a goal and an obstacle. A: The vertical dotted line is a fixed, exocentric reference line used to define the observers direction of locomotion ϕ, the direction of the goal (ψ_g), and the direction of the obstacle ψ_o; d_g and d_o correspond to the distance from the observer to the goal and obstacle, respectively. B: The goal and obstacle angles are defined in an egocentric reference frame with respect to the observers direction of locomotion. Cited from [Fajen and Warren 2003].

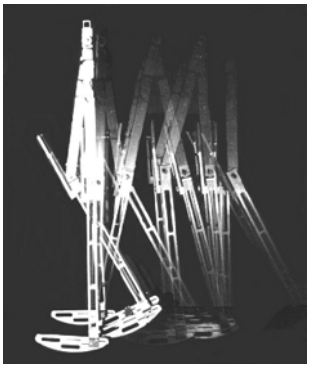

Figure 2.13: A duplicate of one of McGeer's machines from *Human Power and Robotics Lab, Theoretical and Applied Mechanics, Cornell Univ.*

2.4 Robotics: from biped to whole body locomotion models

Since the pioneer work of Raibert [Raibert 1986] on walking machines, robotics focused on controlling a legged mechanical designs which perform locomotions. Some of them applied biological inspirations for designing insect robots, quadruped robots, etc (see [Saranli et al. 2001], and [Raibert et al.] for examples). On the contrary, most of them concentrated on the locomotion of lower limbs level through biped walking, and ignoring the articulated upper body.

The main investigated themes were the design of passive walking machines (see [McGeer 1990] for pioneer works, and an application model of these works shown in figure 2.13), or kinematical and dynamical behaviors of bipedal walking (see [Pratt and Pratt 1998], and figure 2.14 for an overview).

With the advent of humanoid robots from Japan (see figure 2.15 for an example), the upper body was more and more integrated into the entire locomotion task. Roboticians tried to control, to make robots walk and did not pay attention on the human-like walking aspect. The classical control models to generate locomotion patterns are based on the Zero Moment Point (ZMP) theory (see an example in [Kajita et al. 2002] and in figure 2.16).

ZMP theory and inverted pendulum are two main methods using for the equilibrium and the dynamics stability during biped walking (see [Vukobratovic and Borovac 2004] and [Kajita et al. 2001]). Humanoid robots are redundant systems, so apart from solving the inverse kinematics/dynamics problem, the posture and the behavior of motions were also considered to obtain the whole body movements [Khatib et al. 2004]. In a recent research, Kanoun et al. [Kanoun et al. 2009] considered the locomotion as a task. A footstep can be parameterized by a translation and a rotation of the target footprint from the support footprint. Thus, two successive footprints can be considered as two virtual bodies joined by a virtual link with three degrees of freedom. By linking this chain to the robot at one of its feet, authors established a direct relationship between the tasks and the configuration of the walk path (see figure 2.17).

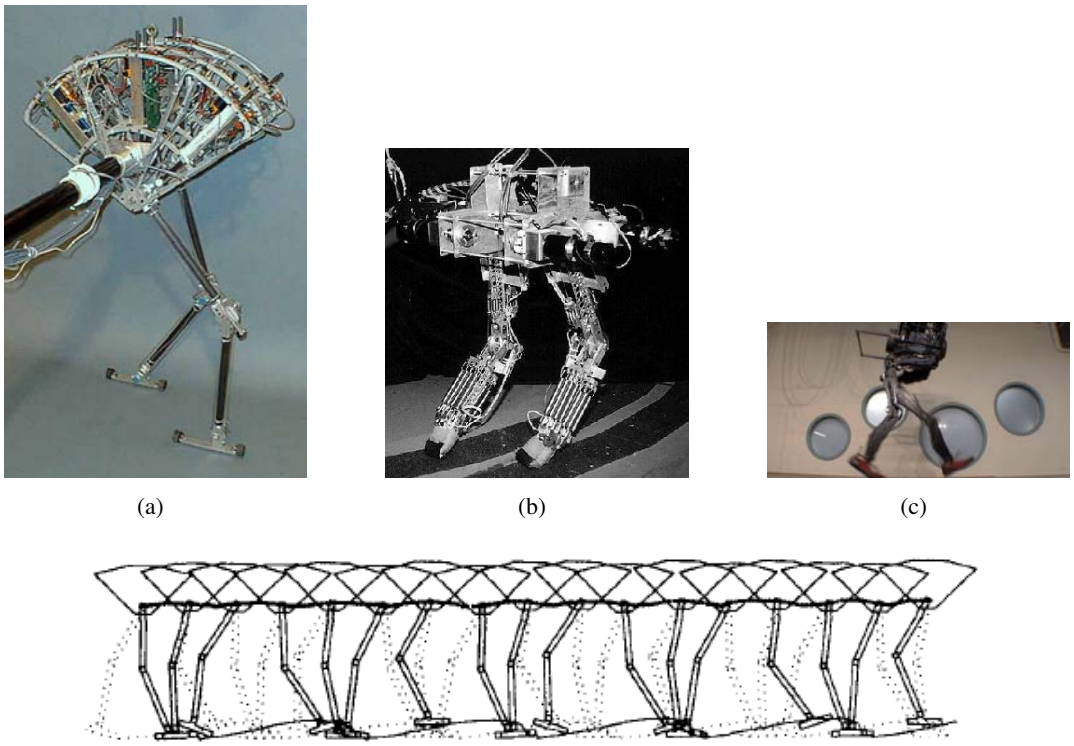

(a) (b) (c)

(d)

Figure 2.14: Some walking biped from MIT Leg Lab. (Spring Flamingo (a), Spring Turkey (b)) and from Boston Dynamics (Petman (c)). A simulation of biped locomotion is shown in (d)

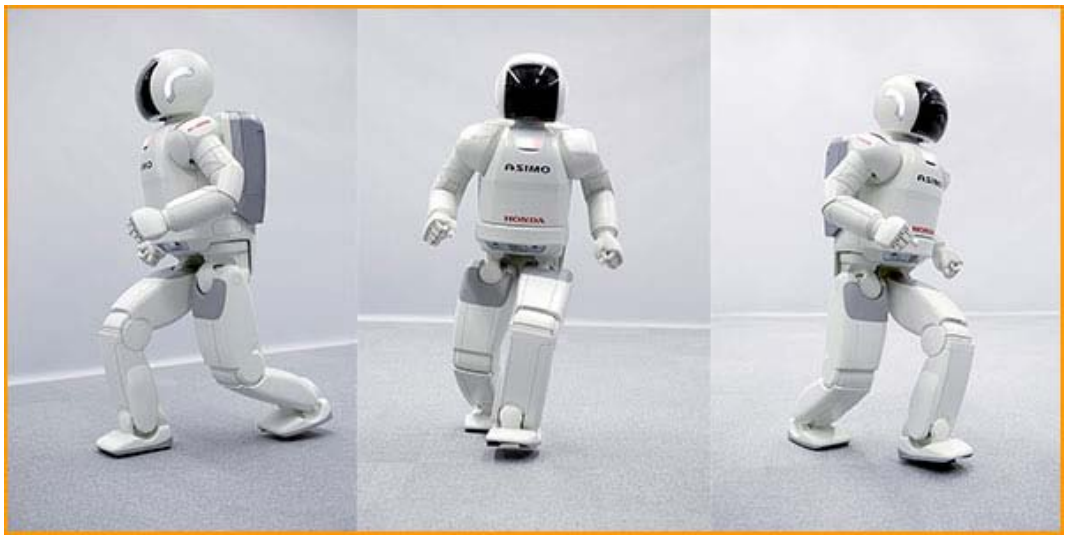

Figure 2.15: Asimo is one of the most flexible robots for walking.

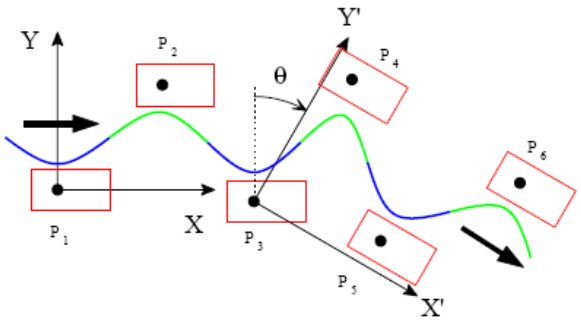

Figure 2.16: ZMP (dark points) on footprints when the robot changes its walking direction in [Kajita et al. 2002]

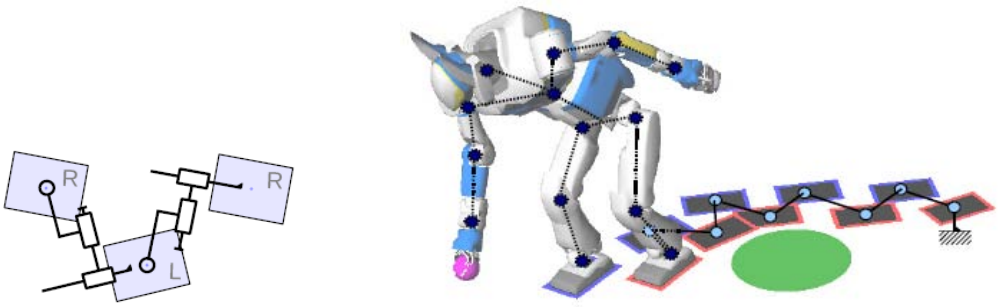

(a) (b)

Figure 2.17: (a) Virtual kinematic chain. (b) The kinematic model of the robot plus virtual kinematic chain. Cited from [Kanoun et al. 2009]

Figure 2.18: A comparison between a simulated and a human runner on a treadmill. The spacing of the images in time for the composite of the simulated and human runner at 0.066 s. Cited from [Hodgins et al. 1995]

2.5 Computer animation: synthesized locomotion

In computer animation, researchers tried to bring human appearance and behavior into virtual environments. The modeling of navigation and locomotion also achieved a great attention. A way of defining motion, commonly known as Motion Control Methods (MCMs), was classified based on the geometric, physical, or behavioral information [Magnenat-Thalmann and Thalmann 1991]. Approaches to synthesize human locomotion were first based on biomechanical knowledge (like in [Zeltzer 1982]) and on physical laws [Hodgins et al. 1995]. Basing on physical information, motion is globally controlled by solving dynamic equations. Hodgins et al. animated athletic behaviors using physically realistic models to perform the desired maneuver. For example, each internal joint τ in running behavior was calculated as:

$$\tau = k(\theta_d - \theta) + k_d(\dot{\theta}_d - \dot{\theta}) \tag{2.8}$$

where k is a gain for the correction of errors in speed, θ and θ_d are the actual and desired facing direction of the runner, respectively. The simulation result is shown in figure 2.18

When the motion capture technique appeared, it became rapidly the most populated one solving two problems of realism: appearance and performance (in term of computation time). This technique allows to record articulated trajectories during specific human motions. Thus, the locomotion study approaches shifted to adapt recorded data to desired context. The core of these approaches relies on signal-processing techniques introduced by [Bruderlin and Williams 1995]. Witkin et al. [Witkin and Popovic 1995] produced new animated sequences of human motions by blending and warping captured motions.

Motion blending was also achieved by using various approaches. Rose et al. [Rose et al. 1998] presented a multidimensional motion interpolation using radial basis functions. The authors called parameterized motions *verbs* and the parameters that control them *adverbs*. Verbs can be combined with other verbs to form a *verb graph*, with smooth transitions between them, allowing an animated figure to exhibit a similar behavior. Figure 2.19 shows an animated result of this work.

The autonomy of locomotion tasks for virtual actors was achieved by mixing motion synthesis techniques with path planning [Pettré et al. 2003], [Choi et al. 2003], and reactive navigation techniques [Reynolds 1987]. For the locomotion animation combined with path planning, realism of followed trajectories (followed path and speed profile) essentially depend on the artistic skills of the animator. The work in [Reynolds 1987] represented the computer animation method based on behavioral information. Reynolds et al. introduced a distributed behavioral model to simulate flocks of birds and schools of fish.

2.6 Summary

In summary, there has been many studies on human locomotions in many different ways. The goal of our work is to create a bridge between the life science community integrating human locomotion studies and the engineering community. In particular, we base on the robotics knowledge (nonholonomic and holonomic motions) to understand the control strategy of neuroscience via the mathematical model. Then, we exploit these properties in computer animation via a developed locomotion controller. The

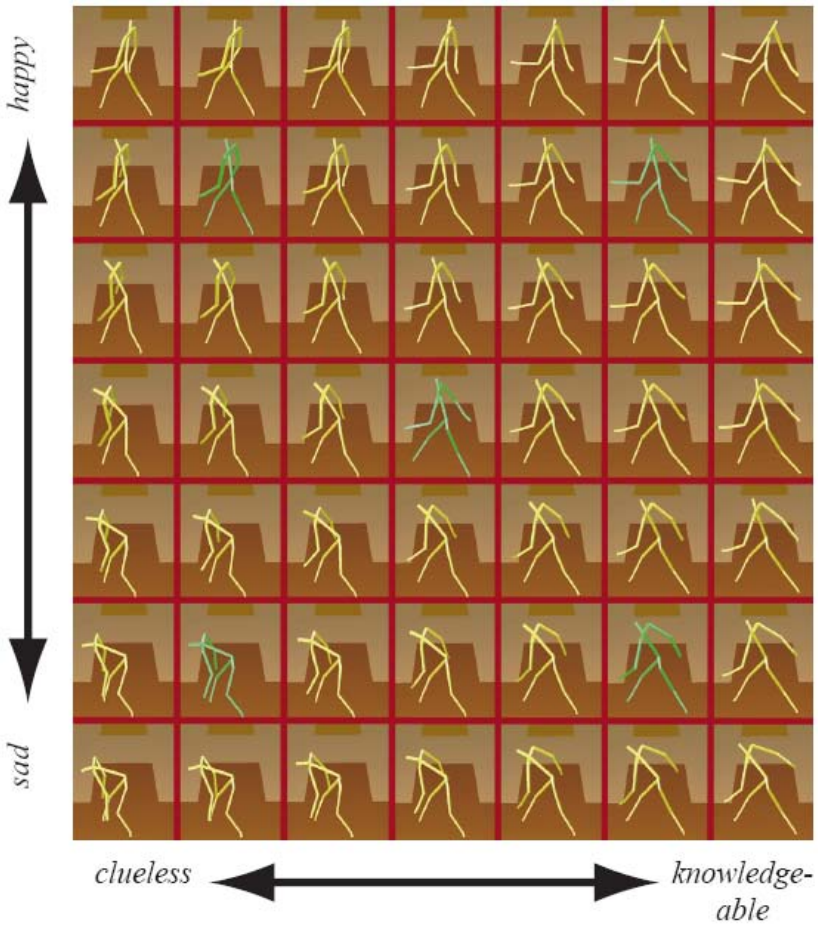

Figure 2.19: A walk sampled across two emotional axes. The green figures are the example motions. The rest are created through the verb/adverb mechanism. Cited from [Rose et al. 1998]

next chapters present our initial work, the experimental study, the modeling study and the application study respectively.

3

A nonholonomic-based model approach

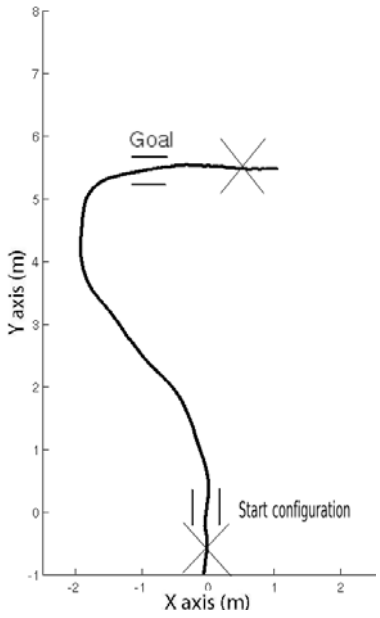

Figure 3.1: The protocol used in our previous work. Two doors were placed at start and final configurations. To exclude the positive and negative acceleration effects at the beginning and at the end of trajectories, we just kept these trajectories in the interval of two doors. Cited from [Arechavaleta et al. 2008a]

In this chapter, we first talk about our previous work, then emphasize our approach in the thesis. The goal of our work is to understand the shape of human trajectories during walking. Our previous work focused on two main problems:

- Everybody (in term of statistically homogeneous sample) shares the same locomotor strategy
- Human locomotion trajectories proved a nonholonomic nature integrated in a model
- The shape of these trajectories are explained via an optimal control tool

3.1 Stereotype nature of human walking paths

Human locomotion was investigated in a goal-oriented task where subjects had to walk to and through a doorway starting from a fixed position and orientation in space (figure 3.1).

With such a protocol, we found that subjects had the *stereotypy* of walking paths (geometric stereotypy, see figure 3.2) and the stereotypy of velocity profiles (kinematic stereotypy), but they had a variability of foot steps. That means humans may share the same locomotion control strategy, especially in trajectory planning level rather than in stepping level.

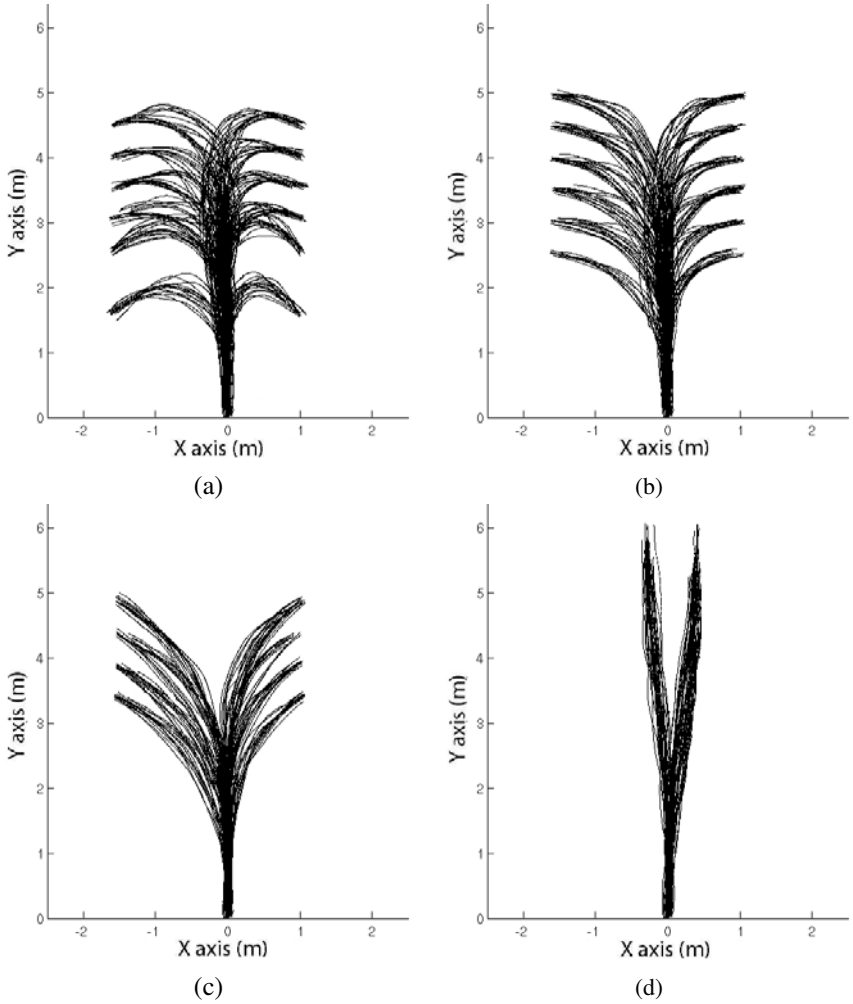

Figure 3.2: Recorded trajectories in our previous experiment [Hicheur et al. 2007]. They are classified into four categories: (a) High Curvature (HC), (b) Medium Curvature (MC), (c) Low Curvature (LC) and (d) Straight (S), respectively. The trajectories are those of the torso.

3.2 Nonholonomic nature of human walking

Let us consider the motion of a car (or a car-like robot). We use two parameters of acceleration (gear) and orientation (driver) for controlling the car to move in a space specified by three parameters of position and orientation [Laumond 2001]. This kind of motion is caused by the integration of car's orientation into its corresponding position. Such a motion in wheeled robots (including car-like robots) represents a *nonholonomic* constraint. This constraint doesn't reduce the dimension of the reachable space, but it reduce the dimension of differential movement space (velocity direction space). It forces wheeled robots to move tangentially to their main axis. But how humans walk? Humans can move with the same way that a nonholonomic system does? From observation of forward human walking, we tested in [Arechavaleta et al. 2008a] the *hypothesis* that human walking can also be described as a nonholonomic system. We compared three reference frames: head, torso, and pelvis to choose which frame steers the human locomotion (see figure 3.3). The study showed that the torso (shoulders) is the best frame accounting for the hypothesis (see figure 3.4)

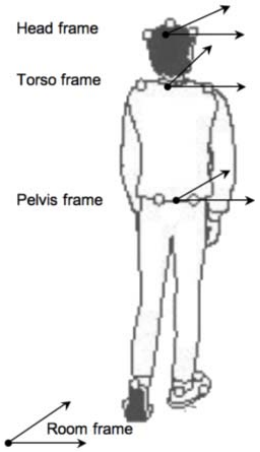

Figure 3.3: Definition of the local frames in [Arechavaleta et al. 2008a]. The position and the direction of the frames are deduced from the motion capture markers located respectively above the ears, on the shoulders and on both sides of the hip.

Then, we proposed a simple differential model (extensively used in mobile robotics [Laumond et al. 1998]) integrating the nonholonomic constraint:

$$\begin{pmatrix} \dot{x} \\ \dot{y} \\ \dot{\theta} \end{pmatrix} = \begin{pmatrix} \cos\theta \\ \sin\theta \\ 0 \end{pmatrix} v_f + \begin{pmatrix} 0 \\ 0 \\ 1 \end{pmatrix} \omega \tag{3.1}$$

where (x, y, θ) is position and orientation of the mid-point of two shoulders, and v_f, ω are *forward* velocity and *angular* one. Simulated (integrated) trajectories were similar to recorded trajectories in terms of the geometric shape. And this model can predict 87 percent of all trajectories in the experimental database.

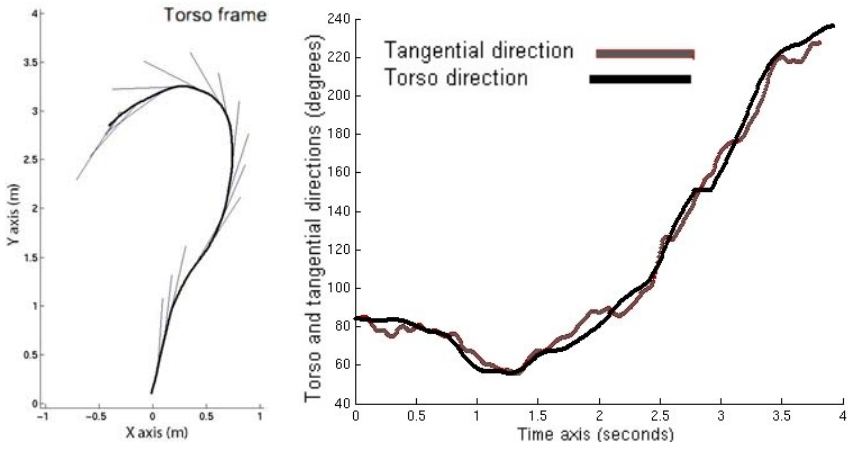

(a) (b)

Figure 3.4: A trajectory and the corresponding tangential direction profile of torso. (a) shows the trajectory followed by torso frame and its direction. (b) shows the torso direction profile and the tangential direction, two direction curves coincide verifying the hypothesis. Cited from [Arechavaleta et al. 2008a]

3.3 Numerical synthesis of human walking trajectory

We first extended the model in equation (3.1) and used an optimal control tool to predict trajectories:

$$\begin{pmatrix} \dot{x_T} \\ \dot{y_T} \\ \dot{\varphi_T} \\ \dot{\kappa_T} \end{pmatrix} = \begin{pmatrix} \cos\varphi_T \\ \sin\varphi_T \\ \kappa_T \\ 0 \end{pmatrix} u_1 + \begin{pmatrix} 0 \\ 0 \\ 0 \\ 1 \end{pmatrix} u_2 \tag{3.2}$$

The optimized criterion was the minimization of the curvature derivative. The analytical solutions (solved by using Pontryagin Maximal Principle) underlined that optimal trajectories are composed of clothoid arcs [Arechavaleta et al. 2008b]. That means each trajectory has a finite sequence of elementary clothoid arcs. Such a sequence may be phrased as, for instance, "Start turning left while increasing the curvature during τ_1 second, then decrease the curvature during time τ_2 and finally increase the curvature during time τ_3". These combinations generate "words" that account for the strategy during intentional locomotion.

This section concentrates on the numerical synthesis of human locomotion (essentially done in my master thesis [Truong 2007] and published in [Laumond et al. 2007]). We proposed that the concatenation of clothoid arcs implies words of trajectories. Thus, we numerically characterize the optimal paths by the number of concatenated clothoid arcs. We can define a clothoid as the curve satisfying the following equation:

$$\kappa(\tau) = \pm c\tau, \quad \tau \in (-\infty, \infty) \tag{3.3}$$

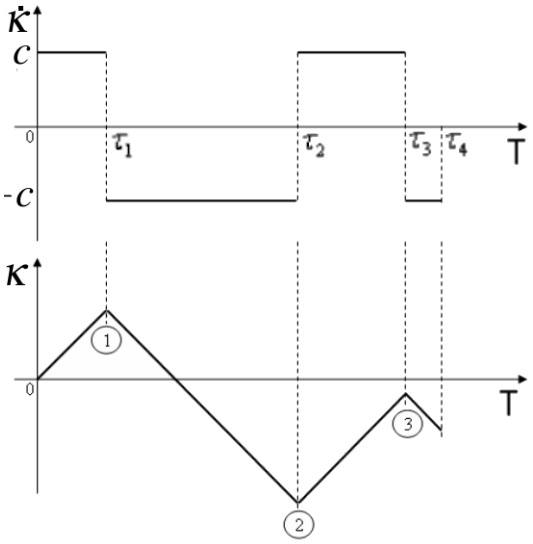

Figure 3.5: The concatenation point between two clothoid arcs is called a "switching point". At each switching point the curvature function contains a local extremum and the derivative of the curvature has a discontinuity.

where the sign $\pm$ defines the orientation of each piece of clothoid:

$$\begin{array}{rll} & u_2(\tau) \equiv c, & \kappa(\tau) \to \infty \\ or & u_2(\tau) \equiv -c, & \kappa(\tau) \to -\infty. \end{array} \tag{3.4}$$

The concatenation point between two clothoid arcs is called a *switching point*. At each switching point the curvature function contains a local extremum and the derivative of the curvature has a discontinuity (see figure 3.5). From the preceding reasoning, our numerical approach consists to determine the number of switches and the order of switching points of each optimal path. The method is based on the local analysis of the curvature. To be more precise, at each local extremum of the curvature there exists a switching point. The aim of the synthesis problem is to compute the partition of the 3-dimensional space according to the sequences of the switching points. To compute the synthesis for our optimization problem, we first sampled the reachable space considered in the experimental protocol $(x, y, \theta) \in \mathbb{R}^2 \times \mathbb{S}^1$. We defined the point $(0, 0, \pi/2)$ as the origin of the configuration space ($\kappa = 0$ at the starting and goal configurations). We computed the approximation of the space by a grid decomposition technique. The grid resolution was $(0.2m \times 0.2m \times 10deg)$ and the grid range from $[-2, 2] \times [3, 9]$ in position. Then, the analysis has been carried out by the following steps:

1. $\mathbb{R}^2 \times \mathbb{S}^1$ is partitioned with 36 slices according to the direction θ.
2. For each θ-slice, we computed numerically all the optimal trajectories from the origin to each vertex in the grid.
3. At each θ-slice, we determined the regions mapping the types of optimal paths. Each region corresponds to a set of optimal trajectories containing the same ordered combination of clothoid arcs in terms of their orientations.

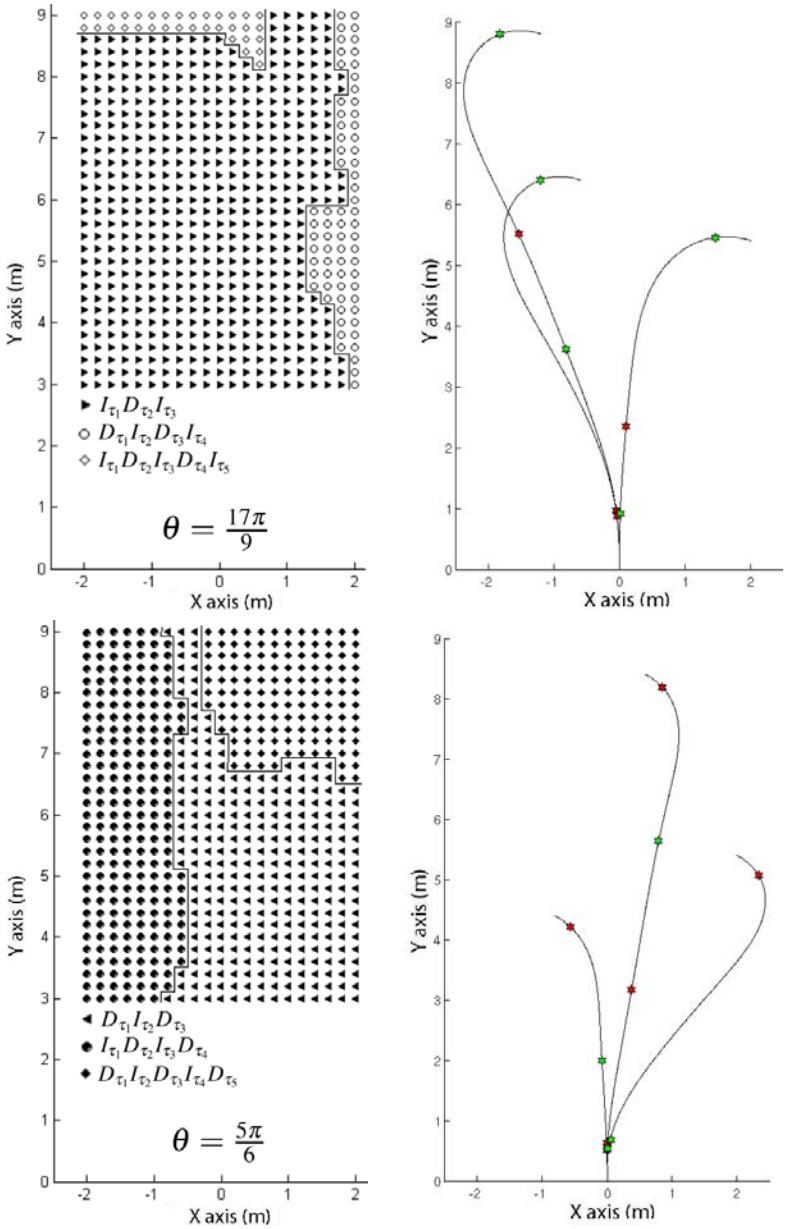

Figure 3.6: *Top-left: The partition of the slice* $\theta = \frac{17\pi}{9}$. *Bottom-left: The partition of the slices* $\theta = \frac{5\pi}{6}$. *Right: Some examples of representative optimal trajectories for different regions.*

By considering that the curvature κ of an arc of a clothoid can either increase (I_τ when $u_2 = c$) or decrease (D_τ when $u_2 = -c$) for a given time τ, we then found experimentally that only 6 combinations appear:

$I_{\tau_1} D_{\tau_2} I_{\tau_3}$,
$D_{\tau_1} I_{\tau_2} D_{\tau_3}$,
$I_{\tau_1} D_{\tau_2} I_{\tau_3} D_{\tau_4}$,
$D_{\tau_1} I_{\tau_2} D_{\tau_3} I_{\tau_4}$,
$I_{\tau_1} D_{\tau_2} I_{\tau_3} D_{\tau_4} I_{\tau_5}$,
$D_{\tau_1} I_{\tau_2} D_{\tau_3} I_{\tau_4} D_{\tau_5}$.

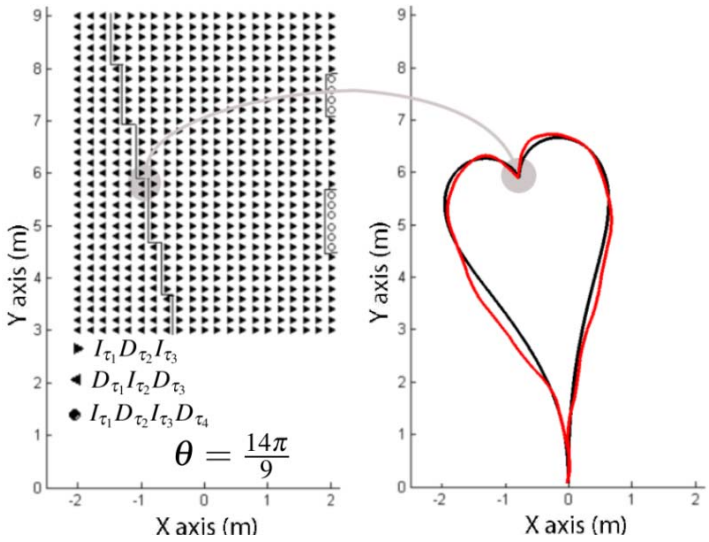

Figure 3.7: An example of two configurations belonging to two adjacent cells. The real (thin black) trajectories performed by the same subject with respect to predicted (bold) optimal trajectory. Cited from [Laumond et al. 2007]

We call these sequences the words of human locomotion. Figure 3.6 shows two θ-slices with their representative optimal trajectories for different regions.

Figure 3.7 shows an interesting case: at a configuration on the common border of both cells, there exist exactly two optimal trajectories with the same cost and a completely different shape. This means that the two completely different strategies used by the same subject to reach two close configurations in terms of optimizing the derivative of the curvature (see [Laumond et al. 2007] for more details).

4

The appearance of holonomic behaviors in neighboring space

4.1 Methodology

The goal of this chapter is to complete the study of the nonholonomic behavior hypothesis proposed in the thesis of Arechavaleta [Arechavaleta 2008]. Naturally, humans perform the nonholonomic behavior through exhibiting trajectories where the body orientation supports the tangent direction of motion. Nevertheless, in very specific situations, when targets are just nearby from the departure point, sideward or diagonal steps are performed (see figure 4.1), and they are types of holonomic motions. In these cases, the hypothesis is not any longer true, and the equation (3.1) is not validated either.

This thesis presents the combination between nonholonomic and holonomic properties in the human locomotion context. It is based on the methodology of human walking study using the accessible domain in free space. In particular, locomotion trajectories were recorded in neighboring space, and via statistical data, we would understand the nonholonomic/holonomic property of human walking. Our approach underlies several questions:

1. When (where) the holonomic appears? i.e. when the hypothesis is no longer true? And how can holonomic and nonholonomic behaviors combine together in human locomotion?
2. There exists a model unifying holonomic and nonholonomic motions explaining trajectories of recorded data? If these trajectories are assumed to be optimal ones, the model can predict them, and which is the corresponding criteria?
3. How to take into account the appearance of holonomic movements in global trajectories for deducing a whole body movement produced by a locomotion controller?

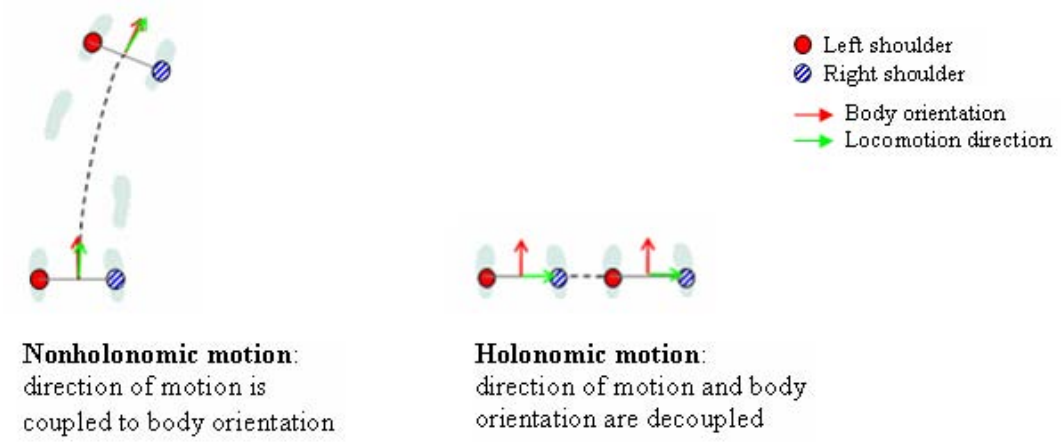

Figure 4.1: Two typical motions, the left one is of nonholonomic behavior, and the right one is of holonomic behavior.

We address these questions in chapter 3, 4, and 5 respectively.

4.2 Nonholonomic-holonomic segmentation tool

4.2.1 Segmentation function

To study the behavior of human locomotion in neighboring space, we developed an analytical tool (function) for analyzing the nonholonomic characteristic during a general human movement (i.e. a hybrid movement including the holonomic and nonholonomic movements). The goal of this function is to extract the nonholonomic behavior segments from any locomotor trajectory. This segmentation is based on the characteristic of nonholonomic movements in which the trajectory tangent direction is approximate to the movement direction. We consider here the movements of both shoulders to study the nonholonomic/holonomic characteristic of human locomotion. These movements were recorded by the motion capture system as the sequence of discrete points $x(t)$, $y(t)$. We calculated and compared the orthogonal direction of shoulders and the tangent direction of the corresponding trajectory. The nonholonomic/holonomic behavior depends on whether the deviation is smaller/larger than a threshold. This threshold (*tol* in function 1) was selected by a heuristical process based on the behavior of the observed curve of the deviation from many tested scenarios. If the threshold is too big, we obtain many trivial holonomic motions, and vice versa, when it is too small, we neglect some quasi-holonomic behaviors (essentially caused by combining diagonal steps and body rotations). Finally, we chose a threshold of 15°. The implementation is shown as function 1.

We used both left and right shoulder trajectories for exploring the human locomotion in the neighboring space so as to not ignore nonholonomic behavior from one of them (see figure 4.4 for the illustration of holonomic behaviors and figure 4.3 for the illustration of nonholonomic ones).

The tangent direction θ_T of the mid-point was calculated from its each coordinate (x,y) of the

Function 1: The function for segmenting nonholonomic/holonomic behaviors of any trajectory

input : Sequence of discrete points $x(t)$, $y(t)$ of human trajectories
output: Segmentation of nonholonomic/holonomic behaviors for these trajectories

begin
Step 1: calculate the tangential direction of mid-point of shoulders θ_T, of the left shoulder θ_{TL} and of the right shoulder θ_{TR} as equation (4.1);
Step 2: calculate the orthogonal direction of shoulders θ_S as equation (4.2) and equation (4.3);
Step 3: deduce the deviation between them (see figure 4.2)
Step 4: determine holonomic/nonholonomic segmentations of the trajectory:
If $|\theta_S - \theta_{TL}| < tol$ *or* $|\theta_S - \theta_{TR}| < tol$ **Then**
nonholonomic behavior;
Else
holonomic behavior;
End
end

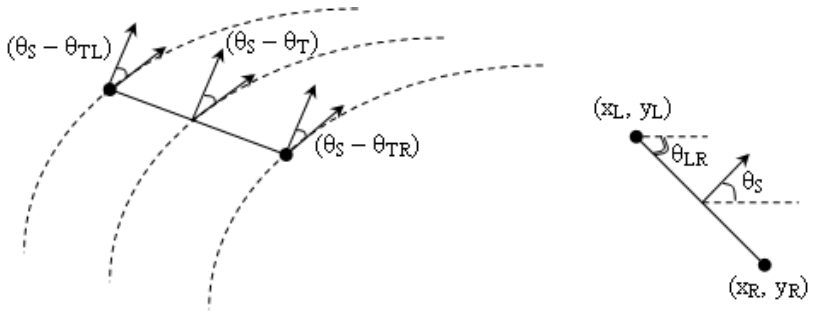

(a) (b)

Figure 4.2: An illustration for the angles calculation in a trajectory. (a) The deviation of orthogonal direction of shoulders θ_S and the tangential direction θ_{TL}, θ_{TR}. (b) The orthogonal direction of shoulders θ_S is calculated from the left-right shoulder vector

.

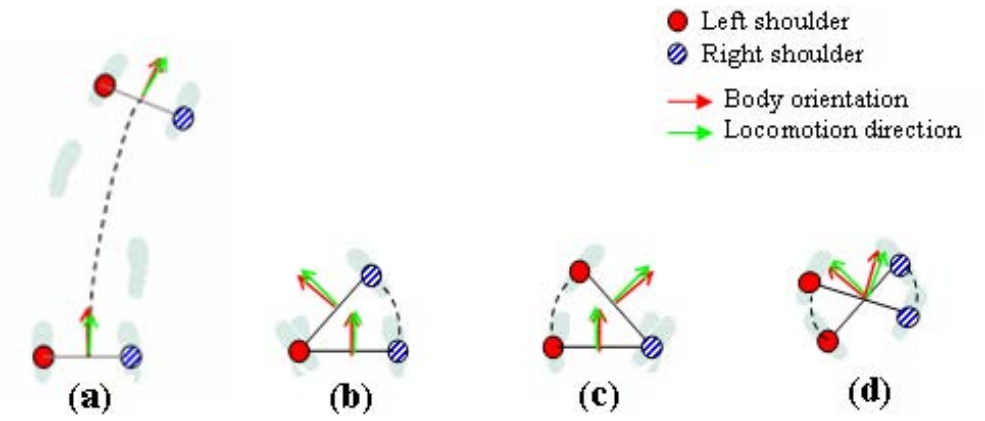

Figure 4.3: Some types of nonholonomic movements during human locomotion. (a): The normal walking. (b): The left spin turn motion: the right shoulder movement is nonholonomic. (c): The right spin turn motion: the left shoulder movement is nonholonomic. (d): The spin turn on the spot: movements of both left and right shoulders are nonholonomic. In these cases, the orthogonal direction of shoulders and the tangential direction of shoulders trajectories are approximative

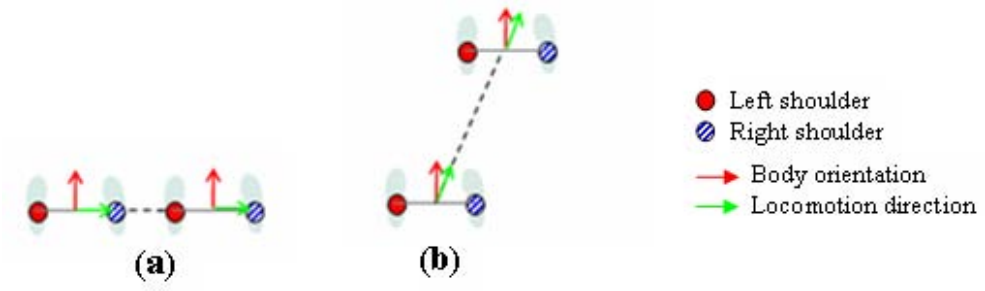

Figure 4.4: Two types of holonomic movements during human locomotion: the sideward step motion (a) and the diagonal step motion (b). In these two cases, the orthogonal direction of shoulders and the tangential direction of shoulders trajectories are very different.

corresponding recorded trajectory:

$$\theta_T(t) \leftarrow \frac{y(t+\Delta t) - y(t-\Delta t)}{x(t+\Delta t) - x(t-\Delta t)} \tag{4.1}$$

Similarly, we calculated θ_{TL} and θ_{TR} for left and right shoulders. The orthogonal direction of shoulders θ_S is implied by the left-right shoulder vector θ_{LR} (see figure 4.2 (b)) as:

$$\theta_{LR}(t) \leftarrow \frac{y_R(t) - y_L(t)}{x_R(t) - x_L(t)} \tag{4.2}$$

$$\theta_S(t) = \theta_{LR}(t) + \frac{\pi}{2} \tag{4.3}$$

We considers a hybrid movement including normal walking, some diagonal steps and some sideward steps (see figure 4.5 (b)). Movements of two shoulders were recorded by the motion capture system. The deviation between tangential and orthogonal direction of the acquired trajectory is then calculated (shown in figure 4.5 (a)). With a chosen tolerance of 15° (the red line in figure 4.5 (a)), holonomic and nonholonomic segmentations were detected by the function 1 (in 4.5 (c)).

4.2.2 Validation of the segmentation function

4.2.2.1 Noise filtering

The segmentation function presented in the above section is used for the online mode. In the case of noise appearances (an example in figure 4.6), the function segments a small interval of the holonomic behavior. In order to get more precise information about holonomic/nonholonomic behaviors for statistic analysis, we modify this function to a off-line function.

This off-line function detects intervals whose values (the deviation of tangential direction a and body orientation) are smaller than the chosen tolerance. If noises appear in these intervals, a low-pass filter is used to eliminate them.

4.2.2.2 Boundary of nonholonomic and holonomic movements

Diagonal steps are the cases of holonomic motions. The deviation of the tangential direction and the body orientation is 90 degree when we perform a sideward step. The deviation converges to zero when we walk forward to reach the target in front of you. Thus, at the boundary of forward walking and sideward step, we supplemented a subfunction distinguishing these two types of walking. In these two cases, the deviation is smaller than the tolerance, and the difference of initial and final body orientations deduces the behavioral segmentation. In figure 4.8, $\theta_i = \theta_f$ means that the deviation between two configurations is smaller than 1°.

4.2.2.3 Testing the segmentation function

A subject was asked to perform some scenarios of hybrid locomotions to verify the performance of the segmentation function. We tried to combine holonomic and nonholonomic behaviors into a trajectory to

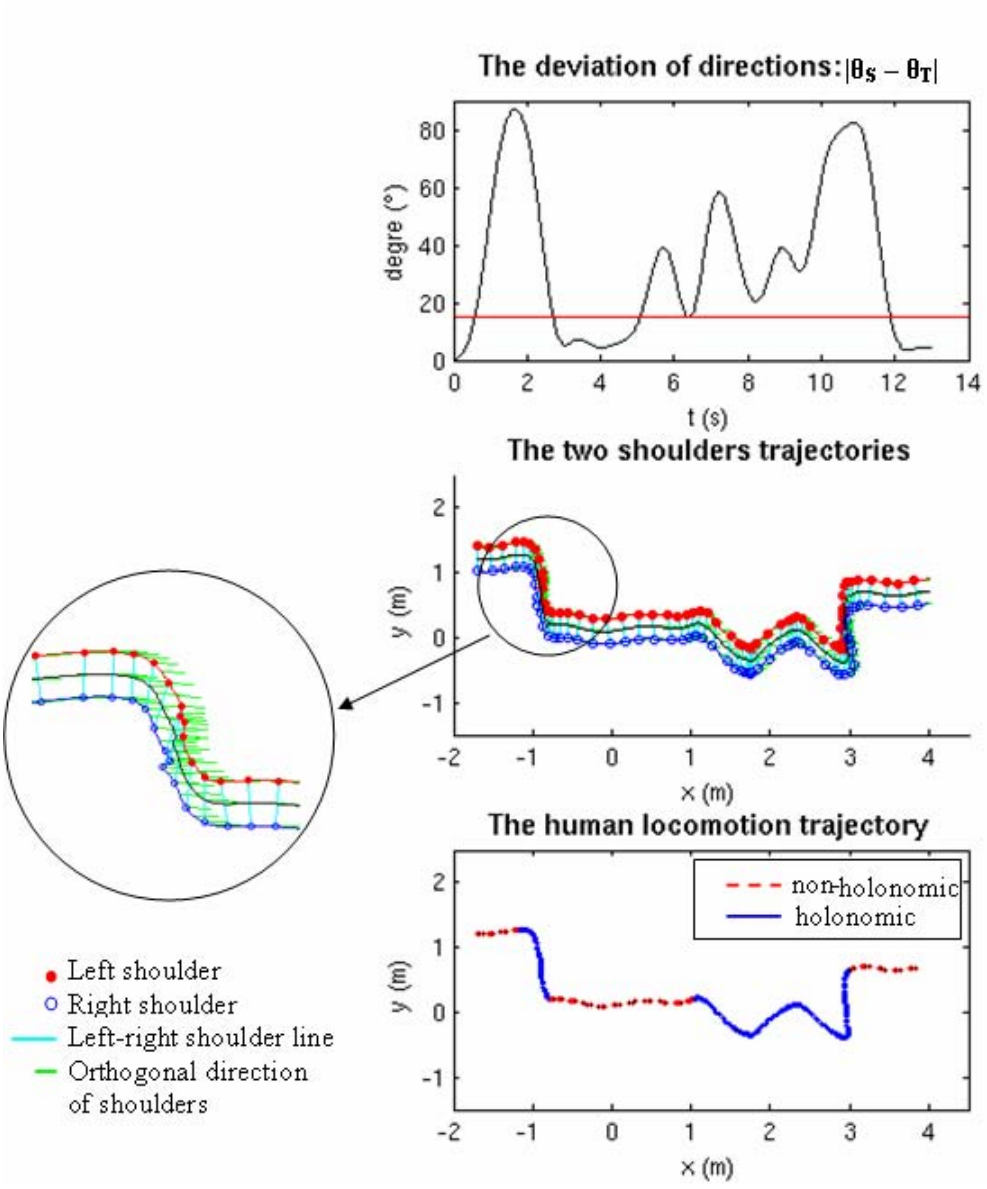

Figure 4.5: A demonstration of the segmentation function during a hybrid movement

.

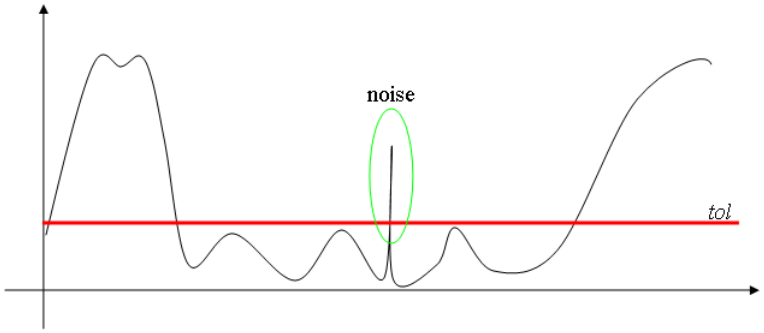

Figure 4.6: A noise appeared in a recorded trajectory

.

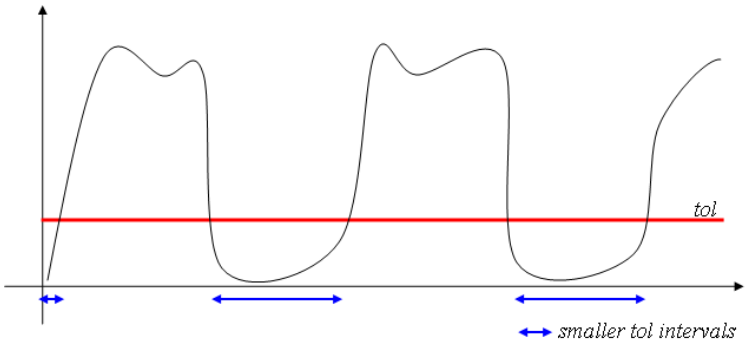

Figure 4.7: An illustration of the detection of intervals whose the deviation of tangential direction and body orientation is smaller than the chosen tolerance (*smaller tol intervals*)

.

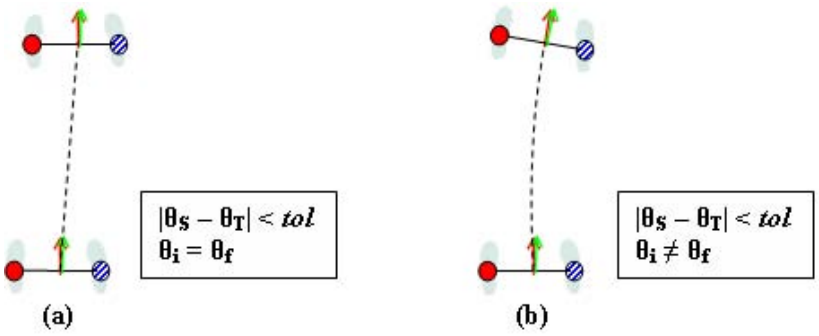

Figure 4.8: Two different types of human locomotion in the boundary of straight walking (a) and diagonal stepping (b)

.

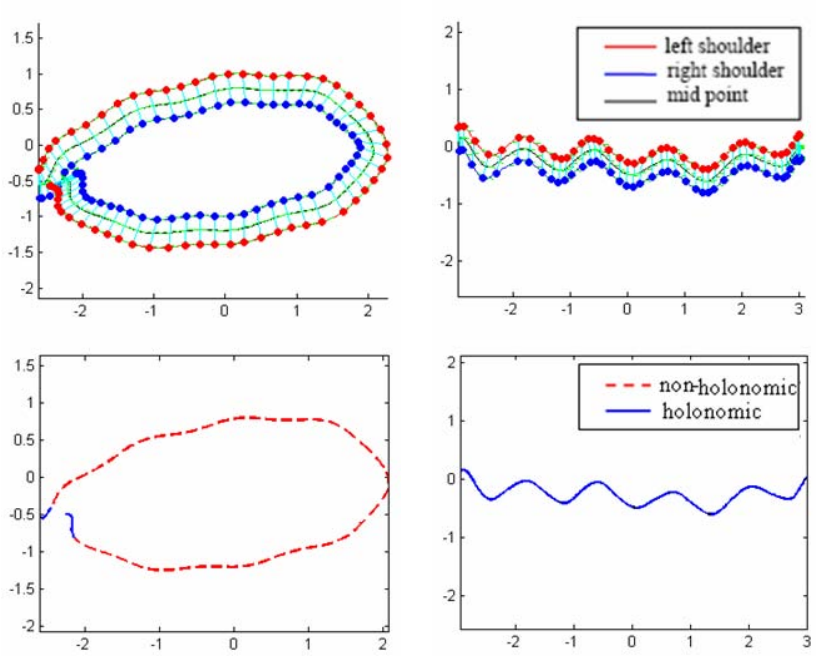

(a) (b)

Figure 4.9: Segmentations of nonholonomic and holonomic behaviors of an oval trajectory (a) and a trajectory including diagonal steps (b)

.

see the continuous transitions between them. Figure 4.9, 4.10 and 4.11 illustrate such a trajectory. The function 1 analyzes holonomic/nonholonomic segments for corresponding trajectories. The results are in agreement with realistic observation and then validate the qualify of the segmentation function.

4.3 Material and method

4.3.1 Subjects

Ten healthy male subjects volunteered to take part in the experiment. The mean age and height were 27 $\pm$ 4 years and 1.77 $\pm$ 0.06 m respectively. They all had normal or corrected to normal vision and none reported any problem with the walking task. Participants gave their informed consent before taking part in the experiment. The experiment was performed in accordance with the ethical standards laid down in the 1964 Declaration of Helsinki.

4.3.2 Experimental setup

4.3.2.1 Motion capture system and calibration

We used MotionAnalysis (Motion Analysis Corporation, USA) motion capture system to record the trajectories of body movements. This system (equipped by LAAS-CNRS) consists of 10 cameras placed on a rail system (about 3 meters above the floor) in the $9(m) \times 6(m)$ room. Among these ten cameras,

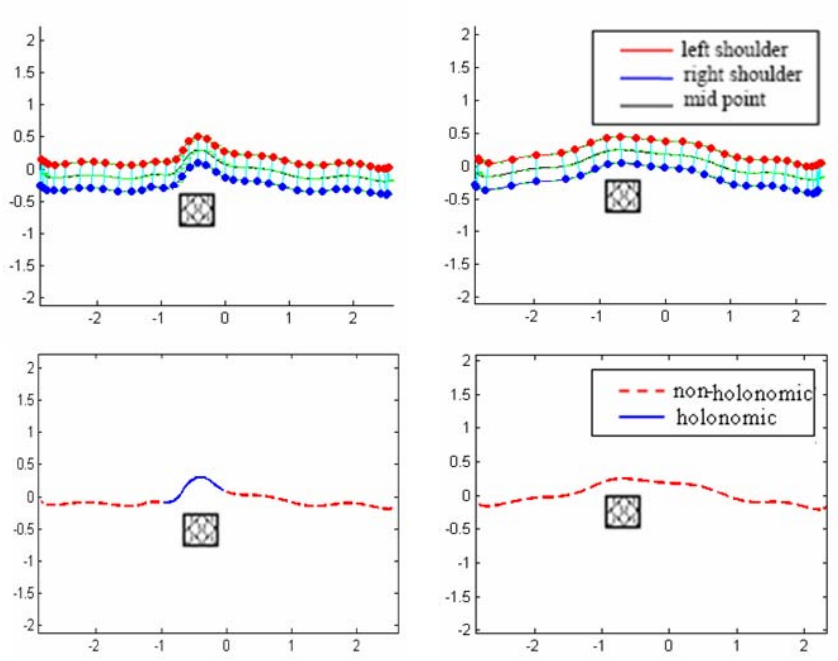

(a) (b)

Figure 4.10: Segmentations of nonholonomic and holonomic behaviors of: (a) a hybrid trajectory including the normal walking and a diagonal step for avoiding an obstacle, (b) a trajectory of normal walking for avoiding an obstacle.

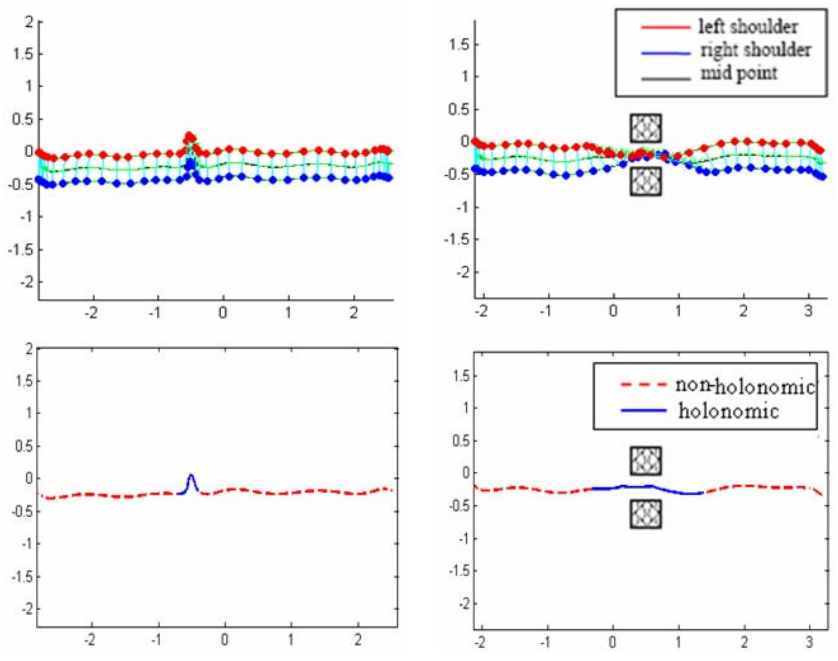

(a) (b)

Figure 4.11: Segmentations of nonholonomic and holonomic behaviors of: (a) a hybrid trajectory including the normal walking and a sideward step, (b) a hybrid trajectory of normal walking and some sideward steps for entering in the middle of two obstacles.

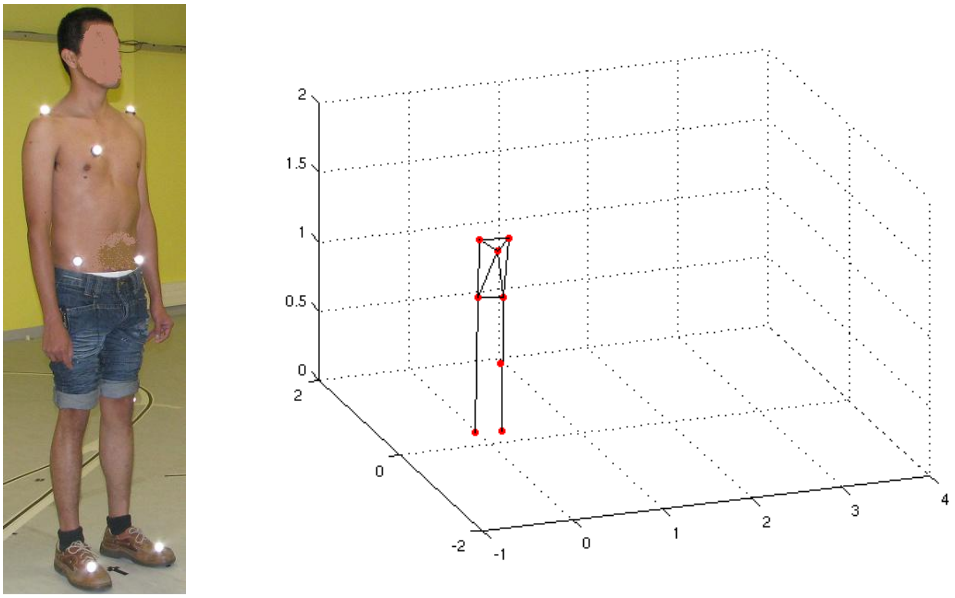

(a) (b)

Figure 4.12: The markers attached on a subject (a) and the makers-linking model simulated on Matlab .

there were six eagle cameras and four hawk ones. Eagle and Hawk cameras use the same high-powered ring lights and have the same limits for marker distances. The difference between the two cameras is that you can use smaller markers with the Eagle cameras.

Coordinates of object's movements are calculated by *triangulation* technique and recorded on the realtime. We guaranteed that at each position in the capture volume, the locomotion of subjects were implied by at least two cameras. The sampling rate used in the experiment was at 100 Hz sampling frequency.

The calibration consists of two processes: static and dynamic. The static calibration used an L-frame attaching 4 markers. These markers were placed in a particular orientation and precise distances apart in order to tell the MotionAnalysis's software (Cortex) the origin and coordinate (XYZ) system of the room. The dynamic calibration used a wand attaching 3 markers. The object of this calibration is to cover the entire capture volume by waving the wand both horizontally and vertically through the cameras field of view. The better the coverage, the better the calibration. The static and dynamic calibrations were done and used for all subjects and trials during the experiment.

4.3.2.2 Marker placement

Subjects were equipped with 8 light reflective markers located on the shoulders, pelvis, and feet for characterizing the human locomotion in the neighboring space (see figure 4.12). We used the midpoint between left and right shoulder markers to determine the body displacement in space. Two markers were located on the pelvis and two others were on the feet (one marker was on each foot), which were placed at the top of the feet to detect the step events. Two markers were located on the thorax and the knee for

Figure 4.13: The arrow used in the experiment. It was placed at the final configuration to reach.

the anti-symmetry of body marker set.

4.3.3 Protocol

Subjects walked from the initial configuration to the different targets. The initial configuration was the same across subjects and trials (indicated on the floor by dark tape, figure 4.15 (a). The targets were indicated by using an arrow placed on the ground at a specific position (x,y) and orientation θ, relative to the initial configuration. Two markers were fixed on the target to get its orientation (see figure 4.13). One hundred and six targets were used in the experiment, which were sampled from a $[-3,3](m) \times [-1,1](m)$ space with orientations as illustrated in figure 4.14. Subjects walked towards for all targets in the sampled space. In total we generated 2120 trajectories, i.e. 10 subjects $\times$ 106 targets $\times$ 2 repetitions.

At the beginning of a trial, subjects stood at standstill while looking directly ahead (see figure 4.15 (b)). They were instructed to align their feet with the tape that indicated the initial configuration. Additionally, they were asked to visually confirm the position of the target before starting to walk. Subjects started walking upon hearing an auditory cue. They were instructed to walk normally and to stop upon reaching the target by facing in its direction (the direction of the arrow). Another auditory cue was played to indicate the end of trial, and subjects walked back to the starting point. The configuration for the next trial was chosen at random and the experimenter moved the target (arrow) to its new position and orientation.

4.3.4 Data processing

All the motion data of 8 markers were recorded by Cortex. For some reasons, a few of raw data appeared gaps (missed data) and noises (when there was a great change of data comparing to their neighbors) in a very short time interval. Thus, we first detected gaps and noises for all raw data. These gaps and noises then were eliminated and the data in the corresponding intervals were interpolated by a spline function. Finally, data were filtered by the anti-alias low-pass digital Butterworth filter in Matlab 7.4.0

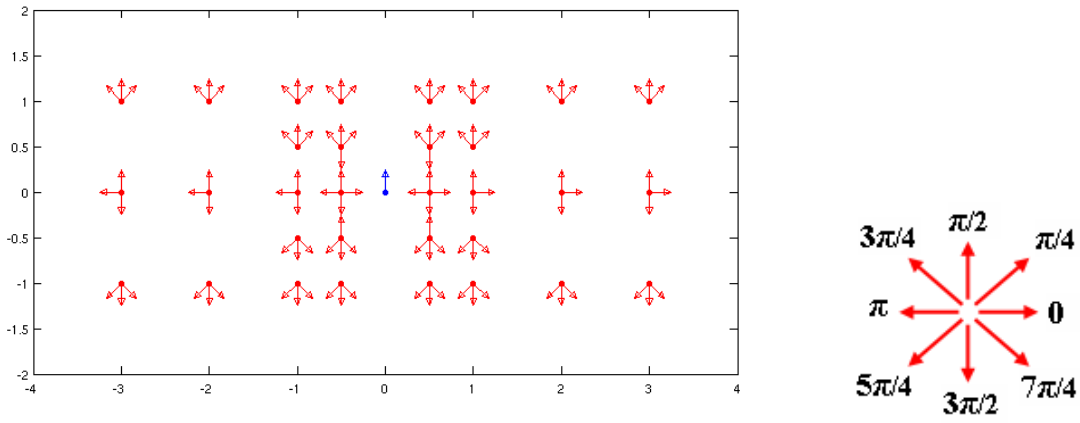

Figure 4.14: The reachable space in the experiment. Subjects always walked from the same initial configuration to randomly selected final ones. The initial configuration was (0,0) of position and $\frac{\pi}{2}$ of orientation (blue arrow). We sampled the room to 32 final positions (16 ones for the left and the right side) in the neighbor of the initial configuration (red arrow). Each final configuration had some investigated orientations, from 0 to $7\pi/4$ (red arrows in the right figure).

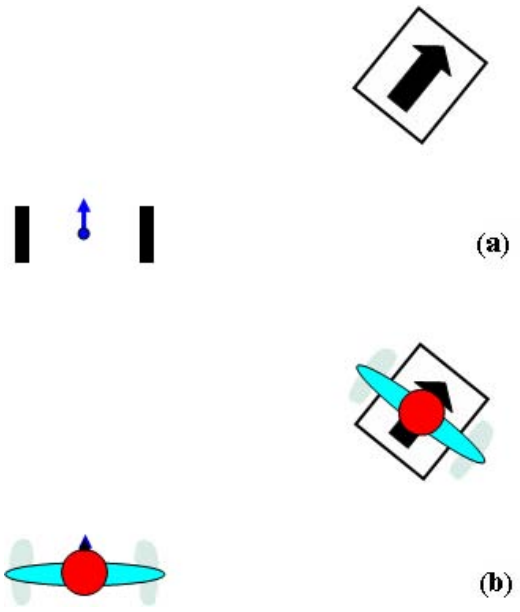

Figure 4.15: Two dark line segments at the initial position and an example of a final configuration determined by the arrow (a). And the upright posture of subjects corresponds to these configurations (b)

with normalized cutoff frequency 0.5 Hz. The shoulder (trunk) frame was used as the body coordinate frame. It means that the position and orientation of body during the locomotion are the position (as in equation (4.4) and equation (4.5)) of the midpoint of the shoulder markers and the direction orthogonal to the shoulder axis (as in equation (4.2) and equation (4.3) respectively).

$$x_{midpoint}(t) \leftarrow \frac{x_R(t)+x_L(t)}{2} \tag{4.4}$$

$$y_{midpoint}(t) \leftarrow \frac{y_R(t)+y_L(t)}{2} \tag{4.5}$$

We computed the linear velocity v such that:

$$\begin{aligned} \dot{x}(t) &\leftarrow \tfrac{x(t+\Delta t)-x(t-\Delta t)}{2\Delta t} \\ \dot{y}(t) &\leftarrow \tfrac{y(t+\Delta t)-y(t-\Delta t)}{2\Delta t} \\ v(t) &\leftarrow \sqrt{\dot{x}^2(t)+\dot{y}^2(t)} \end{aligned} \tag{4.6}$$

4.4 Data analysis: Stereotypy of path geometry

Recorded trajectories were classified into three categories corresponding to relative positions of the goals from the departure point: forward (F), sideward (S) and backward (B) goals. Each of them was also classified into three other categories according to the amount of body turn required: trajectories of low (LC), medium (MC) and high (HC) curvature. So we have totally nine categories such as forward for low curvature (LCF), medium curvature (MCF), high curvature (HCF) and similarly, (LCS), (MCS), (HCS) and (LCB), (MCB), (HCB) for sideward and backward trajectories respectively. In particular LCF, MCF, HCF represent trajectories where the targets were in front of the subjects and the final orientations were $\pi/4$, $\pi/2$, $3\pi/4$ respectively. LCS, MCS, HCS represent trajectories where the targets were on the right/left of the subjects and the final orientations were 0, $\pi/2$, $3\pi/2$ respectively. LCB, MCB, HCB represent trajectories where the targets are behind the subjects and the final orientations were $7\pi/4$, $3\pi/2$, $5\pi/4$ respectively (see figure 4.16).

In order to examine the form of trajectories (in terms of the time and the shape) across subjects and trials for each given target, we calculated the average trajectory and the deviation between the recorded and the average trajectories (see figure 4.17). The mean trajectory $(\bar{x}(t),\bar{y}(t))$ was computed as:

$$\bar{x}(t) = \tfrac{1}{N}\textstyle\sum_{i=1}^{N} x_i(t) \quad and \quad \bar{y}(t) = \tfrac{1}{N}\textstyle\sum_{i=1}^{N} y_i(t) \tag{4.7}$$

where N is the number of recorded trajectories. For a given target we performed the following steps: first the trajectories of all subjects and trials were time-rescaled by using the shortest time trajectory as the reference. After this step, the trajectories have the same final time but they contain different number of points. Then, we used a linear interpolation function to re-sample each trajectory according to the number of points contained in the reference trajectory (shortest time trajectory). After this step, the trajectories are transformed to paths (i.e. they are represented by the same number of points and with the

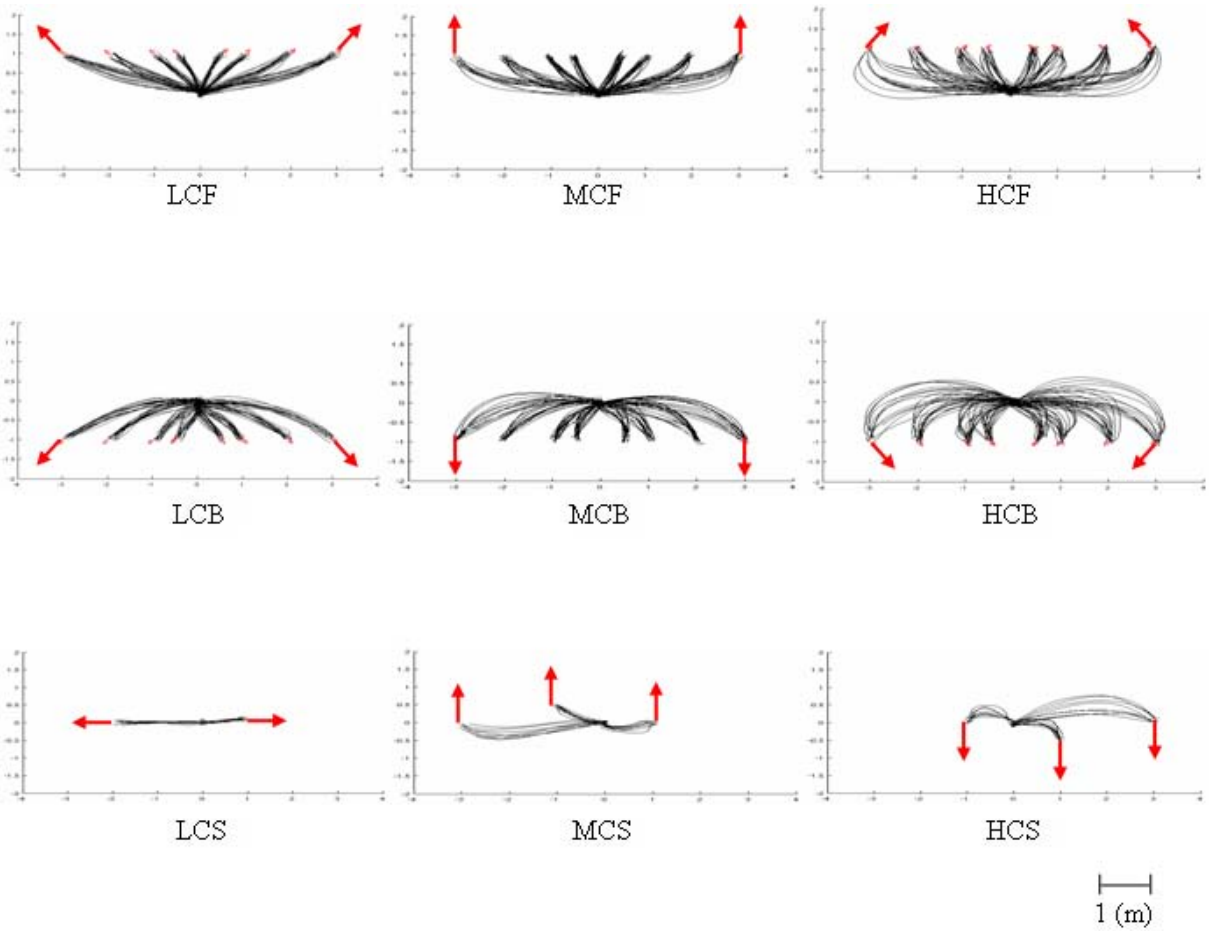

Figure 4.16: Classification of recorded trajectories in terms of curvature induced by the deviation between final orientations and the initial one. The first line is for *LCF*, *MCF*, *HCF*; the second line is for *LCB*, *MCB*, *HCB* and the third line is for *LCS*, *MCS*, *HCS* respectively

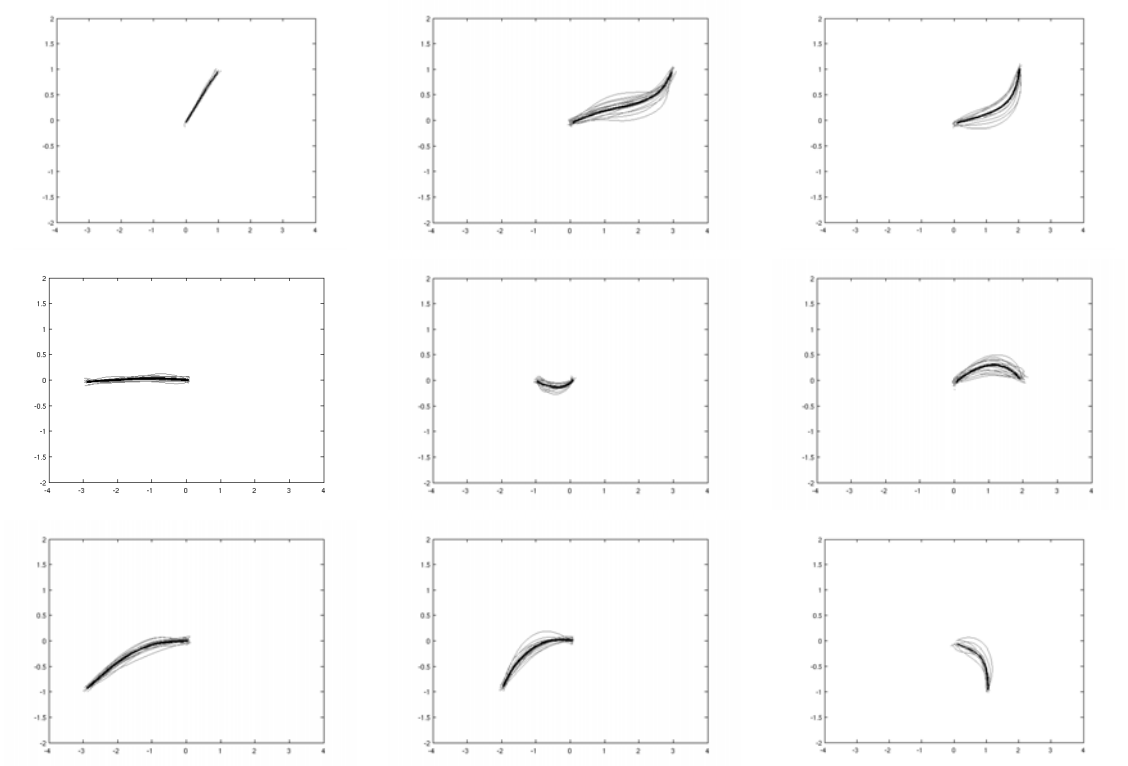

Figure 4.17: The mean trajectory (black) is computed for all targets. The first line is for *LCF*, *MCF*, *HCF*; the second line is for *LCS*, *MCS*, *HCS* and the third line is for *LCB*, *MCB*, *HCB* respectively

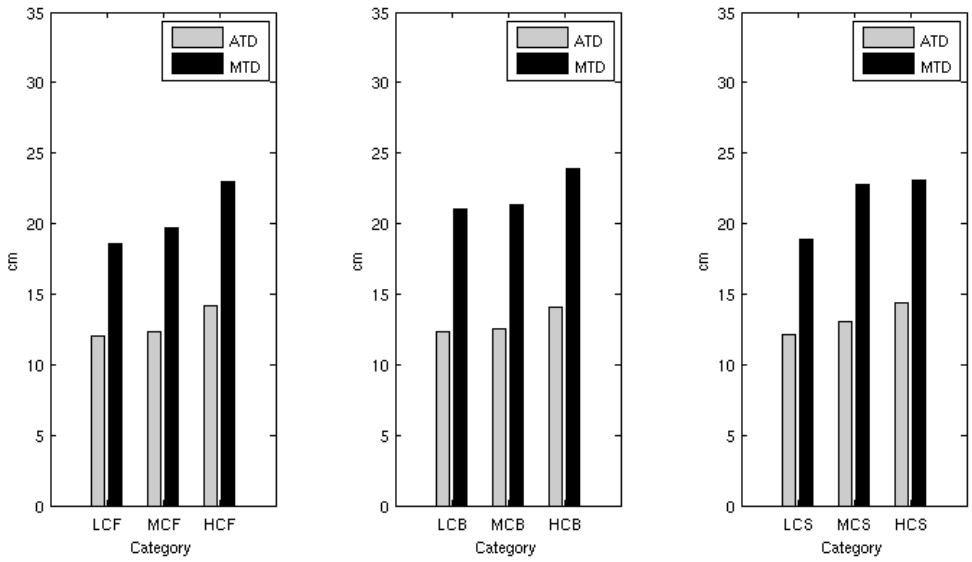

Figure 4.18: Geometric deviations of locomotor trajectories. The comparison between the averaged and maximal trajectory deviations (ATD) and (MTD) for: LCF, MCF, HCF in the left figure, LCB, MCB, HCB in the middle figure and LCS, MCS, HCS in the right figure respectively

same duration). The trajectory deviation TD is defined as the sum of the instantaneous distances between the averaged $(\bar{x}(t),\bar{y}(t))$ and the actual $(x_i(t),y_i(t))$ trajectory:

$$TD(t) = \sqrt{\frac{1}{N}\sum_{i=1}^{N}((x_i(t)-\bar{x}(t))^2+(y_i(t)-\bar{y}(t))^2)} \tag{4.8}$$

The averaged and maximal deviations between the recorded and the mean trajectories are denoted ATD and MTD respectively. This procedure was repeated for all tested targets.

Figure 4.18 illustrates the path geometric stereotyped behavior for each category. We observed that ATD is less than 14 cm while MTD is less than 23 cm for the 212 targets. We also observed that TD grows when the curvature of the trajectory increases.

4.5 Stereotypy of path behavior: holonomic-nonholonomic-holonomic segments

Using the nonholonomic function, we realized that most of the trajectories are composed of three segments, two holonomic behavior segmentations at the beginning and at the end, and one nonholonomic behavior segmentation between them (see figure 4.19 (a)). At the beginning, subjects take a small step to orient towards the target, and at the end, they adapt the final direction with another small step. In the middle interval, they walked normally, such that the nonholonomic property was satisfied.

For higher curvature trajectories, we found a similar result. However, the holonomic behavior segments were longer because subjects have to make a bigger adaptation to approach the goal (see figure 4.19 (e)).

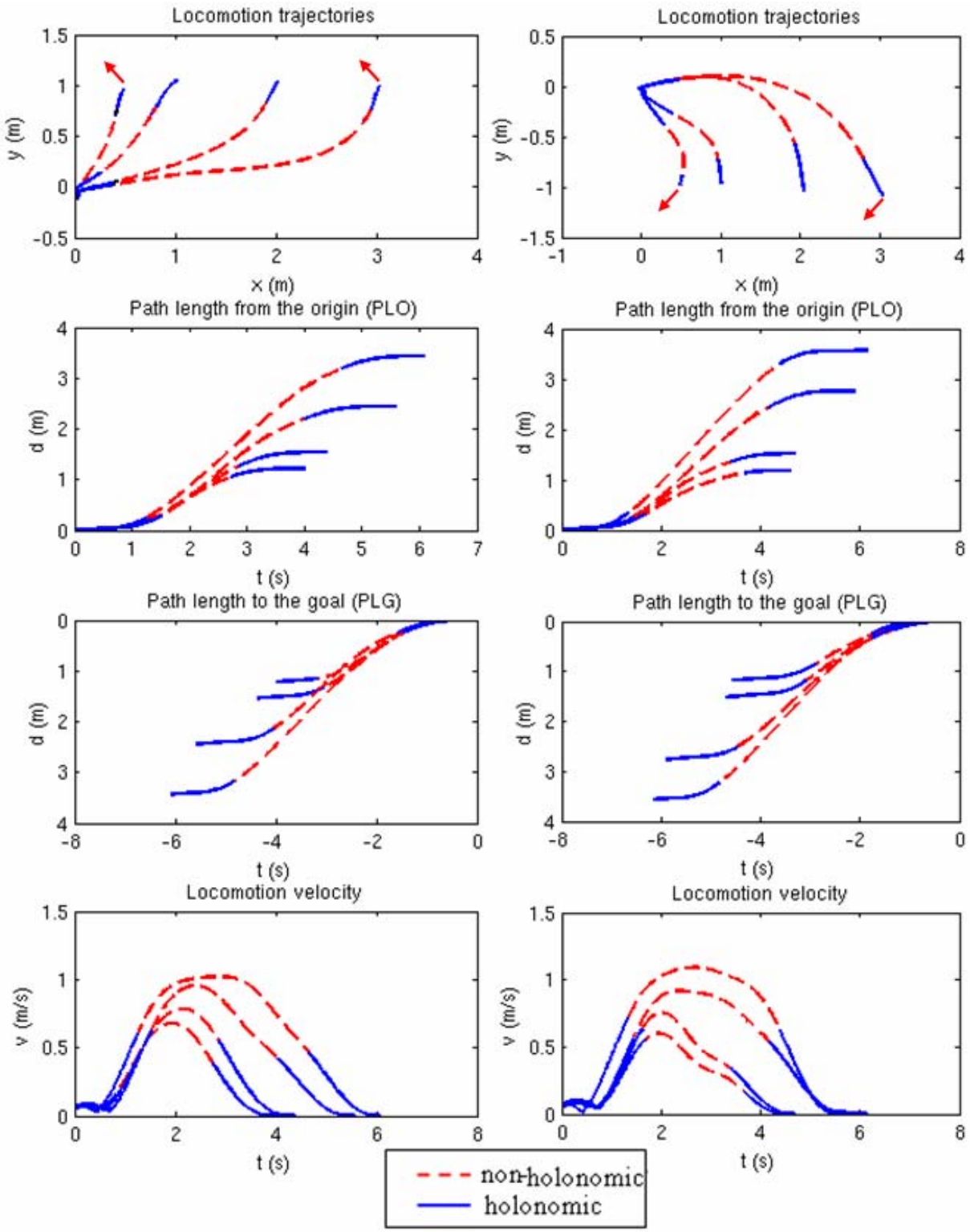

Figure 4.19: Nonholonomic/holonomic parts for trajectories of which final orientations are $\frac{3\pi}{4}$ (for (a), (b), (c), (d)) and $\frac{5\pi}{4}$ (for (e), (f), (g), (h)). (a), (e) Nonholonomic/holonomic segmentations of corresponding trajectories. (b), (f) The dependency of holonomic parts on *PLO*. (c), (g) The dependency of holonomic parts on *PLG*. (d), (h) The dependency of nonholonomic/holonomic parts on the locomotor velocity.

The analysis of free motion trajectories confirms that indeed there is a strong relationship between body orientation and direction for human locomotion. Only very short trajectories are holonomic (e.g. to a target 0.5 m to the right or left), but for longer motions, a nonholonomic phase appears in the middle part while the beginning and end phase are marked by holonomic behavior, i.e. there is a dependency of the behavior on the distance from origin and goal. The analysis also shows that there is a correlation of nonholonomic behavior and stable speeds.

4.5.1 The dependency of holonomic parts on the path length to the origin/goal

In order to investigate the holonomic, nonholonomic behaviors at the beginning and at the end of trajectories, we computed two path lengths (PLO) and (PLG) from equation (4.9). PLO is the path length from the origin to the end of holonomic part at the beginning of trajectories (indicated by instant t_O). PLG is the path length from the beginning of holonomic part at the end of trajectories (indicated by instant t_G) to the goals.

$$\begin{aligned} PLO &= f(t) = \int_0^{t_O} v dt \\ PLG &= g(t) = \int_{t_G}^{T} v dt \end{aligned} \tag{4.9}$$

where T is the total time duration of the corresponding trajectory. As the linear velocity v varies with respect to time, so we used an numerical calculation of the integration:

$$\begin{aligned} PLO &= h_O \left[\tfrac{v_0+v_n}{2} + v_1 + ... + v_{n_0-1} \right] \\ PLG &= h_G \left[\tfrac{v_{N-n_G+1}+v_N}{2} + v_{N-n_G} + ... + v_{N-1} \right] \end{aligned} \tag{4.10}$$

where $h_O = t_O/n_O$, $h_G = (T-t_G)/n_G$, with n_O and n_G are the number of points used to calculate PLO and PLG respectively. N is the number of points corresponding to the time T.

The averaged PLO and PLG (across subjects and trials) for each of the nine categories were also computed. From the observation of path behavior stereotypy, we recognized that PLO across different targets of each category were similar to each other. Similar remark was found in PLG. Figure 4.19 illustrates examples of PLO ((b), (f)) and PLG ((c), (g)) for two categories HCF and HCB respectively. Note that PLG in these figures were shifted with respect to two axes (time and path length) to have the same final instant:

$$PLG = g(t) = f(T) - f(t) = \int_0^T v dt - f(t) \tag{4.11}$$

The averaged PLO ($Mean$), the corresponding average deviation (AD), maximal deviation (MD) between PLO across subjects and trials were calculated in figure 4.20 for each category above. We found that the mean PLO was about 0.3 m that AD is less than 5 cm while MD is less than 15 cm for almost targets. Using ANOVA for the statistical analysis, we found that PLO have no difference across subjects and trials (with all p-values $p > 0.01$).

Similarly, the above indices were calculated for PLG as in figure 4.21. We found that PLG increases relative to the curvature of categories, from 0.2 m for LCF to 0.35 m for HCF.

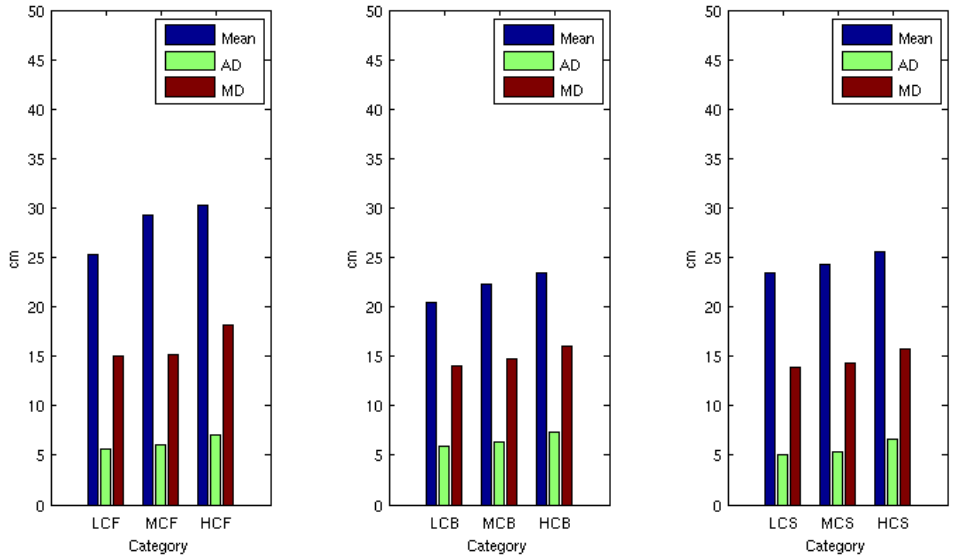

Figure 4.20: The average *PLO* (*Mean*), average deviations (*AD*), maximal deviations (*MD*) across subjects of nine categories of locomotor trajectories

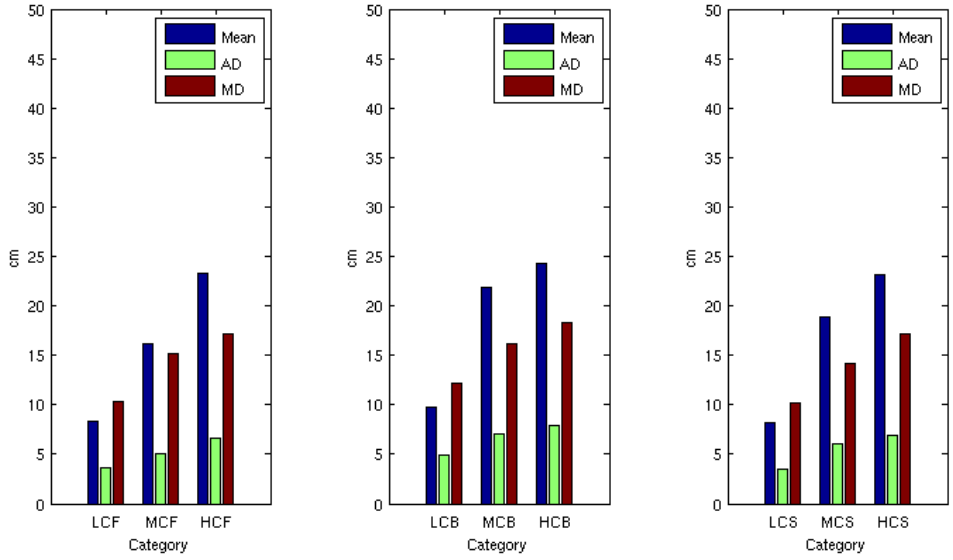

Figure 4.21: The average *PLG* (*Mean*), average deviations (*AD*), maximal deviations (*MD*) across subjects of nine categories of locomotor trajectories.

4.5.2 The dependency of nonholonomic/holonomic parts on the velocity

In previous work [Arechavaleta et al. 2008a], we proposed the nonholonomic behavior for nominal walking at nearly constant velocity. With our protocol, subjects started and stopped with the null velocity. We still observed nonholonomic parts in the middle of trajectories with nearly stable velocity. And there were also the appearance of holonomic parts at the beginning and at the end of these trajectories with the variation of velocity, i.e. the acceleration at the beginning and the deceleration at the end (see figure 4.19 (d), (h) for more detail). At nearly constant velocity (tangential velocity), we tend to do a nonholonomic motion because the movement is essentially caused by tangential velocity. But when there is change of velocity, holonomic motion appears, and it is the consequence of orienting to the target. In a small space in the experiment, at the initial point, subjects performed a hybrid movement of angular, tangential and lateral velocities to adapt the final orientation. Thus, the angular and lateral velocities were considerable and the tangential velocity was then limited. The movement was then a combination of a diagonal step and a rotation step, so holonomic behavior was exhibited. On the contrary, nonholonomic parts depend on the stable tangential velocity without lateral velocity factor.

4.6 The disappearance of the behavior stereotypy in the neighbor of the origin

In cases above, corresponding trajectories are composed mostly part of nonholonomic behavior, and only some small intervals of holonomic behaviors for dynamic adaptation. However, for the nearby target, 50(cm) on the right or the left of the initial point (see figure 4.22 (a)), subjects preferred doing one sideward step for approaching the final configuration. Based on the segmentation function, we found that corresponding movements are completely holonomic. There is then no holonomic-nonholonomic-holonomic segmentation stereotypy.

It seems that in the neighborhood of the origin, subjects just performed one step to reach the goal. And such a step is almost diagonal or sideward step for orienting toward targets (not considering targets we can perform forward steps). Figure 4.23 (a) shows a $0.5(m)$ radius holonomic zone, from experimental data analysis with the help of the segmentation tool. Thus, the distance from the origin to the goal is very important to have an appearance of holonomic motions. However, the deviation of the orientation between initial and final configurations also contributes a significant effect. Figure 4.22 (b) shows trajectories with different final positions in the neighborhood of the origin, because of the disadvantage of the target's orientations, subjects performed few steps (combining diagonal steps and the rotation) to reach the goal. In these cases, the holonomic-nonholonomic-holonomic behavior was still displayed but most part of trajectories was dominated by holonomic behavior. Additionally, figure 4.23 (b) presents the same target with different orientations. With such final configurations, humans can not perform a direct step to reach the goal because of the joint rotation limits of the human body. Thus, a completely holonomic segment can not be displayed.

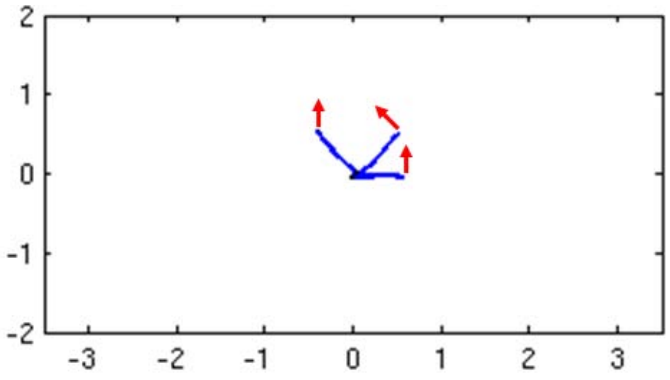

(a)

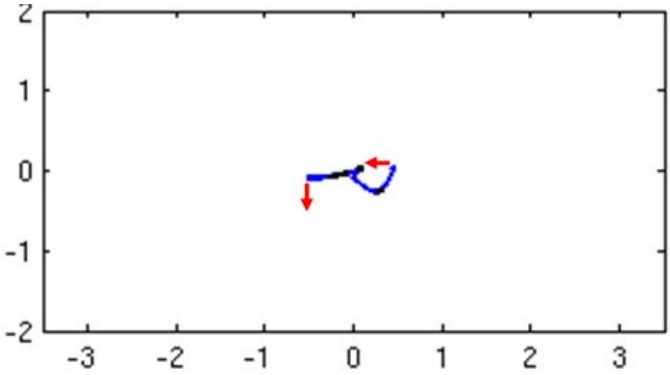

(b)

Figure 4.22: Examples of holonomic behaviors in the neighborhood of the origin. (a) shows one sideward step on the right, and one diagonal step for the targets with different orientations ($\pi/2$, $3\pi/4$ on the left and the right, on red arrows). (b) also shows trajectories with few hybrid steps to reach different targets with orientations π and $3\pi/2$.

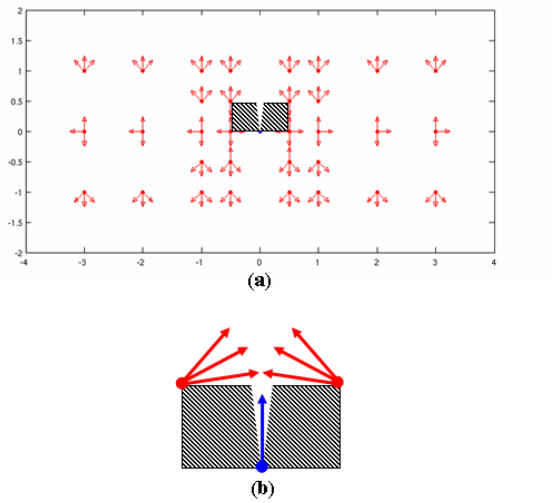

Figure 4.23: (a) The proposed $0.5(m)$ radius holonomic zone, (dark downward diagonal zone) from experimental data observation. The small white zone in the middle of dard zone is the case when subjects walked straight. We didn't consider here the backward walking, so the dark zone is in front of the origin. (b) some examples of the differences between the initial orientation (blue arrow) and final configurations (red arrow). In these case, humans can not perform a direct step toward the target.

4.7 Discussion

4.7.1 Choice of protocol

The aim of this protocol was to study the relationship between body orientation and direction of motion during goal-directed human locomotion in nearby space. In [Arechavaleta et al. 2008a], [Hicheur et al. 2007], authors used the protocol with the "door" to determine the initial configuration and targets, then subjects performed nonholonomic motions. However, in the neighboring space, it is really difficult to apply this protocol because the door prevents lateral movements to reach the target. Thus, the main issue was to find a way for imposing the final orientation so as not to ignore the possibility of nonholonomic and holonomic movements in the neighbor of the origin. We tried to test three proposed protocols such as "Arrow imposed on the ground", "Meeting one person" and "Climbing on a small step-ladder". Finally we chose the protocol: "Arrow imposed on the ground" because it was presented as an appropriate manner to obtain movements without any constraint in the neighboring space (figure 4 (a)).The protocol "Climbing on a small step-ladder" and "Meeting one person" well conducted subjects to the desired configuration but it was not easy to know the exact final position determined by the step-ladder or mannequin position.

With the "door" protocol, we found a stereotypy of nonholonomic behavior for each entire trajectory, and a stereotypy of nearly constant velocity profile. In our case, when replacing the door by an arrow at final configurations, most trajectories are composed of the holonomic-nonholonomic-holonomic segmentation behavior called the path behavior stereotypy. We acquired the belt-shaped velocity profile with the stable speed in the middle of trajectories represented to nonholonomic behavior. Holonomic segments appear to adapt the orientation essentially caused by the lateral velocity. It depends a lot on

the protocol we choose, and actually, when we used an arrow, there were many more possibilities of walking/stepping for subjects.

4.7.2 Feet-guiding locomotion

During nominal walking (including walking straight and turning), the head anticipates the change of entire body direction [Grasso et al. 1996], and it plays a role of guiding the locomotion [Pozzo et al. 1990]. Authors in similar studies also mentioned such a hierarchical control of movement called *top-down* approach.

In [Arechavaleta et al. 2008a], authors chose the shoulders as the most appropriate frame for steering human locomotion in terms of satisfying the nonholonomic motion hypothesis. That study also adapted the *top-down* approach by using the trunk instead of the head for steering locomotion. However, in the neighboring space of our experiment, the movements of two feet were significantly considered. Let's see an example in which subjects did some steps to approach the target (see figure 4.24). The trajectory of shoulders in this example mostly consisted of holonomic behavior caused by diagonal steps. But the trajectories of feet (especially when we observed the trajectory of the left foot from the experiment-recorded video) might express the nonholonomic behavior quite well. It seems that in this case, the feet played the role of guiding the locomotion. Movements of two shoulders were mutually dependent, and shoulders moved dependently between two feet. So at each instant, the combination of movements of shoulders and feet keeps the dynamic stability of human body.

Such feet-guided locomotion in terms of *podokinetics* were proposed in [Mergner et al. 1993], [Gordon et al. 1995] and [Weber et al. 1998]. Podokinetics describes the *bottom-up* sensorimotor control. It means that the rotation of feet guides the rotation of trunk for spatial orientation and control of trajectory curvature during natural locomotion. In the above example, the feet-guiding locomotion represented effectively the nonholonomic property. In this case, the nonholonomic behavior of locomotion relates to the bottom-up approach. Hence, the nonholonomic nature seems to be a combination of the top-down and bottom-up control strategy. Such a combination was studied in [Earhart and Hong 2006] for turning in rotating treadmill.

4.7.3 Similarity of holonomic property and asymmetric footstep

During straight-ahead walking, the symmetry of body movements facilitates segment coordination. During curved walking, many temporal and spatial features of the movement of the inner and outer leg become asymmetric [Courtine and Schieppati 2003a] and [Courtine and Schieppati 2003b]. However, the feet placement is quite symmetric in this case. And that still ensures a nonholonomic behavior for shoulders movements. But in the case footsteps are asymmetric in our experiment, the shoulders movements adapted to maintain equilibrium against the inertial forces that threaten balance. As a consequence, the holonomic behavior occurs. So, in walking along a curved trajectory, the footsteps are asymmetric, then (likely) featuring holonomic capacities.

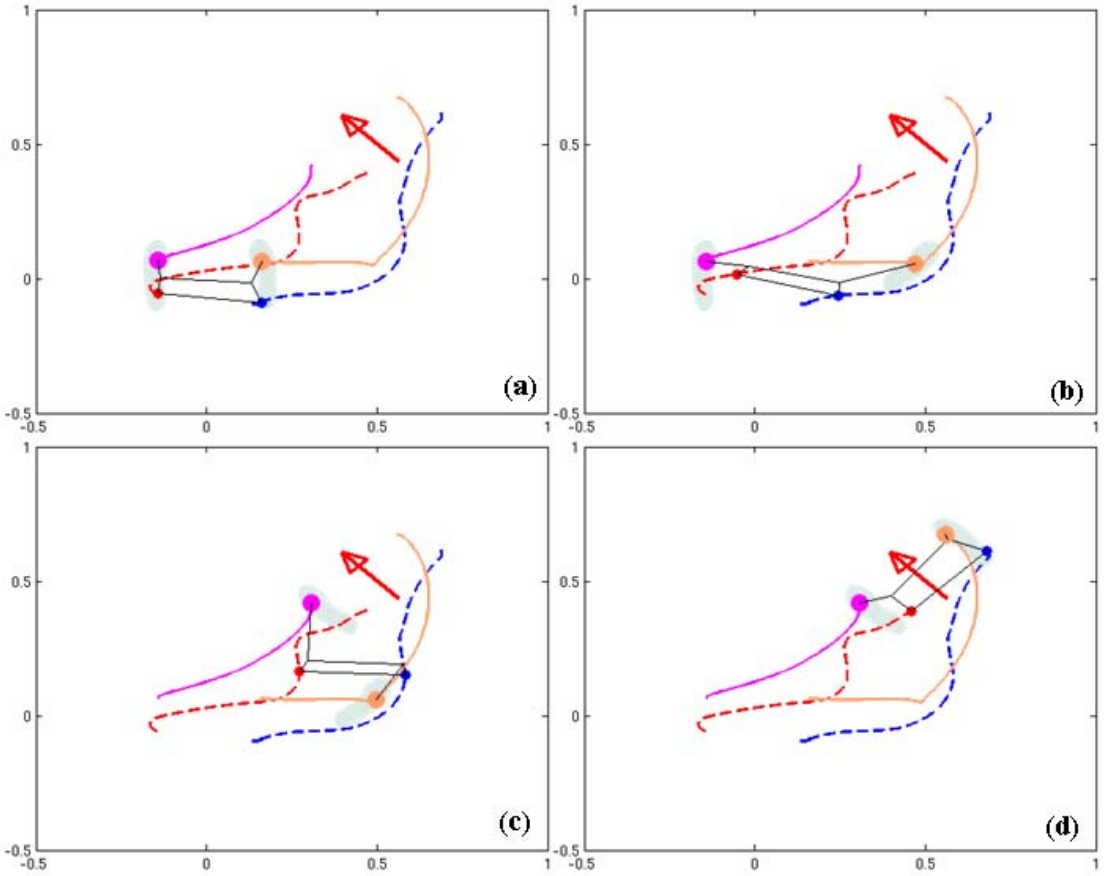

Figure 4.24: Comparison between shoulders and feet movements for a trajectory with final configuration is $3\pi/4$ (left and right shoulder trajectories are in red and blue, left and right foot trajectories are in violet and brown). The left foot (and the right foot for the later part of its trajectory) performs a nonholonomic behavior, and the feet guide the movement, shoulders only follow the feet and keep the stability during moving. Black lines show the projection from the top of shoulders and legs links in cases of: (a) Initial position, (b) Diagonal step to orient toward the target, (c) Normal step at the middle interval and (d) Diagonal step to reach the target.

4.7.4 Stepping level and locomotor trajectory level planning

In [Hicheur et al. 2007], authors found the spatial variability of the foot placements, i.e. the order of foot placement is not the same for all the subjects, or for a subject with different trials. But in neighboring space, only one type of foot placement for each target has been observed from experiments because the number of steps is small and the footprints at the initial configuration is the same for all subjects. Why do humans perform the stereotypy of foot placement for short trajectories (when they just do few steps) instead of for long trajectories? Which control strategy combines the stepping planning level in the nearby space and trajectory planning level in the large space during the human locomotion? In the study of gait initiation planning [Bertucco and Cesari 2009] (inspired from the work in [Klapp 1975]), authors found that pre-planning control was presented for the shortest times while a feedback control was applied during the action ongoing for longer movement times. The result brings to light how a control strategy is selectively coupled and constrained by task parameters: movement time, distance and accuracy. Our locomotion model in the next chapter associates to these characteristics.

4.7.5 A completed human locomotion model

This work refines the study in [Arechavaleta et al. 2008a], on the nonholonomic nature of the human locomotion by showing that dynamic effects at the beginning and at the end of the motion induce holonomic behaviors. Then, the nonholonomic-based model used in [Arechavaleta et al. 2008b] should be modified for both capabilities of holonomic and nonholonomic movements of human trajectories. In a recent study [Mombaur et al. 2008], authors have proposed a model in which we consider the movements of sideward direction and forward direction at the same time. It might be a feasible solution for us because it includes the lateral movements instead of only the nominal direction movement during human locomotion. The continuous transition between holonomic and nonholonomic behaviors will also be considered in our model. In the sections above, the holonomic factor in this model can be deduced from the distance and the orientation difference between initial and final configurations.

5

Inverse optimal control approach to locomotor trajectory modeling

My personal contribution in this chapter is to provide the experimental data for an inverse optimal control approach unifying holonomic and nonholonomic behaviors. This work was essentially done by Mombaur [Mombaur et al. 2010] during the time when she was the invited researcher at LAAS-CNRS.

5.1 Problem statement

In our approach, we consider locomotion as the level of the trajectory of a body's reference point rather than the complexity of the system with many kinematic joints. In the intentional locomotion, which is

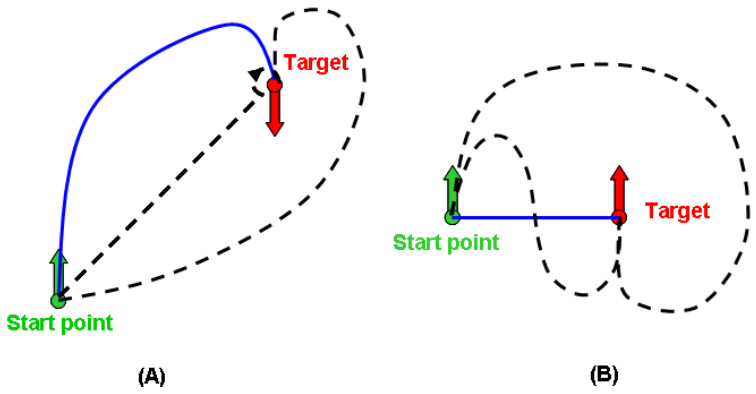

Figure 5.1: Two examples of goal-directed locomotion whose targets are near the start point.

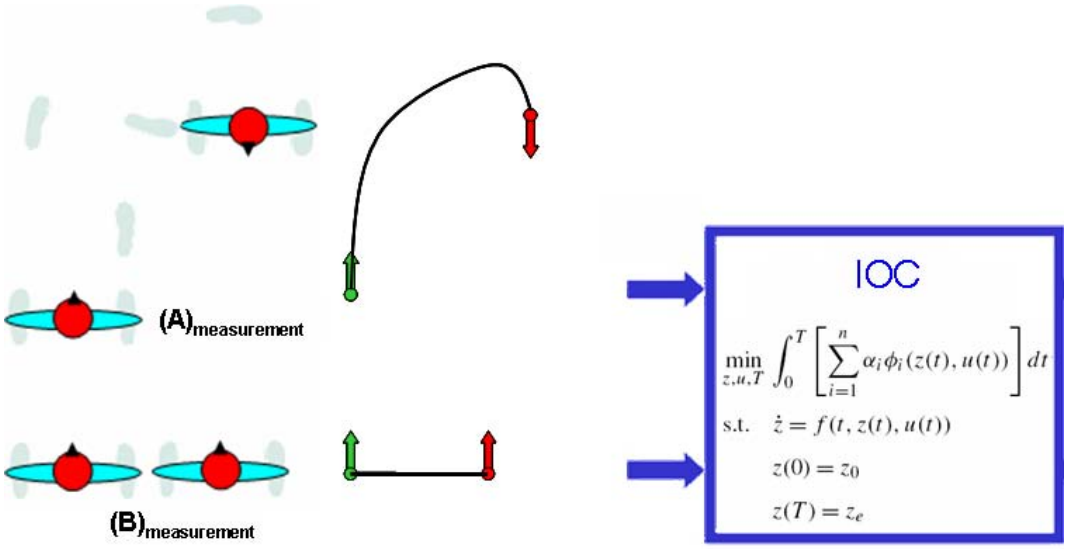

Figure 5.2: An illustration of inverse optimal control approach for two cases in figure 5.1. $A_{measurement}$ and $B_{measurement}$ are the real trajectories for the case A and B respectively.

the shape of the trajectory to go from one configuration to another configuration.

Figure 5.1 shows two typical examples of different targets. Humans can reach these targets by some different ways (including the dash lines and solid lines), by observing the experimental data, we found that they chose the solid trajectories (in both cases (A) and (B)). So, if we consider trajectories of human locomotion are optimal, which is the criteria explaining the shape of them?

We also recognize that the chosen trajectory in (A) represents the nonholonomic behavior while the chosen trajectory in (B) represents the holonomic one. Thus, whether the choice of nonholonomic behavior in (A) is different from the choice of holonomic behavior in (B)? And whether there is a switching factor or just a continuous transition between them?

The goal of this chapter is to propose a mathematical model including both nonholonomic and holonomic modes of locomotion that can explain the shapes of trajectories humans choose. To do that, we present here an inverse optimal control approach: human locomotor trajectories are given from the experiment as optimal trajectories, a set of $(model, costs\ function)$ was formulated to produce the solutions that fit well the experimental locomotion data. And actually, the choice between holonomic and nonholonomic behavior is not accomplished by a switching model.

5.2 Inverse optimal control approach

The objective of this approach is to find a cost function that explain the shape of trajectories. Figure 5.2 shows a demonstration of this approach. We have two trajectories of two cases in figure 5.1 as two optimal solutions. With the model unifying the holonomic and nonholonomic behaviors, we identify a multi-objective function that can give calculated trajectories approximate to measured trajectories.

The inverse optimal control can be solved as a numerical optimization as bi-level problem (see

[Mombaur et al. 2010] for details). In this case, the cost function can be expressed as a sum of multi-attribute functions with corresponding weight. And the problem of determining the "best" objective function thus is transformed into the problem of determining the best weight factors α_i.

We present in the following sections the model and the cost function used in the inverse optimal control solver.

5.3 A model unifying nonholonomic and holonomic behaviors

In this section, we present a dynamic model in the optimal control problem formulation. Recalling that our model is out of scope of the multi-joint dynamics in a locomotor system with many degrees of freedom. We concentrated on the movement of whole body represented by a reference point in the plane. A simple model of equation (3.1) describes such a movement associating to the nonholonomic nature. We adapt here the model proposed in [Mombaur et al. 2010] taking into account the certain situations where the motion becomes holonomic due to the appearance of lateral velocity components v_l:

$$\begin{pmatrix} \dot{x} \\ \dot{y} \\ \dot{\theta} \end{pmatrix} = \begin{pmatrix} \cos\theta \\ \sin\theta \\ 0 \end{pmatrix} v_f + \begin{pmatrix} 0 \\ 0 \\ 1 \end{pmatrix} \omega + \begin{pmatrix} \sin\theta \\ -\cos\theta \\ 0 \end{pmatrix} v_l \tag{5.1}$$

where θ here is the body orientation - the orthogonal of two shoulders (equation (4.3)). In a general case like figure 5.3 there are enough three velocity components. Tangential velocity is calculated by equation

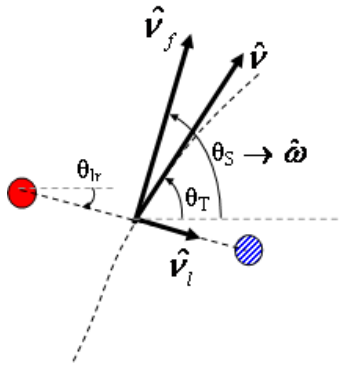

Figure 5.3: Three velocities in a trajectory

(4.6). Angular velocity ω is derived from θ_S:

$$\omega(t) \leftarrow \frac{\varphi(t+\Delta t) - \varphi(t-\Delta t)}{2\Delta t} \tag{5.2}$$

Forward velocity v_f, lateral velocity v_l are calculated with respect to v:

$$v_f = v cos(\theta_S - \theta_T) \tag{5.3}$$

$$v_l = v sin(\theta_S - \theta_T) \tag{5.4}$$

This model is equivalent to the general 3DOF model of a rigid body in a plane with two translations and one rotation. In order to investigate the kinematic characteristics of the locomotion, we used an extension of this model, going down to the acceleration level for all three velocity components:

$$\begin{aligned} \dot{x} &= \cos\theta v_f + \sin\theta v_l \\ \dot{y} &= \sin\theta v_f - \cos\theta v_l \\ \dot{\theta} &= \omega \\ \dot{v}_f &= u_1 \\ \dot{\omega} &= u_2 \\ \dot{v}_l &= u_3 \end{aligned} \tag{5.5}$$

where state variables vector $z^T = (x, y, \theta, v_f, \omega, v_l)$ and control variables u_1, u_2, u_3 denoting the accelerations in forward, angular and lateral direction. The model (5.5) still includes the nonholonomic case for $v_l \equiv 0$, i.e. $u_3 \equiv 0$ and $v_l(0) = 0$. The key property of this model formulation is that it allows transitions from holonomic to nonholonomic behavior and vice versa to happen in a smooth and continuous way, not requiring any discrete switching events.

5.4 Choice of multi-attribute objectives function

The choice of base functions for the multi-objective function was first proposed from the biomechanics knowledge:

- the total time of the path is not defined in advance
  $\rightarrow$ end time T is a free variable;
- humans will generally prefer faster over slower paths
  $\rightarrow$ end time should be minimized
  $\rightarrow$ Thus, we have the first term T of the multi-attribute function and the corresponding coefficient α_0;
- smooth paths are desired, and large variations of velocities should be avoided
  $\rightarrow$ accelerations should be minimized
  $\rightarrow$ Thus, we have three terms u_1, u_2, u_3 of the function and three corresponding coefficients α_1, α_2, α_3;
- the cost of forward and orthogonal components of motions must be computed differently, i.e. the associated weights should be independent;

From the observation of recorded trajectories, we found that:

- humans always adapt their body orientation towards the goal which starts right at the beginning of the motion
  $\rightarrow$ minimize the angle dependent term: the difference between the body orientation and the direction towards the goal
  $\rightarrow$ Thus, we have an another term Ψ of the function and the corresponding coefficients α_4.

The objective function is then:

$$\Phi_i(T,z(t),u(t)) = \alpha_0 T + \alpha_1 \int_0^T u_1^2(t)dt + \alpha_2 \int_0^T u_2^2(t)dt + \alpha_3 \int_0^T u_3^2(t)dt + \alpha_4 \int_0^T \Psi^2(z(t),z_e)dt \quad (5.6)$$

with

$$\Psi(z(t),z_e) = \arctan\left(\frac{y_e - y(t)}{x_e - x(t)}\right) - \theta(t), \; -\pi \leq \Psi(z(t),z_e) \leq \pi \quad (5.7)$$

5.5 Identification of the objectives of human locomotion

This section presents computational results of applying inverse optimal control to identify the objective function to match the human locomotion trajectories described in chapter 4. With the large amount of recorded data, we have made our selections of trajectories for the identification along the following reasoning:

- Since our goal was to establish a model of open-loop human walking based on the average stereotypical behavior, it did not seem reasonable to investigate individual subjects trajectories. So we arbitrarily selected five different subjects, and investigated trajectories of these subjects corresponding to different scenarios (a scenario is characterized by a target position and orientation).
- We first solved inverse optimal control for five subjects per scenario. We did this for a number of different scenarios, and each time identified the best parameters of the objective function. We found that the these parameters in all cases were very similar. That deduces a hypothesis that the optimization criterion actually is the same in all cases.
- Thus, we arbitrarily selected five different scenarios (across five subjects each) and determined the set of objective functions parameters α_i that produced the best overall fit between optimization model and measurements for all five cases. We found that five scenarios are enough to collect the parameters in the cost function. The results of these simultaneous computations are presented in section 5.5.1.
- Finally, we evaluated the performance of the function by testing the model in other scenarios arbitrarily chosen. The results of these tests are shown in section 5.5.2.

5.5.1 Simultaneous inverse optimal control of multiple scenarios

Here we describe the results of inverse optimal control which was simultaneously applied to five different locomotion scenarios. The set of objective function parameters identified by inverse optimal control are

α_0 =1
α_1 =1.2
α_2 =1.7
α_3 =0.7
α_4 =5.2

The objective function that best reproduces measurements therefore becomes

$$\Phi_i(T,z(t),u(t),p) = T + 1.2\int_0^T u_1^2 dt + 1.7\int_0^T u_2^2 dt + 0.7\int_0^T u_3^2 dt + 5.2\int_0^T \Psi^2(z(t),z_e)dt \qquad (5.8)$$

The weight factor corresponding to the orthogonal direction is about 1.5 the weight factor of the forward direction which, in combination with the orientation towards the goal induced by the last term, leads to a clear preference of forward walking, but leaves the possibility for orthogonal motions whenever they are more efficient in this measure. The weight factor of the rotational term is smaller, i.e. large accelerations in rotational direction are less punished, but it is present to balance too large accelerations produced by the last term.

The top left part of figure 5.4 shows the five arbitrarily chosen scenarios. The remainder of the figure shows the results of inverse optimal control for all five cases. The solid line in all sub-figures represents the respective computed optimal trajectory for the identified set of objective function parameters. The five dashed lines denote the measured trajectories of the five subjects used as bases for the computation. The fit in all cases is very good, taking into account that the model equations and optimization functions are always a simplification, and that no perfect fit can be achieved.

5.5.2 Validation of identified cost function

Figure 5.5 shows the fit of the optimal control model established above, applied to two arbitrarily chosen test cases, and the respective measurement data. The targets chosen are (x_e, y_e, θ_e) = (1, 0, 0) and (x_e, y_e, θ_e) = (-1, 1,π/4). The model still represents a good approximation of the data.

5.6 Discussion

We present a simple objective function that has only five componentstotal time, as well as square terms of the accelerations in forward, orthogonal and rotational direction, and a last term minimizing the squared difference between body orientation and direction to the target. It is generally agreed upon that acceleration is an important quantity for human motion if studied from a global perspective, and that sensing of acceleration is with the vestibular organ is crucial for all human movement. In addition to these five terms, authors of [Mombaur et al. 2010] have studied the influence of some objectives frequently discussed in the biomechanical literature such as:

- Velocity and jerk dependent terms: adding velocity terms such as v_f, v_l and ω or jerk terms to objective function 5.8 does not contribute to a better match between experiments and optimal control model, but makes it worse. Inverse optimal control determines the corresponding weight factors to be zero.It then seems that the objective function of overall human locomotion trajectories does not depend on these terms.
- Energy, work or efficiency related terms: Since the kinetic energy of the whole system is proportional to the corresponding squared velocity terms and since there are no contributing factors to the objective function, kinetic energy in that sense cant be either.

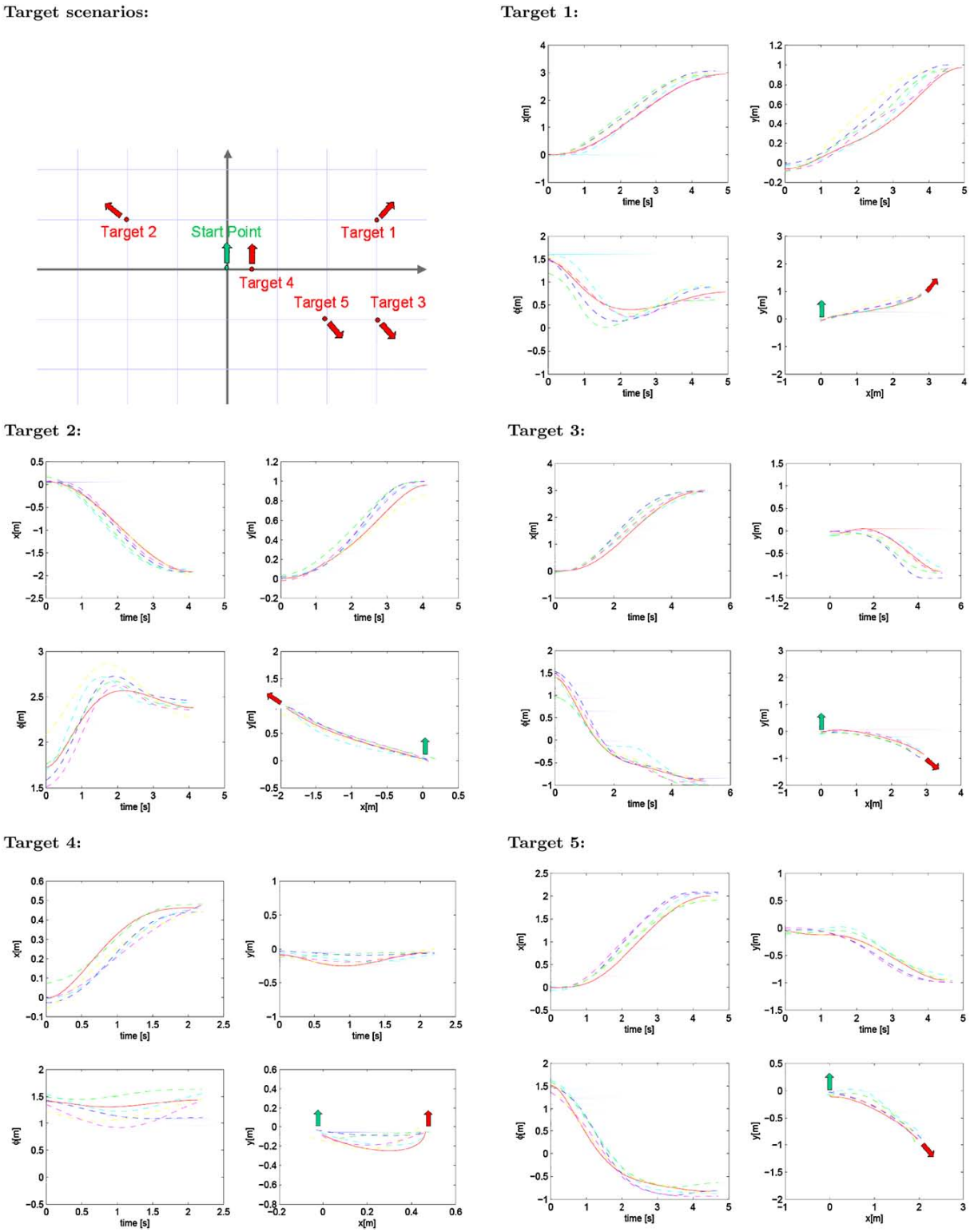

Figure 5.4: Results of inverse optimal control performed simultaneously for five scenarios. The top left sub-figure presents the five arbitrarily selected scenarios. The other sub-figures show the fit between the measurements (5 dashed lines in each case, representing 5 different subjects) with the respective optimal trajectory (solid line) produced by the objective function identified by inverse optimal control

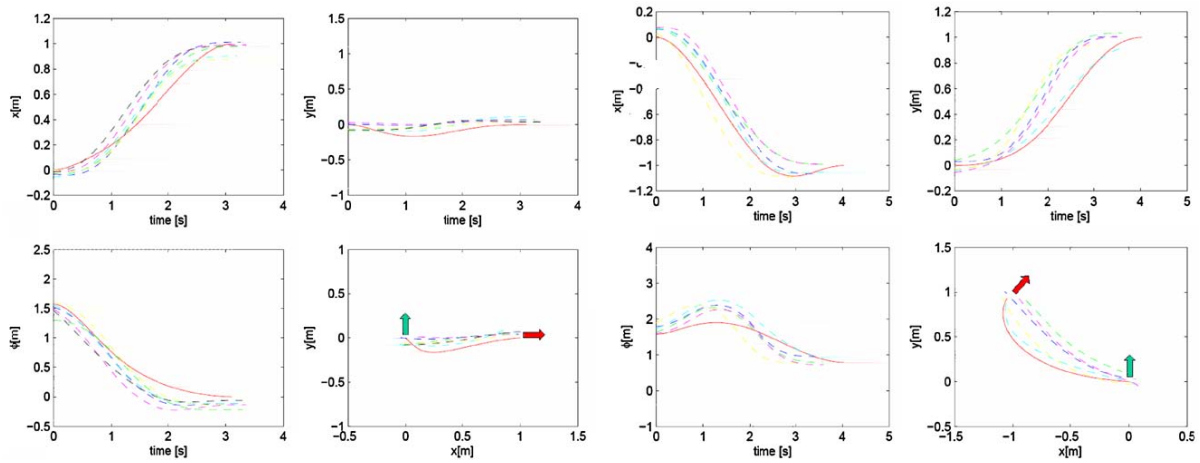

(a) (b)

Figure 5.5: Validation of optimal control model on two test scenarios

Our current work aims at extending the experimental basis of human locomotion as well as the optimal control models to targets that are further away from the origin. We are currently also extending our computational and experimental research on the shape of natural locomotion paths towards the inclusion of obstacles – fixed obstacles as well as moving obstacles, e.g. other persons. A hypothesis to be verified by our current research is that the locomotion trajectories in the presence of obstacles are optimized using the same optimization criterion as in free space, but additionally satisfy obstacle avoidance constraints.

6

Reactive synthesizing of human locomotion combining nonholonomic and holonomic behaviors

6.1 Integrating three velocities into a locomotion controller

This chapter presents a general locomotion synthesis method for digital actors which enables combining nonholonomic and holonomic walk behaviors. Our motion synthesis technique is based on a motion capture blending method. Such a method is able to transform a low-dimensional trajectory describing the global displacement of a digital actor into a high-dimensional motion which involves all the degrees of freedom of the digital actor body. We extend previously existing motion blending techniques [Pettre and Laumond 2006] to reach this goal. More precisely, we consider lateral velocity as a new input of the motion synthesis problem, whereas only tangential and angular were initially considered. Thus, the digital actor locomotion is controlled from 3 inputs in our approach: the tangential velocity, the angular velocity and the lateral velocity. The chapter describes the major steps of our approach. At pre-processing, we analyze some motion captured locomotion cycles to build a Motion Library. The content of the library is projected into the Control Space. Then, at runtime, input (i.e., desired walk velocities) is also projected into the Control Space. We deduce a selection of motion captured locomotion cycles from the library, which are finally interpolated to generate a locomotion animation for digital actors. The newly generated locomotion cycle exhibits the desired input velocities. The locomotion controller enables a human figure to follow predefined paths; the controller can thus be used in the context of locomotion planning for solving high-level goal reaching problems. We show examples of applications in the Results section. We also use the method proposed in [Mombaur et al. 2010] to obtain global trajectories between two desired configurations based on an inverse optimal control approach.

There were some previous studies using the motion blending technique to generate desire motions.

An original interpolation technique was presented in [Unuma et al. 1995] in which Fourier expansions were used to interpolate motion data in the frequency domain. Willey and Hahn [Wiley and Hahn 1997] provided an interpolation technique for synthesizing motions located regularly in the parameter space. Park et al. [Park et al. 2002] exploited this technique to control locomotion in a continuous change of inputs for the retargeting problem. Whereas Kovar et al. [Kovar et al. 2008] constructed motion graph that encapsulated connections among the motion database. The motion graph consisted of original motions and automatically generated transitions. Finally, motion can be generated simply by building walks on the graph. Boulic et al. [Boulic et al. 2004] proposed a *versatile walk engine* producing reactive movements that can change continuously desired speed (e.g. linear and angular speed) or target position at any time, and this walk engine was used for a different biped characters. Our method shares the same objective. But our work fundamentally based on the combination of recorded motion instead of kinematic analysis in [Boulic et al. 2004].

Recently, some authors proposed many interesting controller from the physical-based approach. The motion synthesis is not greatly changed, but they improve locomotion by some optimization techniques. Jain et al. [Jain et al. 2009] viewed the motion as a sequence of solutions to the constrained optimization problem formulated at every time step. Abe et al. [Abe et al. 2007] focused on the multi-objective control with frictional contacts such as foot contact for balancing and pose tracking to maintain the active body motion. Simbicon [Yin et al. 2007] is a locomotion controller which also can animate locomotions for all directions: forward, backwards and sideward. Not like our controller, this one based on few kinematics poses with a robust balance strategy for walking and running. We also concentrate in kinematic parameters to control locomotion, but using the velocities rather than some specific poses.

6.2 Structure of the locomotion controller

Our locomotion controller includes two main processes: Off-line building of the Motion Library and On-line full-body motion synthesis (see figure 6.1 for the global architecture of our method).

Off-line, we construct a Motion library which contains various human locomotions recorded from motion capture system. Motion captures are carefully recorded to satisfy our needs. Locomotion cycles are extracted from motion captures. Average velocities $(tangential,\ angular,\ lateral)$ are extracted for each cycle (respectively denoted as $(\hat{v}, \hat{w}, \hat{v}_l)$). Noting that we used tangential instead of forward velocity because it is more intuitive for users to control directly the (total) velocity of human locomotion than trying to imply forward velocity. The Motion Library building process is presented in section 6.4.

The On-line animation process consists of interpolating cycles from library to synthesize movements with desired instantaneous velocities. This On-line process is composed of two components: Control space and Blending space. Given an input, cycles are selected from the library based on their characteristic average velocities. The Control Space structures the content of the library to enable this selection step: each locomotions cycle is projected as a 3D point into the control space, their coordinates are the average velocities. The resulting points cloud is structured using a 3D Delaunay triangulation. Given input (v_d, w_d, v_{l_d}) is also projected into the control space. At each instant of animation, the input point is contained in a tetrahedron whose four vertices map to four locomotion samples (neighbors).

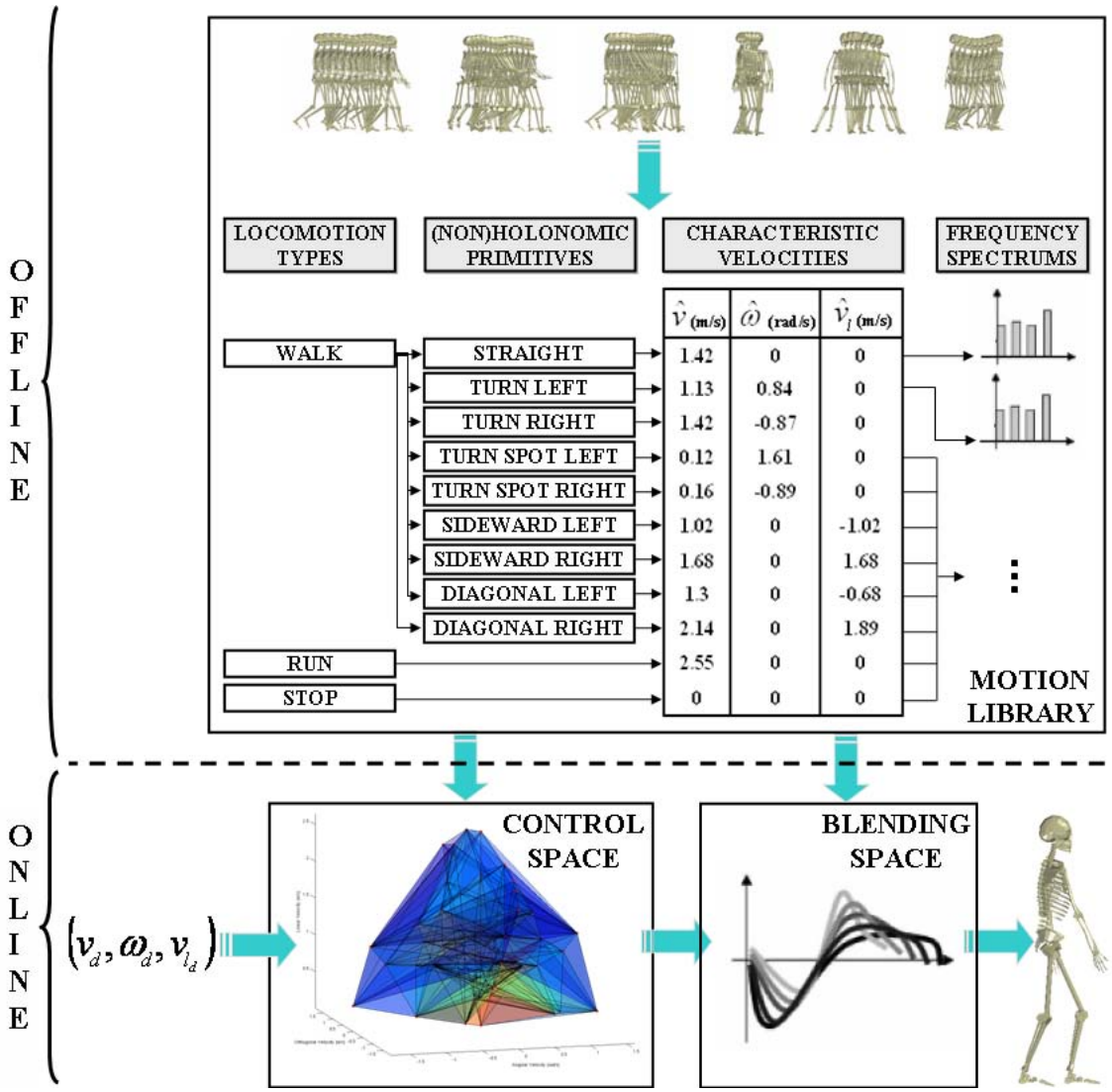

Figure 6.1: Architecture of the locomotion controller.

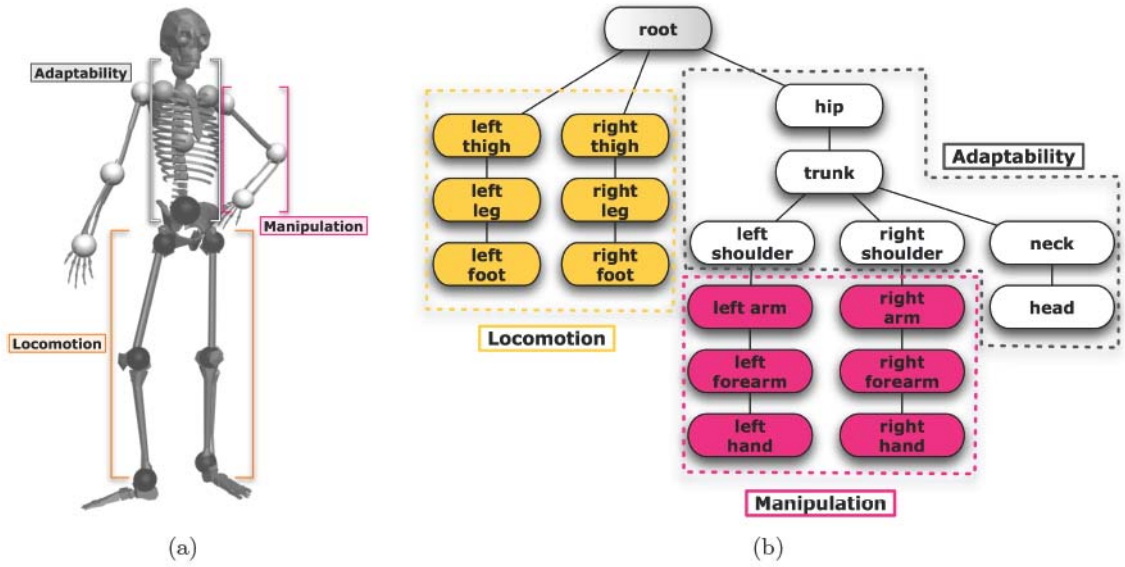

Figure 6.2: (a) Eugene's DOFs are decomposed in three groups: locomotion, manipulation and adaptability. (b) Hierarchical structure of a Eugene. The edges represent the articulated joints and the nodes represent the rigid-bodies that link them. (from [Esteves 2007])

These neighbors are finally interpolated. Angular trajectories of each degree of freedom are expressed as Fourier expansions to enable such an interpolation (Blending space). A new locomotion cycle with desired velocity features is synthesized.

Control space and Blending space are presented in section 6.5 and section 6.6 respectively. Finally, some examples of animated locomotions are showed in the section 6.7.

6.3 Avatar model and interface

Our locomotion controller generated joint angles for whole body movements. We can use a very simple model with links between articulated joints and visualize on Matlab interface. But for more complicated and more human-like animations, we profited the available tools for path planning in KineoKppInterface [Laumond 2006] accompanied with Eugene avatar (see figure 6.2).

6.4 Motion library - Motion capture database

Figure 6.3 showed stages of the Motion library. Main parts of this architecture are presented in following sections.

6.4.1 Human locomotion acquirement

We used the same motion capture system (described in chapter 4) in an area $(4 \times 6(m))$ (figure 6.4). A single subject was equipped with 38 light reflective markers located on his whole body (see appendix A,

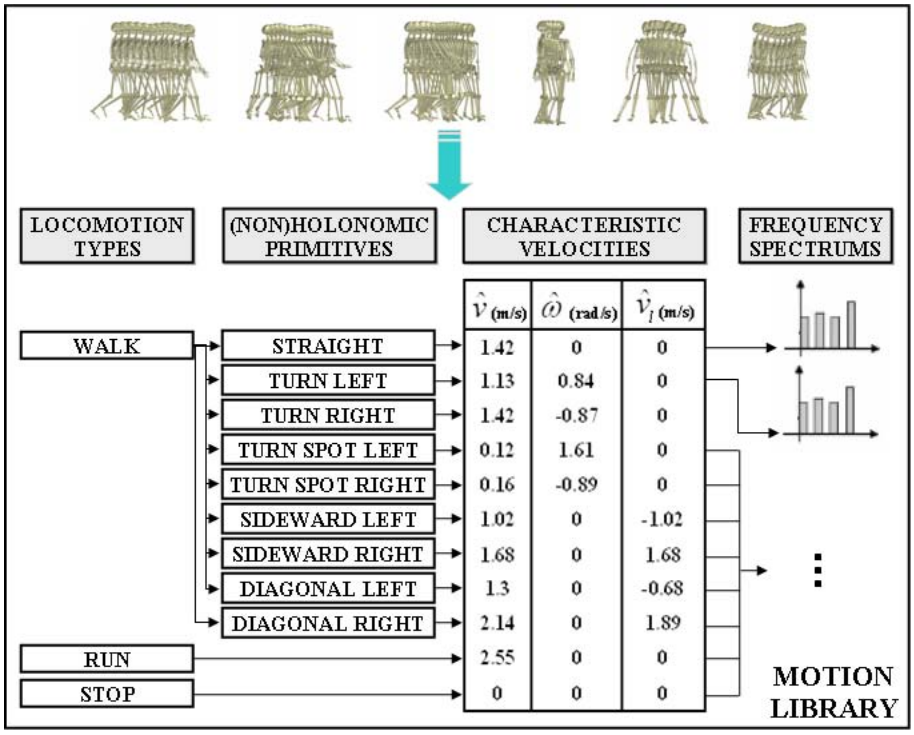

Figure 6.3: Architecture of Motion Library.

figure A.1). These markers were attached on his head, neck, shoulders, spine, pelvis, legs and arms in order to acquire principal joint motions during walking. The subject was asked to perform all trials with a constant speed and in a natural way (like daily human walking).

Our purpose is to collect human locomotions with various velocities. These velocities are inferred from 3 basic locomotions: walk on a straight line, turn on the spot and step sidewards.

The two first types of locomotion represent nonholonomic behaviors, they are actually the forward walking on curved trajectories. We observed that by changing the radius of curvature of the followed path, the three characteristic velocities change either. The radius of curvature for straight walking is infinitive and corresponds to positive tangential velocity, whereas the angular and the lateral ones are null. The radius of curvature for turning on the spot converges to zero and corresponds to positive or negative angular velocity only. Therefore, we sampled nonholonomic locomotions along the radii of curvature from zero to infinitive on the left and the right to obtain the variance of tangential and angular velocities (see figure 6.5 (a)). Some examples of these recorded locomotions are shown in figure 6.6.

The sideward walking is an holonomic type of locomotion. In this case, the tangential direction of trajectories is considered. This means that the variation of the tangential direction causes the variation of other velocities. For example, a diagonal walking and a sideward walking have different velocities. As a result, we sampled holonomic locomotions from zero to π to obtain the variance of lateral and tangential velocities (see figure 6.5 (b)). Some examples of these recorded locomotions are shown in figure 6.7.

For each of above types of locomotion, we recorded with 3 levels of tangential velocity: low, normal and fast. Straight running and rest (stop) postures were also captured for answering the needs of various

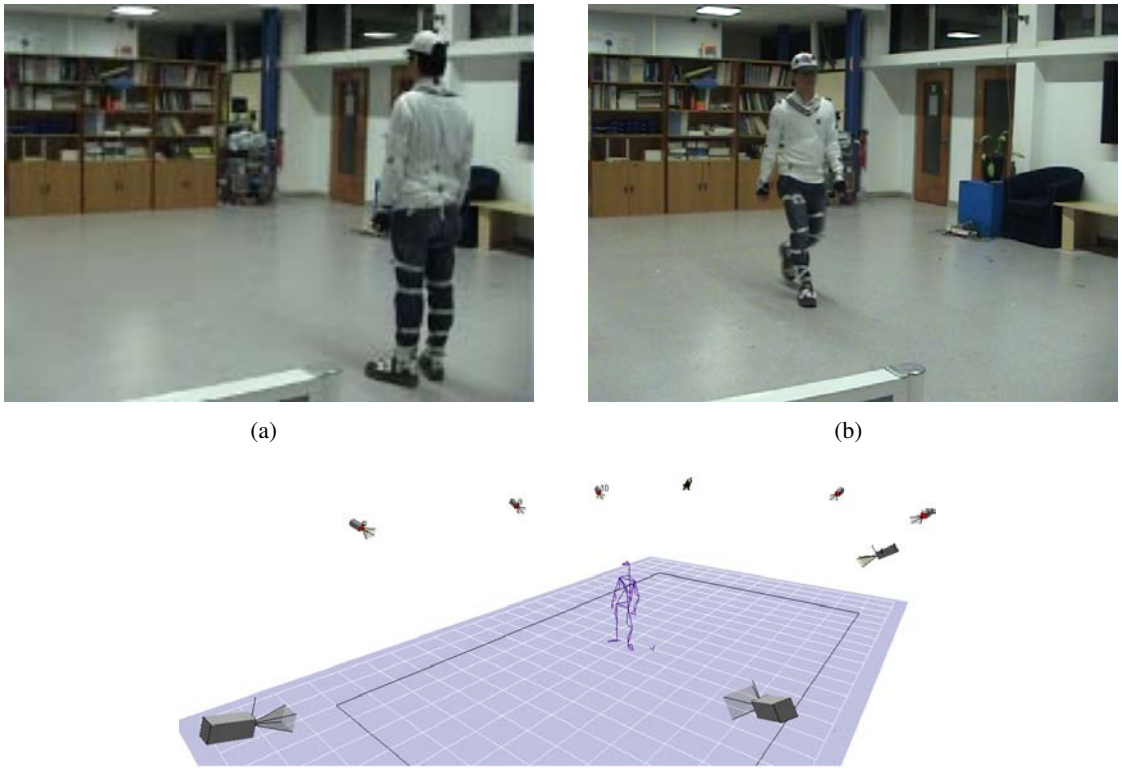

(a) (b)

(c)

Figure 6.4: The subject with markers in motion capture hall using for recording locomotions database (a), (b) and his markers-linked model on the motion capture software Cortex (c).

scenarios. The subject performed 68 captures (68 locomotion primitives) total to compose the Motion library.

6.4.2 Cycles extraction

After having recorded data we extracted one cycle from each entire locomotion sample (see figure 6.8 for an example). In order to interpolate and blend motions from recorded locomotions, all locomotion cycles of the motion library have the same posture (the left toes push off) at starting position (see figures 6.6 and 6.7 for the left push off postures at the beginning).

6.4.3 Average velocities calculation

Three velocities of each capture were calculated in its corresponding trimmed cycle by deriving the trajectory $(x_t, y_t, z_t, \theta_t)$ of the mid-point of two shoulders (see chapter 5 for the calculation).

First, we computed analytically the geometrical pattern corresponding to each locomotion sample in its trimmed cycle. The geometrical pattern is a line segment for locomotions on a straight line (including straight walking and sideward, diagonal steps). And it is an arc of circle for curved locomotions including turning left/right/on the spot. The equation of the corresponding geometrical pattern was computed by

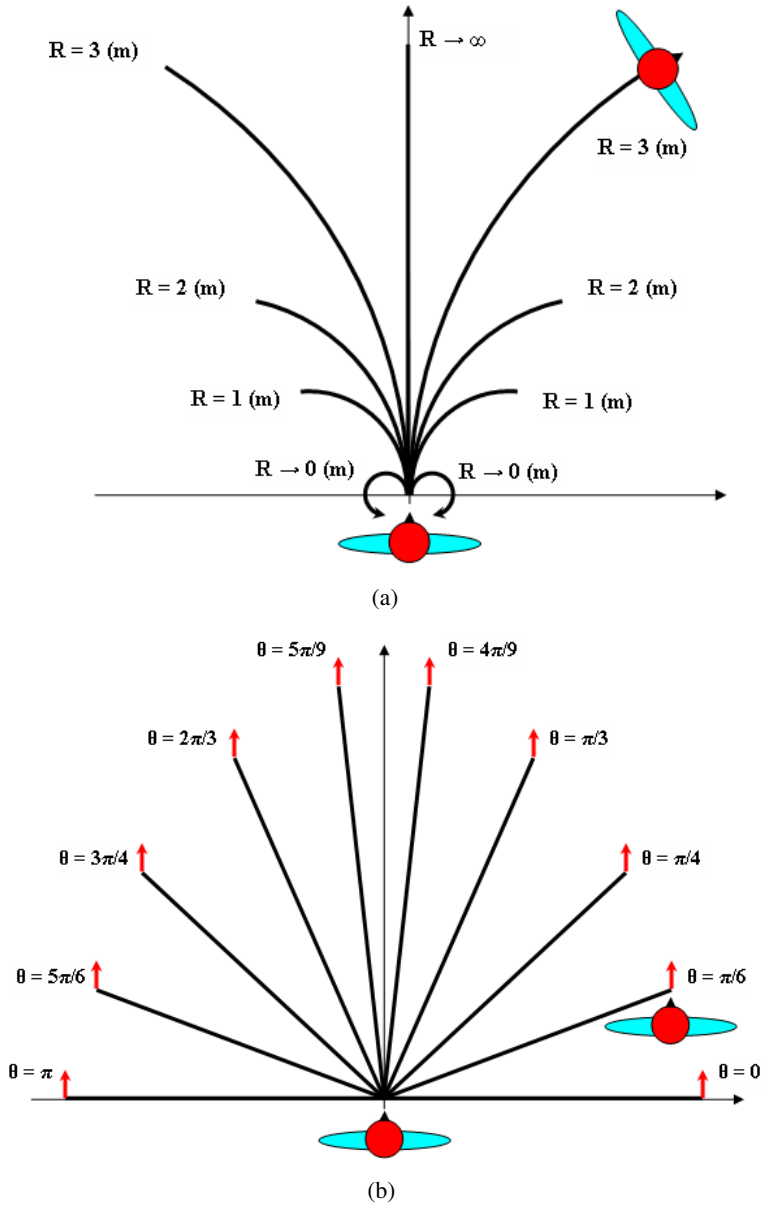

Figure 6.5: The reachable space of locomotions in the library. (a) Nonholonomic locomotions sampled by curves from radius 0 (turn on spot) to radius $1(m)$, $2(m)$, $3(m)$ (turn on the left, right) and infinitive radius (walk on a straight line). (b) Holonomic locomotions sampled by tangent direction θ of trajectory from initial to final configuration. This tangent direction θ represents sideward steps (θ are 0 and π) and diagonal steps (θ are from $\pi/3$ to $5\pi/6$). In these cases, the orthogonal direction of shoulders and tangent direction of corresponding trajectory are very different.

the least square fitting technique. Figure 6.9 illustrates such a process for walking in a straight line (from the first figure to the second one on the top and the third one on the top). The identified trajectory $(\hat{x}_t, \hat{y}_t, \hat{z}_t, \hat{\theta}_t)$ was then used to calculate the average velocity $\hat{v}, \hat{\omega}, \hat{v}_l$ of the corresponding motion sample.

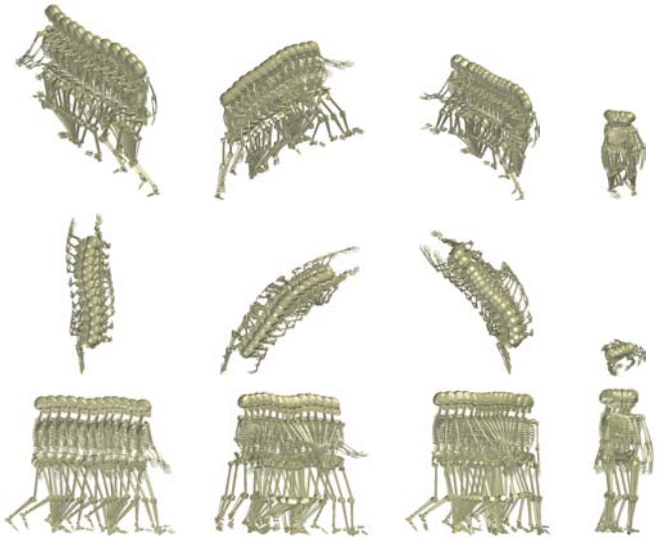

(a) (b) (c) (d)

Figure 6.6: Some nonholonomic locomotions in the library: Walking on a straight line (a), Turning on the right (b), Turning on the left (c) and Turning on the spot (d). Figures from up to down are prospective view, top view and side view respectively.

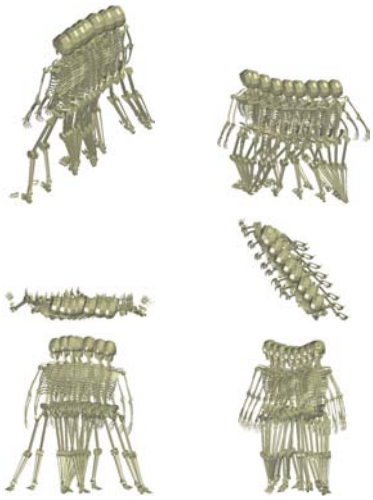

(a) (b)

Figure 6.7: Some nonholonomic locomotions in the library: Sideward step (a), Diagonal step (b). Figures from up to down are prospective view, top view and side view respectively.

6.4.4 Joint angles data of human locomotion

6.4.4.1 Angular joints: from human to avatar

Locomotion is the repetition of periodic motions. We tried to acquire these angular joints by placing 38 markers on whole body. Motion data were recorded as independent markers trajectories (points cloud) using the Cortex software from MotionAnalysis. The cartesian motions of these markers were used to

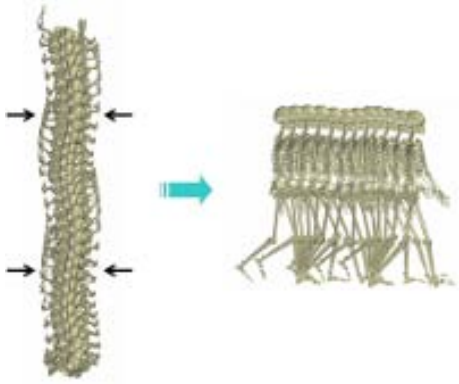

Figure 6.8: A cycle sample from trimming an entire trajectory of walking on a straight line.

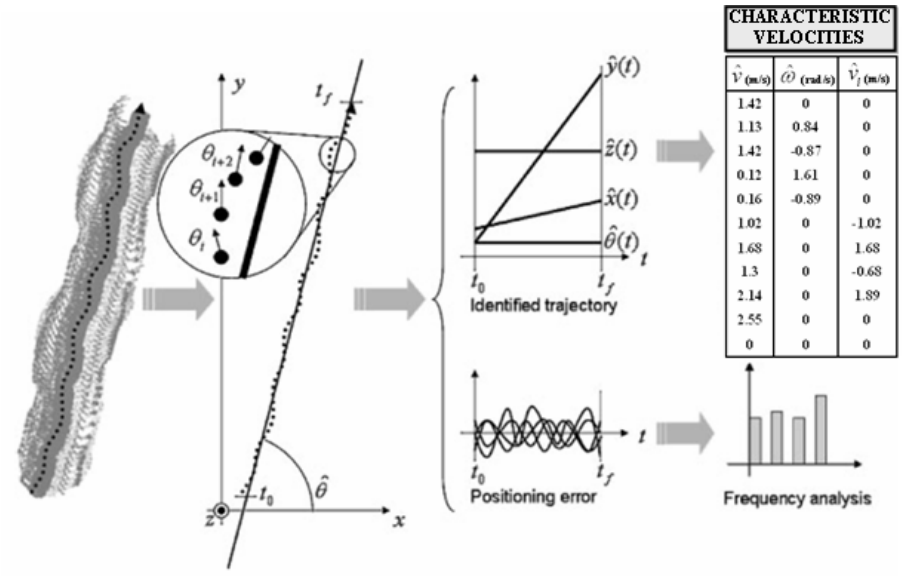

Figure 6.9: An example of motion analysis along a straight line recorded locomotion.

calculate joint angles by using the module Calcium Solver. This application of Cortex uses a Global Optimization method for calculating the best fit of the markers data to the underlying fixed bone skeleton (figure 6.10 (a) to figure 6.10 (b)). All joint angles from this hierarchical kinematics model were then transferred into the avatar Eugene (figure 6.10 (c)) of Kineo Path Planner Interface (from Kineo CAM). See appendix A, figure A.2 for more details of this process.

6.4.4.2 Expression of joint angles data in the frequency domain

Because the motions of most degrees of freedom (head, neck, spine, arms, legs) are periodic and smooth, they are encoded in the frequency domain using a Discrete Fourier Transform. We computed the coefficient pair (α_i, β_i) corresponding to real and imaginary parts of Fourier series expansions. A motion of a degree of freedom is written as:

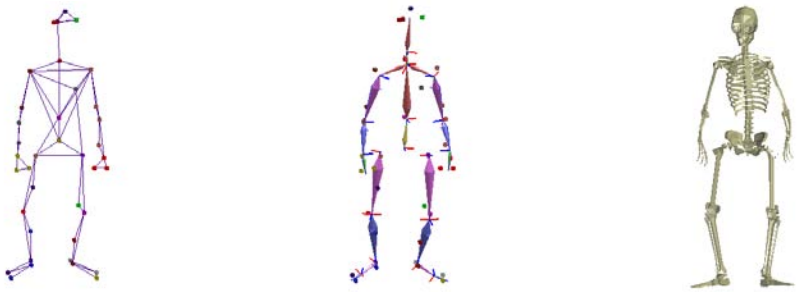

(a) (b) (c)

Figure 6.10: The transfer from the subject to the avatar. He was equipped with 38 markers on whole body. Calcium Solver was used to calculate calcium model (b) from markers cloud model (a). All joint angles of this model were transferred into Eugene model (c) by a parser. See figure A.2 for more details.

$$m(t) = \frac{1}{2}\alpha_0 + \sum_{k=1}^{N} \alpha_k \cos\left(\frac{k\pi t}{T}\right) + \beta_k \sin\left(\frac{k\pi t}{T}\right) \tag{6.1}$$

where N is the number of samples of transform and T is the trimmed cycle of capture. Un like other internal degrees of freedom, the position and orientation of the root (almost) are not periodic. However, due to the oscillations around the followed trajectory, we also extracted the periodic component of the root trajectory. The second and the third figures on the bottom of figure 6.9 illustrate such a process. The *positioning error* was the deviation between computed geometrical pattern $(\hat{x}_t, \hat{y}_t, \hat{z}_t, \hat{\theta}_t)$ and the position of the root $(x_t, y_t, z_t, \theta_t)$ at each instant t.

6.5 3D Control space

6.5.1 Filling the control space

This control space is based on 3 components: tangential, angular and lateral velocities. Each point in this control space is a set of (v, ω, v_l) calculated in the Motion library stage. The space was filled by motion samples stored in motion library. With 68 locomotions recorded, we had a data set of 68 points $(\hat{v}, \hat{\omega}, \hat{v}_l)$. Figure 6.11 shows three basic locomotions corresponding to three points in the space. They are: (1) walking on straight line with constant tangential velocity, (2) turning on the spot with constant angular velocity, and (3) stepping sideward with constant lateral and tangential velocities.

6.5.2 Selecting locomotion samples

Once an input is given in form of a set (v_d, ω_d, v_{l_d}), we have to find motions (neighbors) in library whose characteristic velocities are nearest to it. To do that, data points in the control space have to be structured into a 3D Delaunay triangulation. Figure 6.12 shows a tetrahedron in 3D Delaunay triangulation data structure composed of velocity points cloud in motion library. The input point is found in some tetrahedron. Four vertices of the found tetrahedron represent four locomotion samples used to

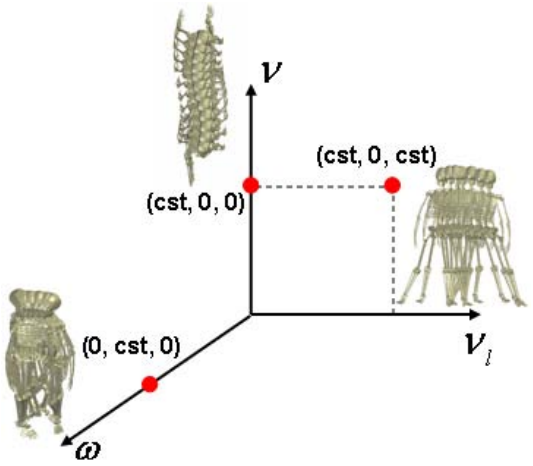

Figure 6.11: 3D control space with three axis corresponding to three velocities. Three red points represent three basic locomotions. Their velocities set $(\hat{v}, \hat{\omega}, \hat{v}_l)$ are respectively $(cst, 0, 0)$, $(0, cst, 0)$ and $(cst, 0, cst)$.

synthesize the desired locomotion (see figure 6.13 for an illustration). By using CGAL (Computational Geometry Algorithms Library) [www.cgal.org 2008], we can always find a tetrahedron containing the input point. The input point has to be in the envelope of the tetrahedra data structure.

6.5.3 Finding weights for selected samples tetrahedron

Four locomotion samples of the found tetrahedron are used to calculate weights to be blended. Among these samples, the sample which velocities characteristics is nearest to (v_d, ω_d, v_{l_d}) has the greatest influence (weights) on the result and vice versa. Weights are calculated by solving below equation system (as an interpolation in Finite Element Method [Bathe 1982]):

$$\begin{cases} a\hat{v}_1 & +b\hat{v}_2 & +c\hat{v}_3 & +d\hat{v}_4 & = & v_d \\ a\hat{\omega}_1 & +b\hat{\omega}_2 & +c\hat{\omega}_3 & +d\hat{\omega}_4 & = & \omega_d \\ a\hat{v}_{l_1} & +b\hat{v}_{l_2} & +c\hat{v}_{l_3} & +d\hat{v}_{l_4} & = & v_{l_d} \\ a & +b & +c & +d & = & 1 \end{cases} \tag{6.2}$$

where $(\hat{v}_1, \hat{\omega}_1, \hat{v}_{l_1})$, $(\hat{v}_2, \hat{\omega}_2, \hat{v}_{l_2})$, $(\hat{v}_3, \hat{\omega}_3, \hat{v}_{l_3})$, $(\hat{v}_4, \hat{\omega}_4, \hat{v}_{l_4})$ is respectively the tangential, angular and lateral velocities set of four selected locomotions (four vertices of found tetrahedron as in figure 6.13). Weights (a, b, c, d) for these four samples are always in $[0, 1]$ because input points are in the envelop of the 3D triangulation data structure. When an input is outside of the envelop, users should change the velocities directive.

6.6 Motion blending

This stage consists of synthesizing a new locomotion from the found weights (a, b, c, d) in the previous stage (see figure 6.14 for the process of the Motion blending).

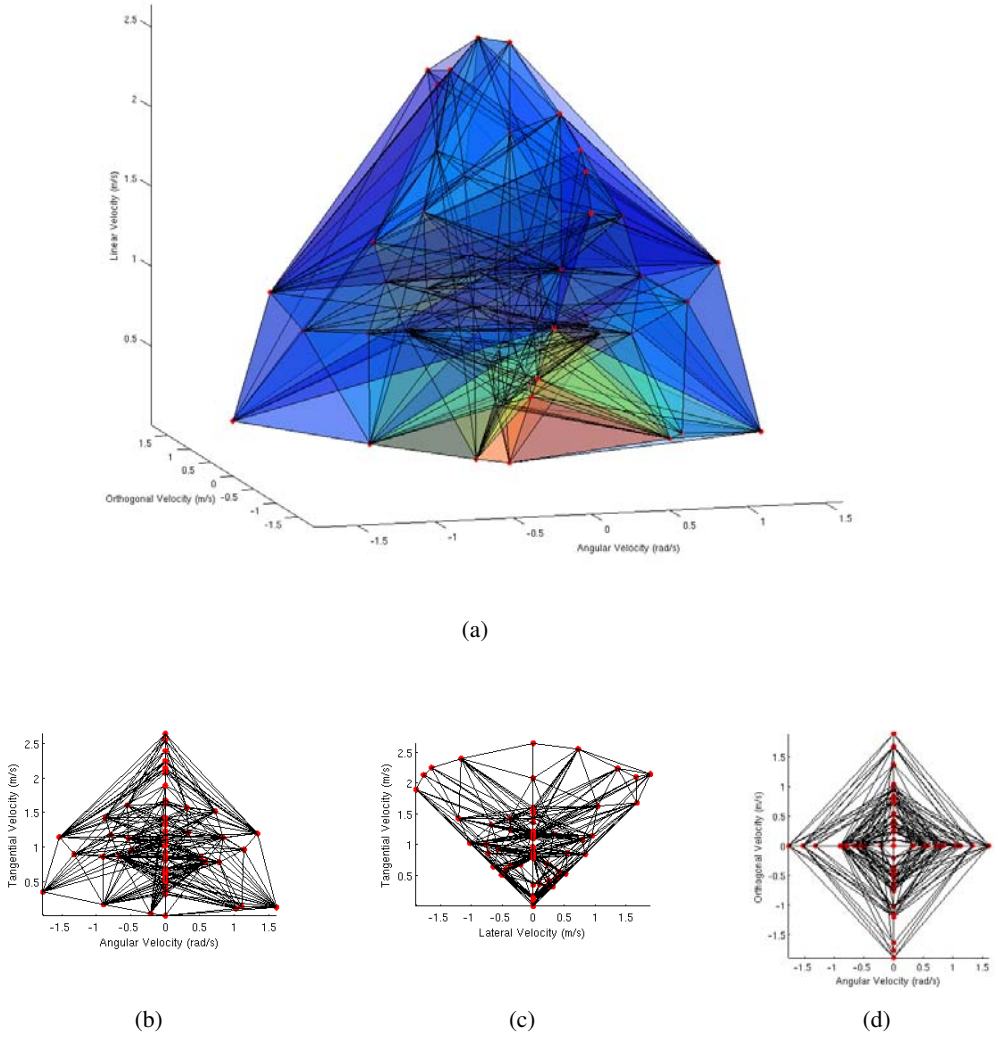

(a)

(b) (c) (d)

Figure 6.12: The control space in from perspective view (a) and its projection into (ω, v) plan (b), (v_l, v) plan (c) and (ω, v_l) plan (d). Red points are vertices of tetrahedra structured by 3D Delaunay triangulation.

We first interpolate the Fourier expansions of the locomotions corresponding to the four vertices of the tetrahedron:

$$\begin{cases} \alpha_i^d = a\alpha_i^1 + b\alpha_i^2 + c\alpha_i^3 + d\alpha_i^4 \\ \beta_i^d = a\beta_i^1 + b\beta_i^2 + c\beta_i^3 + d\beta_i^4 \end{cases} \tag{6.3}$$

where (α_i^d, β_i^d) and (α_i^j, β_i^j) are coefficients pair of joint angles of the desired locomotion and locomotion sample j respectively $(i = 0..N)$. Then (α_i^1, β_i^1), (α_i^2, β_i^2), (α_i^3, β_i^3), (α_i^4, β_i^4) are respectively coefficients pairs of four found samples. These four samples have different cycles, so a new cycle is interpolated as

$$T_d = aT_1 + bT_2 + cT_3 + dT_4$$

Angular trajectories of all degrees of freedom of the animated locomotion will be synthesized in time

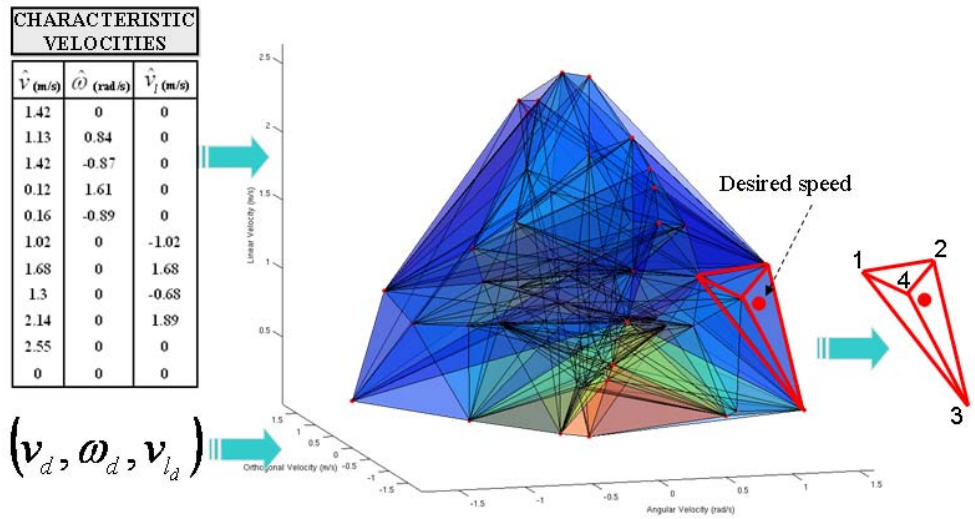

Figure 6.13: Tetrahedron selection process from an input (desired speed). The red tetrahedron is selected from the tetrahedra data structure in the control space.

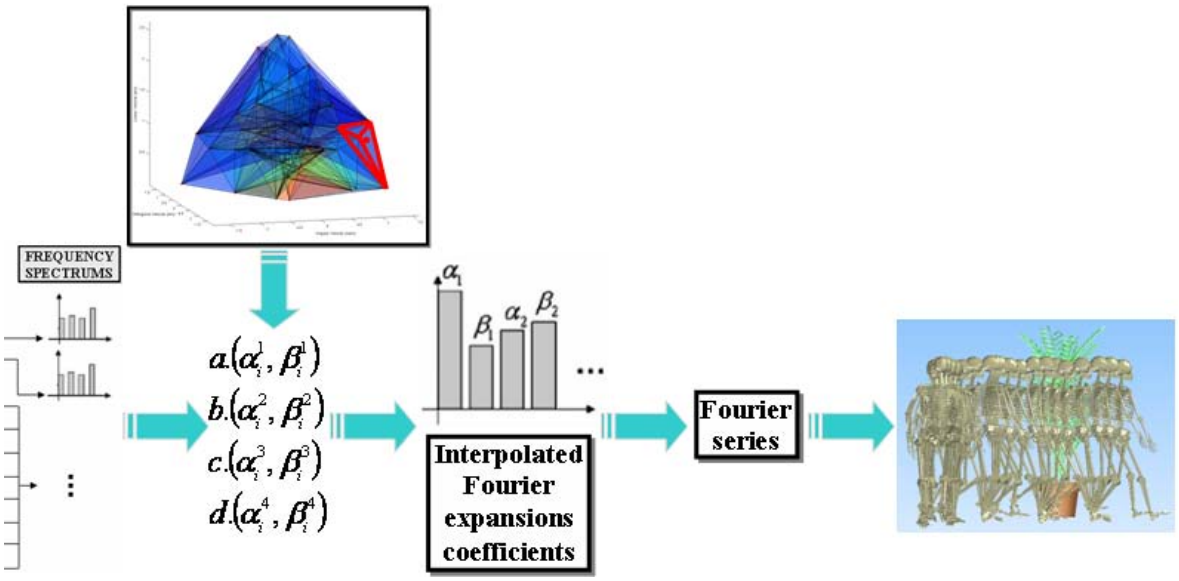

Figure 6.14: Stages of the Motion blending.

domain by Inverse Fourier Transform:

$$m_d(t) = \frac{1}{2}\alpha_0^d + \sum_{k=1}^{N} \alpha_k^d \cos\left(\frac{k\pi t}{T_d}\right) + \beta_k^d \sin\left(\frac{k\pi t}{T_d}\right) \tag{6.4}$$

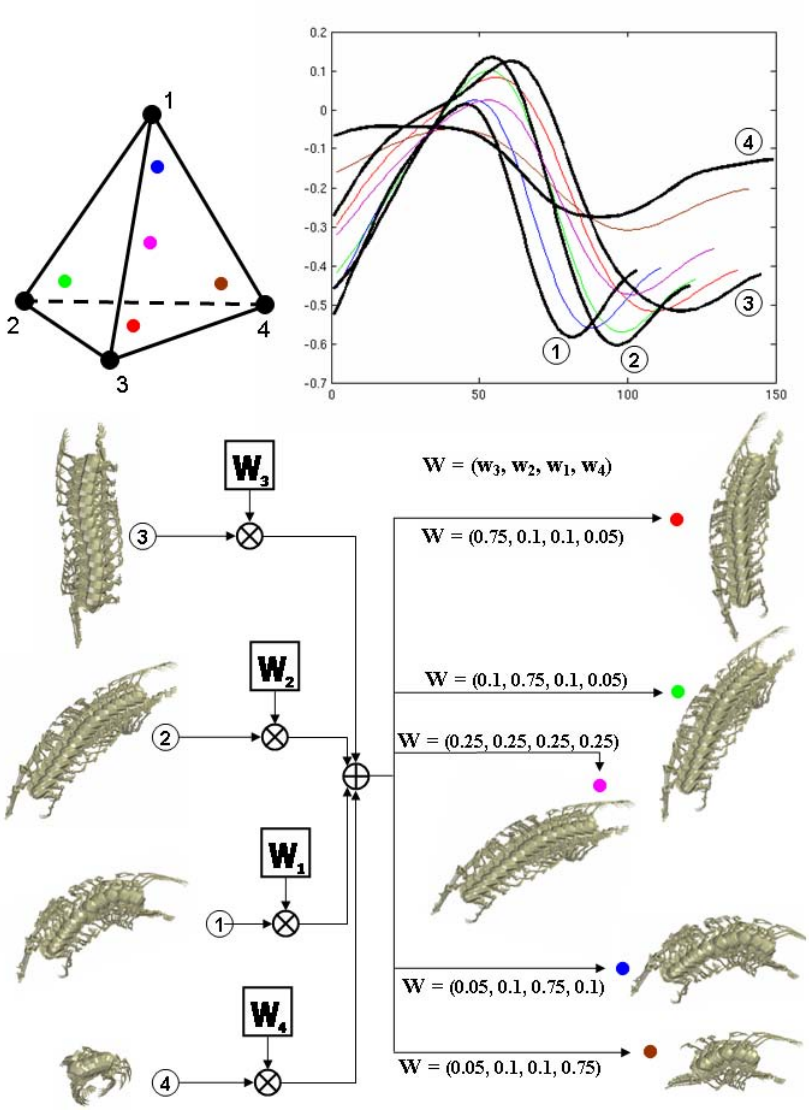

Figure 6.15: Interpolation of four animations. These trajectories are those of right upper leg

6.6.1 Interpolation of periodic signals

Most of joint angles are periodic, they are then blended together to produce other motions. Figure 6.15 presents an interpolation of four animations. The right upper leg joint signals of these four animations are in the sinusoidal form with different cycles. These signals were blended through a weight set $W = (w_1, w_2, w_3, w_4)$ to interpolate five new motions. These motions (five sinusoidal signals different colors) are projected to five corresponding points in the tetrahedron. For example, the new motion in red produced by a great effect of w_3 has a similar form of animation 3. Other new motions (in other color) are produced in the same way. And the motion in violet is the average of four animations. In our locomotion controller, we just accept points representing three corresponding velocities in the envelop of tetrahedra. Thus, only the interpolation was implemented.

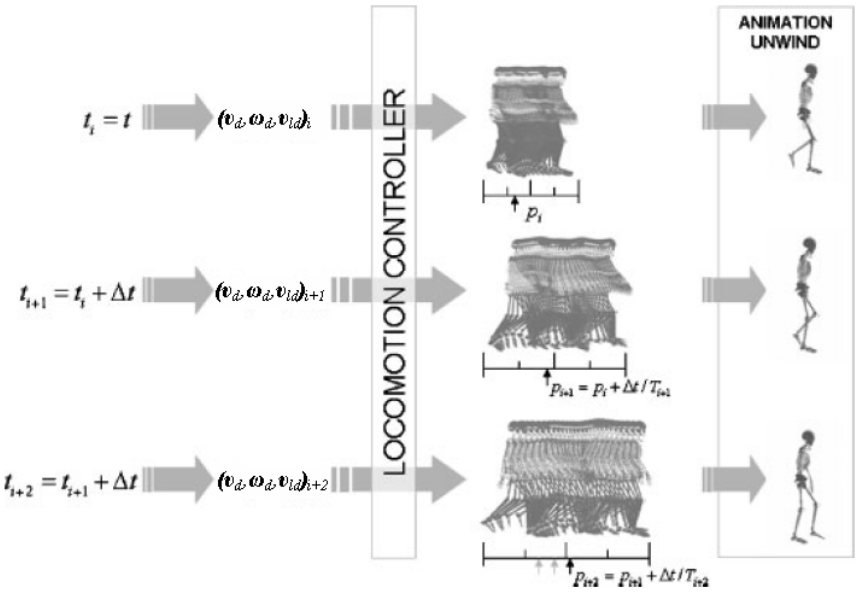

Figure 6.16: Extracting postures in continuous control. Adapted from [Pettre and Laumond 2006]

6.6.2 Continuous animation

For various animations with different velocity levels, we must assure a continuous and smooth change of directives. We adapted the same technique used in [Pettre and Laumond 2006] to extract a posture from a synthesized locomotion. Figure 6.16 illustrates an example of such an animation. The fist line of the figure shows a slow walk cycle T_i and the extraction p_i of a posture at $t = t_i$. When the directive (v_d, ω_d, v_{l_d}) changes to a new normal walk cycle T_{i+1}, the next posture is $p_{i+1} = p_i + \Delta t/Ti+1$ (the second line of the figure). Indeed, we start from the same normalized position with the old cycle and progress to new cycle with respect to its duration. The third line illustrates another new posture.

6.7 Animation results

6.7.1 Reactive locomotions

The perspective of our work is to animate reactive locomotions. For current stage, we present some off-line reactive ones. Desired global paths were pre-defined, and they include parts of which the velocities or tangential directions are varied. Three scenarios are presented in the following sections.

6.7.1.1 Meeting in a corridor

Figure 6.17 presents a scenario of an interaction between two persons in a corridor corner. Each person performs a hybrid locomotion including nonholonomic and holonomic behaviors. Person A goes first along the main corridor, then avoiding the other person B by sideward steps and finally continuing to go ahead (see figure 6.18). The other walker B goes from the left side of the main corridor on a straight line

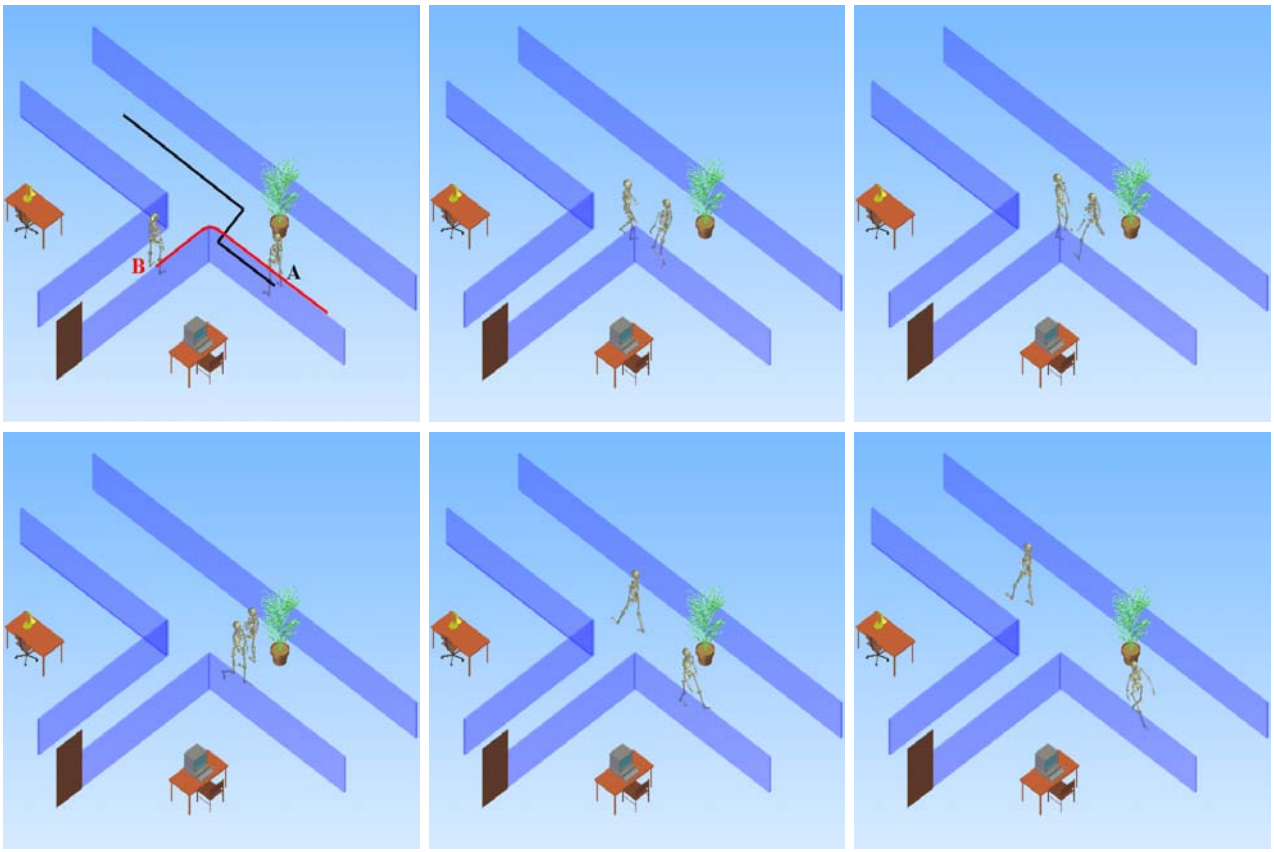

Figure 6.17: Some snapshots in the interaction scenario at the corridor. Two persons start on their initial points. Person A performed a hybrid locomotion (the black lines) of forward walking and sideward stepping. Person B performed a hybrid locomotion (the red lines) of forward walking and right turning.

and turn on his right when arriving in the main corridor (see figure 6.19). He will meet the person A and will stop to let A pass first, then he will continue. The video of this scenario can be found in the link http://homepages.laas.fr/atruong/corridor.avi

6.7.1.2 Catch

The catch scenario was also deduced from a combination of two hybrid locomotions. Indeed, we associated an avoider locomotion and a catcher one. Figure 6.20 shows the started positions of two persons. Both of them first go in two opposite directions. When they see each other, person A turn immediately on the spot and go back to his original direction to avoid person B. And person B starts running to catch B when he sees A. In this novel scenario, A performs a hybrid locomotion of straight walking at the beginning, turning on the spot and again straight walking at the end (figure 6.21). Whereas B performs a hybrid locomotion of straight walking and straight running (figure 6.22).

6.7.1.3 Moving in a narrow environment

Eugene is in the narrow environment and will follow the predefined trajectory as in figure 6.23. Eugene

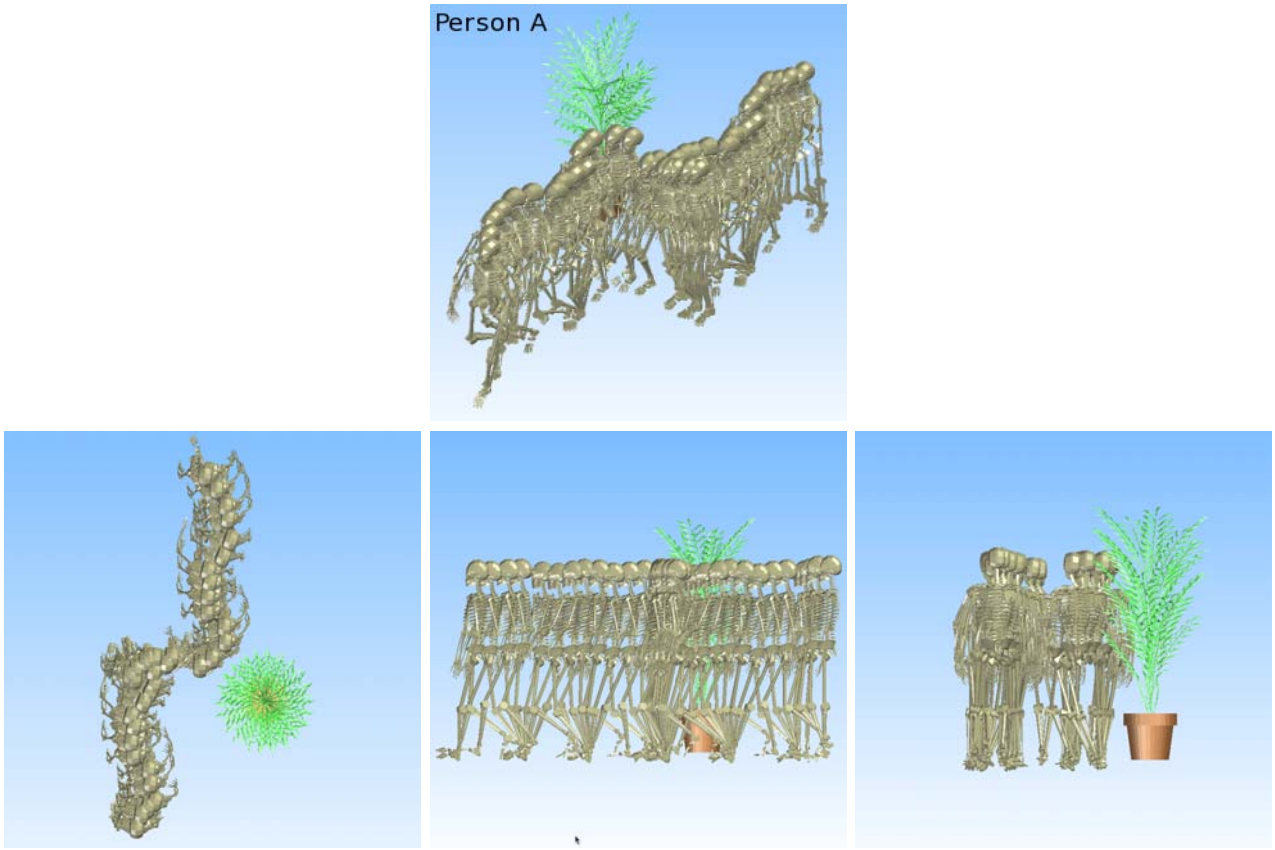

Figure 6.18: Scenario of meeting at a corridor. Person A performed a hybrid locomotion of forward walking and sideward steeping: the perspective view is on the first line, and its three projections are on the second line.

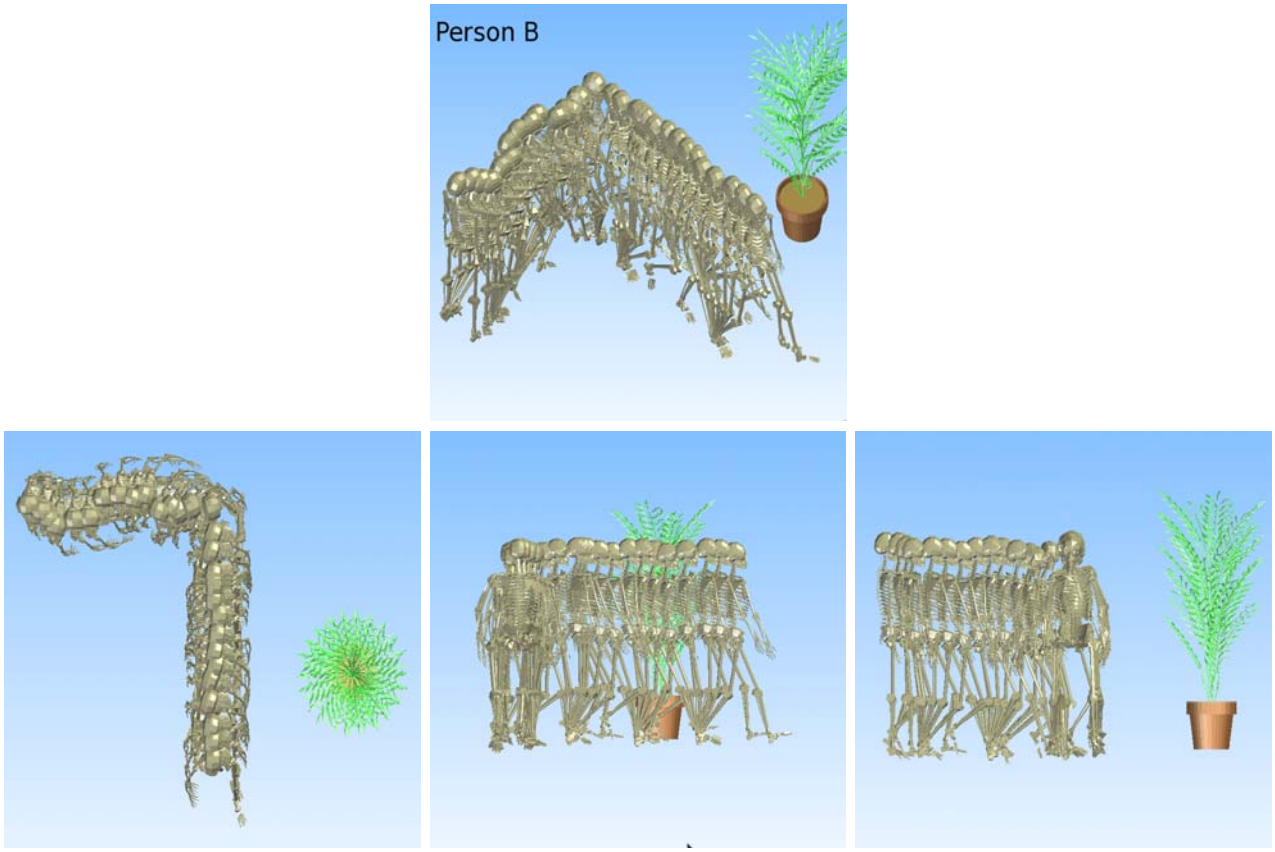

Figure 6.19: Scenario of meeting at a corridor. Person B performed a hybrid locomotion of forward walking and right turning: the perspective view is on the first line, and its three projections are on the third line.

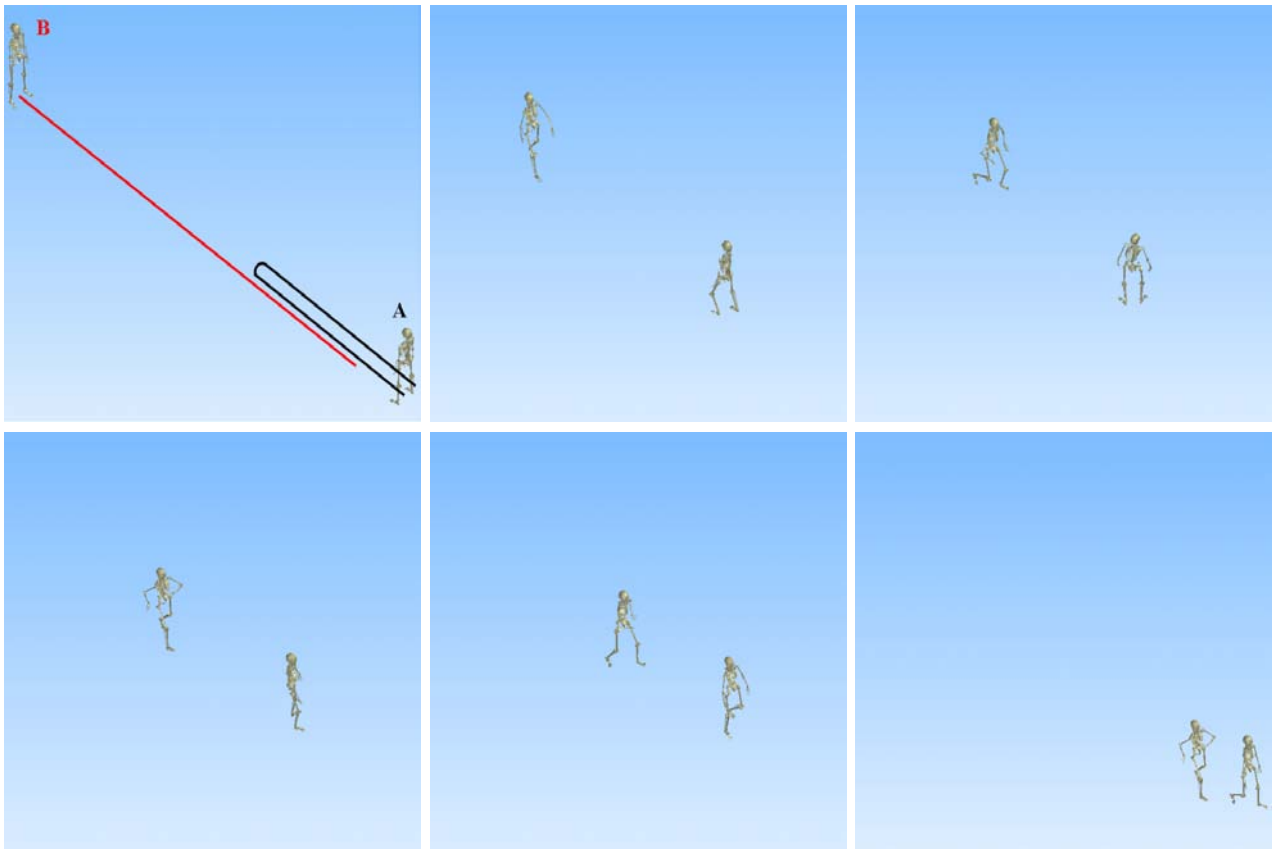

Figure 6.20: Some snapshots in the scenario of catching. Two persons start on their initial points. They performed their hybrid locomotions: the black path for person A and the red path for person B.

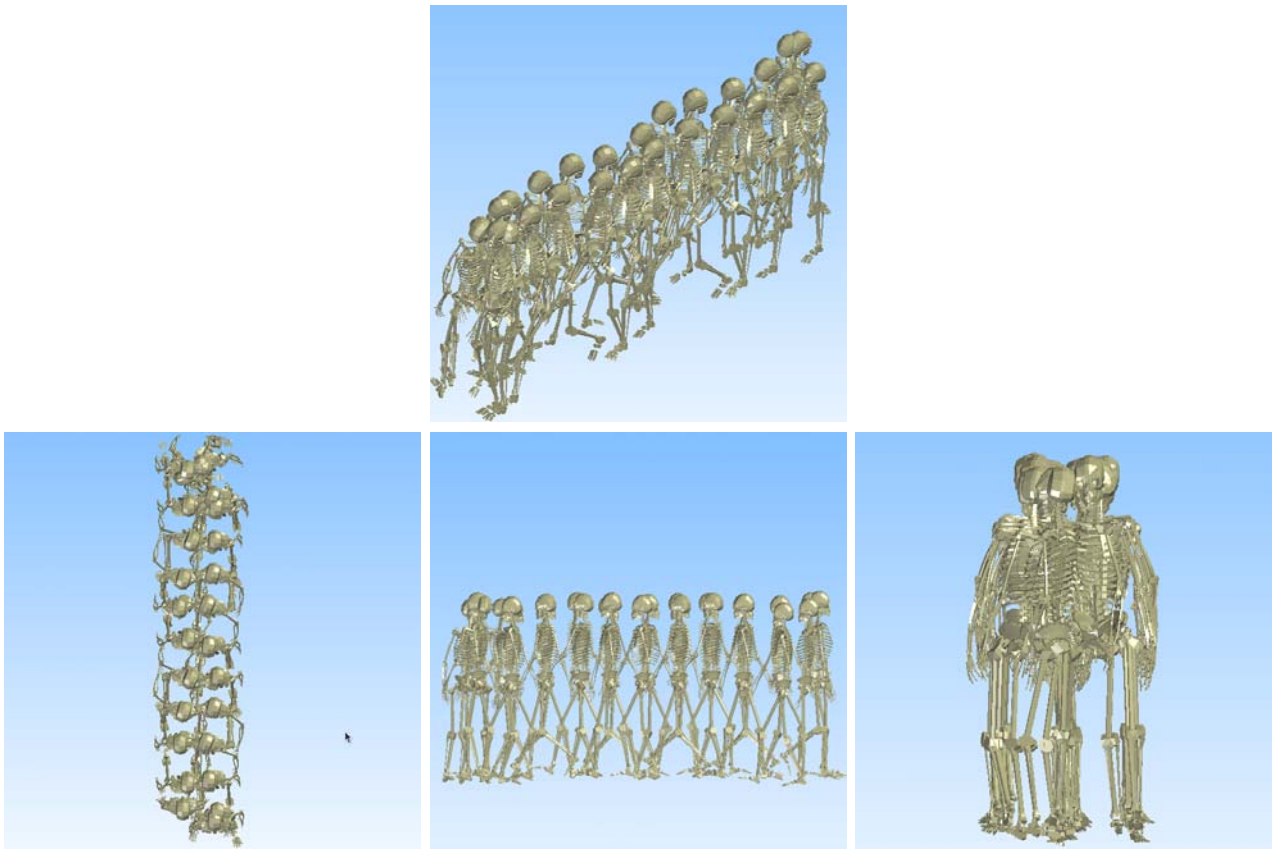

Figure 6.21: Scenario of catching. Person A performed a hybrid locomotion of straight walking and turning on the spot: the perspective view is on the first line, and its three projections are on the third line.

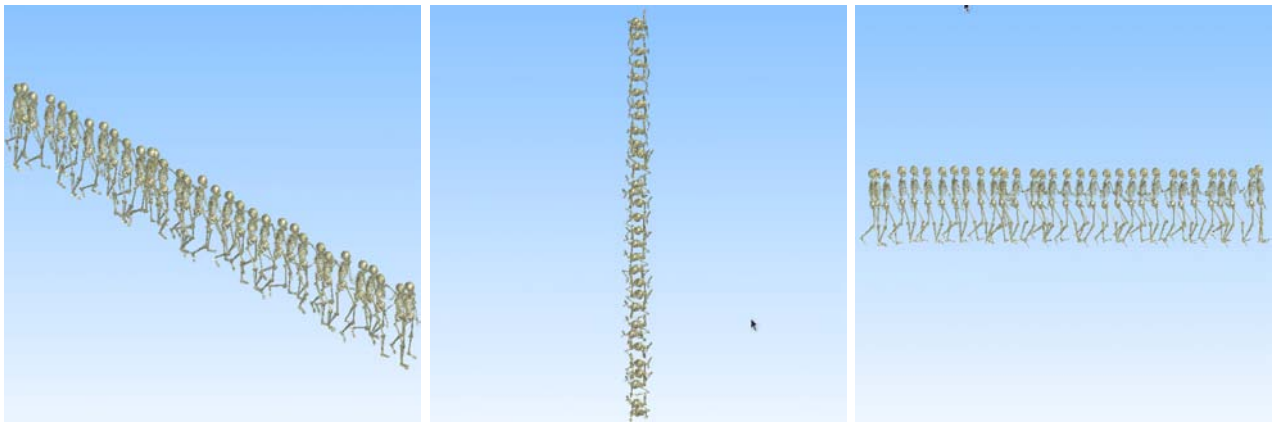

Figure 6.22: Scenario of catching. Person B performed a hybrid locomotion of straight walking and straight running: the perspective view is on the left, and its two projections are on the middle and on the right.

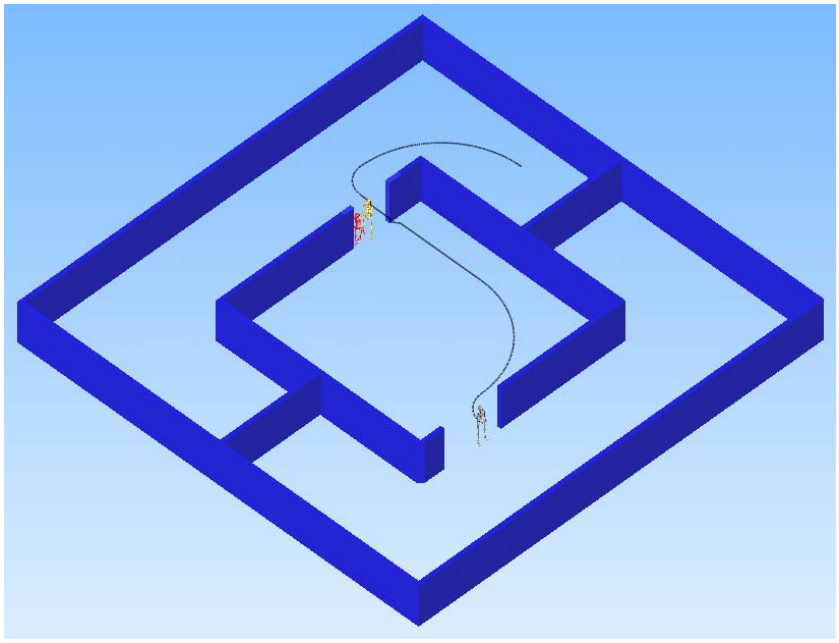

Figure 6.23: Eugene in a narrow environment

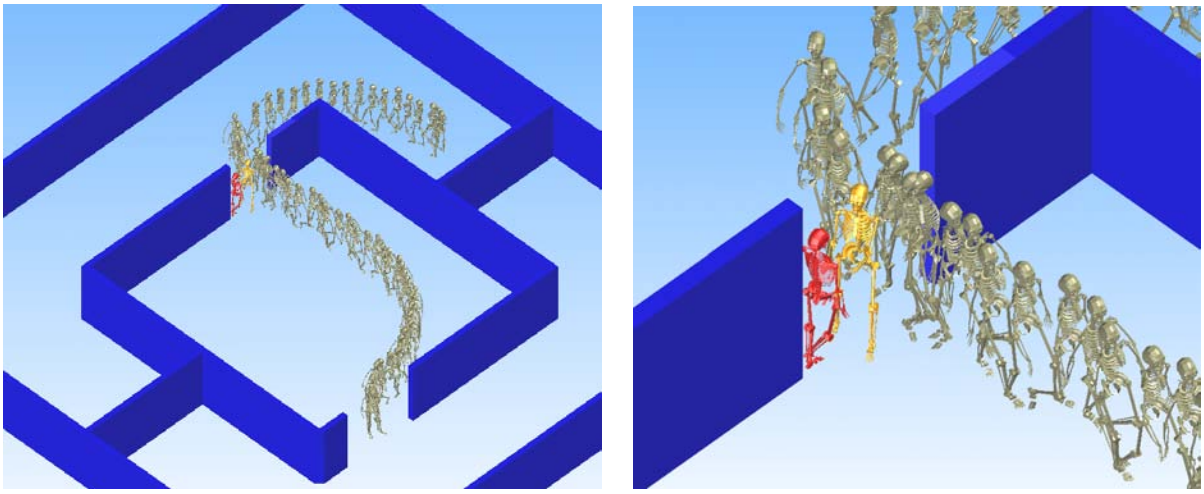

(a) (b)

Figure 6.24: The perspective view of Eugene's locomotion in the narrow environment (a) and the zoom of the transition between forward and lateral locomotions to enter the door (b).

follows different curves during walking (figure 6.24 (a)), especially the transition between the normal walking and the sideward steps in forward direction to avoid two persons talking at the door (see this transition in figure 6.24 (b)).

6.7.2 Intentional locomotions

Some intentional trajectories from initial to final configurations are produced by using the inverse optimal control approach from [Mombaur et al. 2010]. Two such locomotions are presented in figure 6.25 (a) and figure 6.26 (a) for the target on the right and the left respectively.

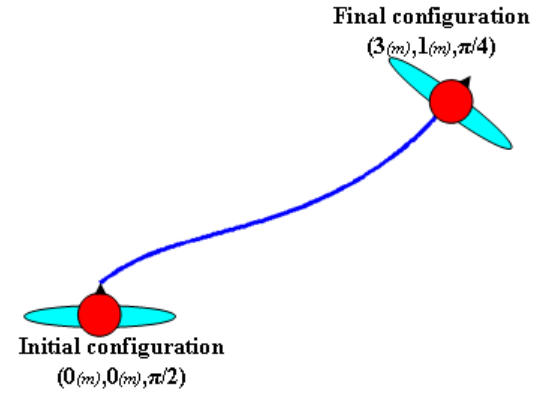

(a)

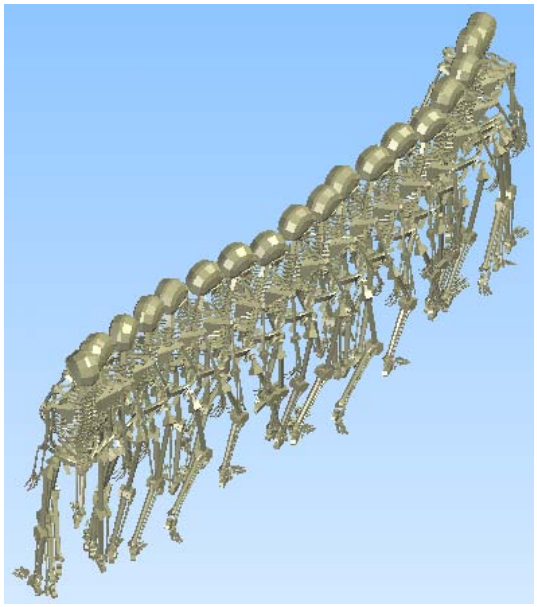

(b)

Figure 6.25: The initial and final configurations of an intentional goal walking when the target is on the right (a) and the corresponding animated locomotion generated by our controller (b).

We chose desired velocities and then generated the locomotions. Postures sequences of the animations were shown in figure 6.25 (b) and figure 6.26 (b). We find that these animated locomotions are close to locomotions acquired from data of human locomotion experiment in the neighboring space.

Like in these data, the mannequin adapts the body orientation to the goal during locomotion.

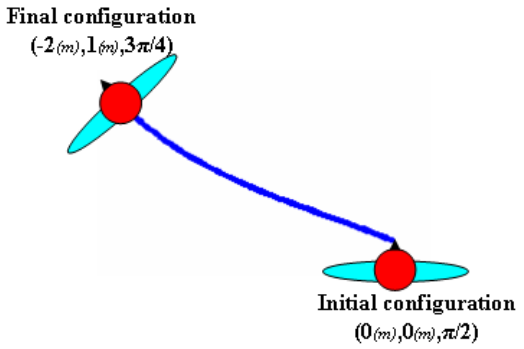

(a)

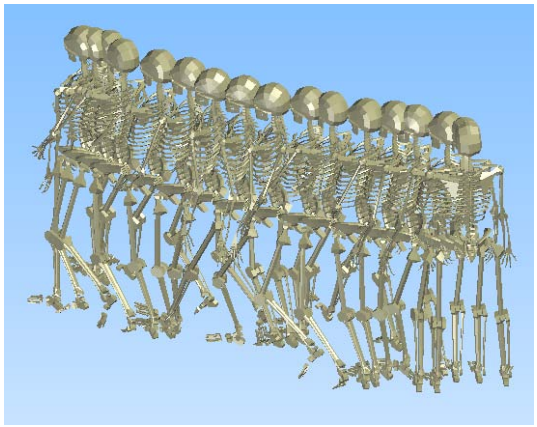

(b)

Figure 6.26: The initial and final configurations of an intentional goal walking when the target is on the left (a) and the corresponding animated locomotion generated by our controller (b).

6.7.3 Performance of the controller

On the computer Dell Precision 390 (Intel DuoCore 2.13 GHz, 2 Go RAM, OS Fedora 12), the computation time measured for the animations above are as following:

Corridor	Catch	Narrow Environment	Intent. Goal Right	Intent. Goal Left
430 (ms)	726 (ms)	1763 (ms)	261 (ms)	185 (ms)

We found that the computation time depends on the trajectory length and the complexity of the trajectory (the change of velocities, directions or locomotion types). We need about 90 (ms) to animate 1 (m) of locomotion. That allows us to develop the controller for further online animations.

6.8 Discussion

Nonholonomic and holonomic locomotions has been combined in our locomotion controller. We produced some feasible locomotions (look like human walking). The ongoing work allows us to animate

locomotions following predefined paths for some interesting scenarios. Moreover, with the optimizer used in [Mombaur et al. 2010], an optimal (human-like) trajectory would be planned and tracked by locomotions generated by our controller. From a top-down approach, we defined a computational model explaining trajectory shape of human locomotion between different configurations. And now, from these different configurations, we could generate "human-like" locomotions. It seems to be an inverse application of top-down approach. Nevertheless, these locomotions were created without any feedback information of equilibrium and contact on the ground. It's just a movement combination of the root - free flyer object and all joints participating in human locomotion. So, the slide of feet on the ground could not be completely eliminated. We tried to reduce the slide by fixing an impacting foot on the ground during the swing phase of the other one. Synthesized locomotions represent feasible movements and satisfy user's directives. Even when the input velocities change suddenly, reactive animations are simultaneously generated and they look like what humans do. Nevertheless, these inputs have to be in the envelop of control space data structure. In the scope of normal walking, the database in our Motion library could synthesize most of human-like locomotions. For further applications, our objective is to control locomotions by using a joystick. It will be another application of the human locomotion controller in human - virtual characters interaction.

7 Conclusion

This thesis is devoted to refine the nonholonomic hypothesis of human locomotion. In intentional locomotions, the holonomic motions appear when targets are nearby the initial point. When targets are farther, a combination of holonomic-nonholonomic-holonomic segments is presented. That is the consequence of the adaptation to final orientations of targets. Statistical results correspond to this adaptation are investigated such as the dependency of holonomic parts on the distance to the origin/goal, or the effect of velocity on the holonomic/nonholonomic behaviors. The "top-down" approach from the previous work was not always exhibited in our current study. In some cases, the "bottom-up" approach e.g. the feet-guiding locomotions deduced a better explanations about the control strategy of human walking. However, this hypothesis is not proved by statistical analysis caused of the lack of the markers on the feet. For the future work on this subject, we can investigate the whole body motions in the initial time of walking and concentrating on the movement of the feet that can reveal the control strategy at the beginning of locomotion.

How about the interpretation of the holonomic-nonholonomic-holonomic segments stereotypy? In the city, on the public places, does human walk like that? We can recognize that in a daily walking, human perform the locomotion in a stable speed and the nonholonomic hypothesis seems to be strongly confirmed. But in some cases, for example when we just exit a shop, or when someone calls us suddenly, we first tend to adapt the noise sources – targets, and then go the reach these targets. Such kinds of locomotions fall in our finding. However, the potential reason of this behavior is that the center of mass of human move from one foot to other during the transition of standing and walking. In the normal walking, the movement of two feet in forward direction guarantees the center of mass is always between them. Another subject of interest is to deepen the link between the locomotion patterns and the "word" introduced in chapter 3. The "word" of locomotion is the hypothesis from the optimization of

derivative of curvature during locomotion. The variation of curvatures influences the locomotion pattern in that case. So, which variations decide our locomotion pattern of holonomic-nonholonomic-holonomic segments? This question might be addressed for perspective of the thesis about locomotion pattern, concerning the work in neuroscience and optimal control theory.

The statistical clues provide an evidence for an inverse optimal control approach unifying holonomic and nonholonomic behaviors in a model. The multi-attribute objectives function identified from statistical data provided a continuous model of the change of holonomic and nonholonomic behaviors. This model remains limited. Actually, energy is an important factor in locomotion as the source of initializing, maintaining and stoping. And it is more important in our case when human walk from rest-to-rest configurations. The variation of energy might reveal something about the characteristics of human locomotion in the initial and final phases. But which energy we need to study as well as the way to measure are not easy to carry out promised goals.

Three velocities from our model are the the key to build a locomotion controller that variously synthesizes reactive motions for virtual characters. Moreover, we can reproduce the intentional locomotions for targets used in the experiment. Thus, from the inspiration of the holonomic and nonholonomic behaviors combination, the control-based approach associated with the inverse optimal control approach provide a general framework to address the naturalness of locomotion in applications such as avatar animation.

With the help of the inverse optimal control solver, our locomotion can reproduce human-like locomotions. From two configurations, we animate the locomotion of a virtual character, and compare this locomotion with human locomotion is the same configurations. This approach is not the imitation from human to avatar, but rather than the way from understanding the shape of human locomotion to regenerate it in an avatar with a movement source (velocities components). The study is also the way to validate our model, our inverse optimal control solver and our locomotion controller.

As general perspectives of our work we may notice:

- the consideration of energetic criteria in addition to the purely kinematic models we have considered,
- the integration of the proposed motion controller in software platform for motion planning and control of human avatars in virtual worlds,
- the possible extension of our models for interactions between humans or for human-robot interactions.

A

Appendices

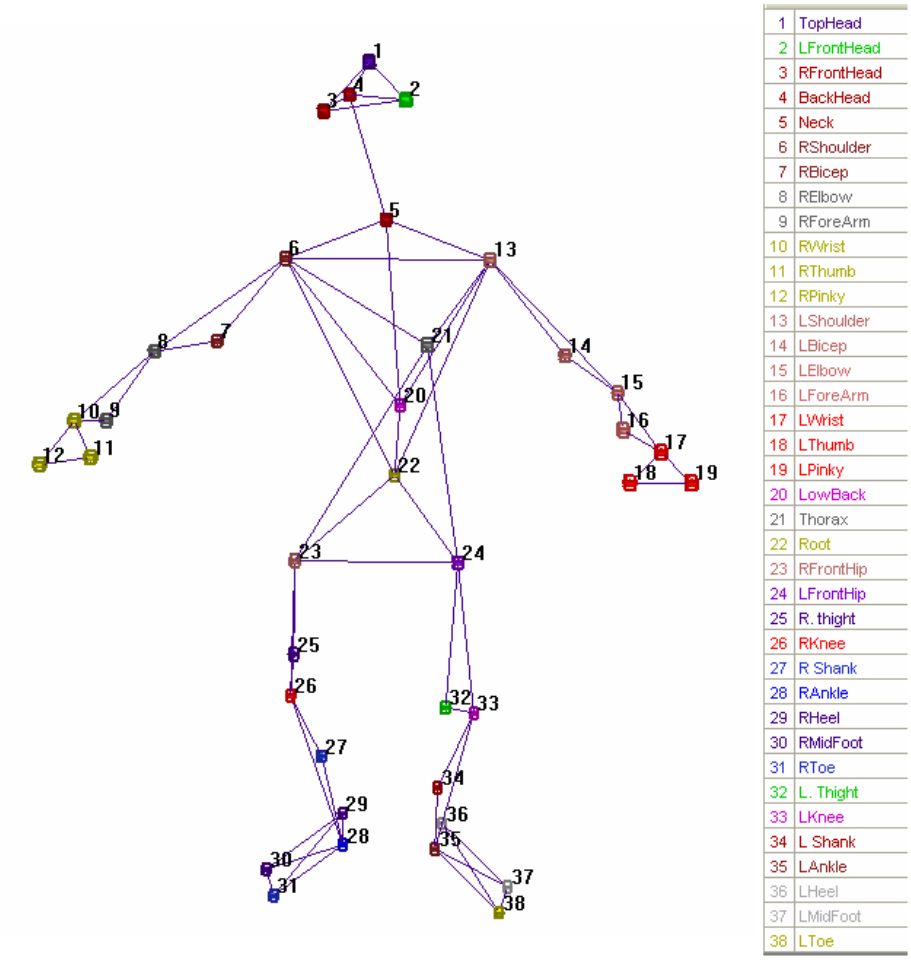

Figure A.1: Markers attached on the subject's whole body

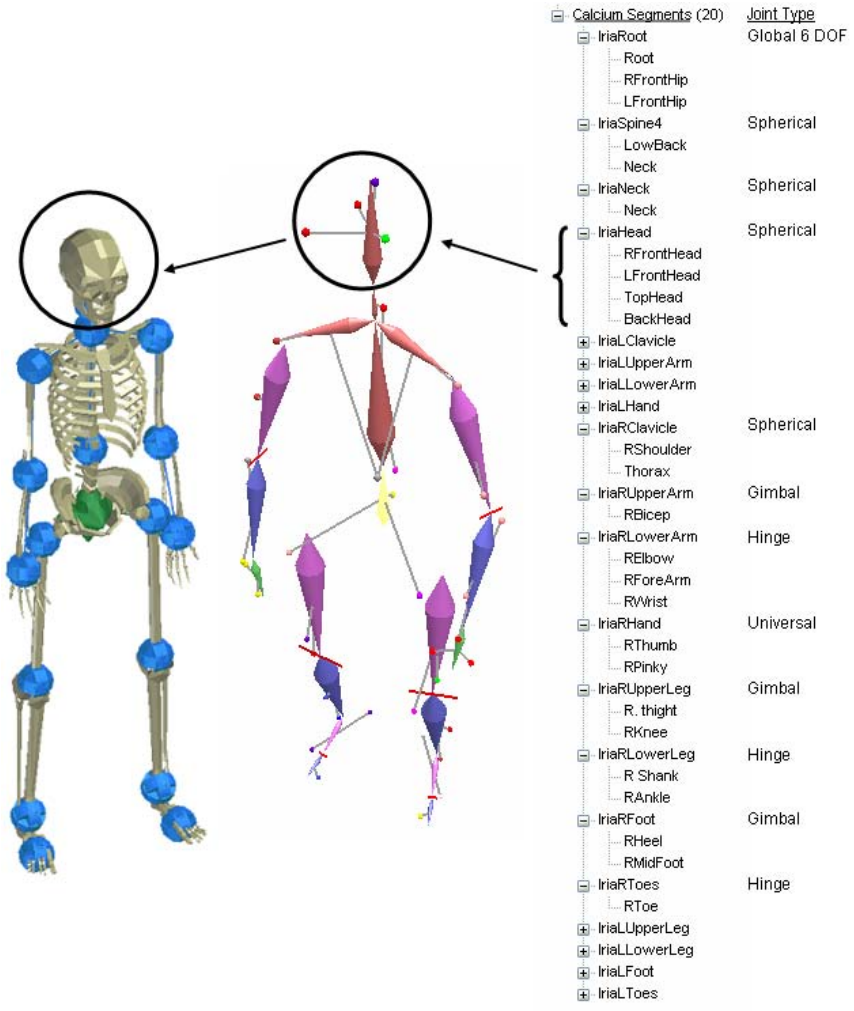

Figure A.2: Hierarchical kinematic model created by Calcium Solver in Cortex. Each joint was defined by a joint type and attached markers (attachments) around it. For example, the head joint is spherical joint and it attached 4 markers to build the head segment

References

ABE, Y., DA SILVA, M., AND POPOVIĆ, J. 2007. Multiobjective control with frictional contacts. In *Proceedings of the 2007 ACM SIGGRAPH/Eurographics symposium on Computer animation*. Eurographics Association, 258. 66

ABERNETHY, B., HANRAHAN, S., KIPPERS, V., MACKINNON, L., AND PANDY, M. 2005. *The biophysical foundations of human movement*. Human Kinetics. 7

ANDERSON, F. C. AND PANDY, M. G. 2001. Dynamic optimization of human walking. *Journal of Biomechanical Engineering 123*, 381–390. 15

ARECHAVALETA, G. 2008. An optimality principle governing human walking. Ph.D. thesis, Institut National des Sciences Appliquees de Toulouse. 31

ARECHAVALETA, G., LAUMOND, J.-P., HICHEUR, H., AND BERTHOZ, A. 2008a. On the nonholonomic nature of human locomotion. *Autonomous Robots 25*, 25–35. 1, 23, 25, 26, 50, 52, 53, 55

ARECHAVALETA, G., LAUMOND, J.-P., HICHEUR, H., AND BERTHOZ, A. 2008b. An optimality principle governing human walking trajectories. *IEEE Transactions on Robotics 24(1)*. 26, 55

BATHE, K. 1982. *Finite element procedures in engineering analysis*. Prentice-Hall Englewood Cliffs, NJ. 75

BERNSTEIN, N.-I. 1967. *The Coordination and Regulation of Movements*. Pergamon Press. 7

BERRET, B., DARLOT, C., JEAN, F., POZZO, T., PAPAXANTHIS, C., AND GAUTHIER, J.-P. 2008. The inactivation principle: Mathematical solutions minimizing the absolute work and biological implications for the planning of arm movements. *PLoS Computational Biology*. 12

BERTHOZ, A. 1993. *Multisensory control of movement*. Oxford University Press, USA. 8

BERTHOZ, A. AND VIAUD-DELMON, I. 1999. Multisensory integration in spatial orientation. *Current Opinion in Neurobiology 9*, 708–712. 7

BERTUCCO, M. AND CESARI, P. 2009. The speed-accuracy trade-off effects on the gait initiation planning. In *The 19th International Symposium of Posture and Gait Research (ISPGR)*. Bologna, Italia. 55

BOULIC, R., ULICNY, B., AND THALMANN, D. 2004. Versatile walk engine. *Journal of Game Development 1,* 1, 29–50. 66

BROGAN, D. C. AND JOHNSON, N. L. 2003. Realistic human walking paths. In *CASA '03: Proceedings of the 16th International Conference on Computer Animation and Social Agents (CASA 2003)*. IEEE Computer Society, Washington, DC, USA. 15, 16

BRUDERLIN, A. AND WILLIAMS, L. 1995. Motion signal processing. In *Proceedings of the 22nd annual conference on Computer graphics and interactive techniques*. ACM, 104. 20

CARLSEN, A., KENNEDY, P., ANDERSON, K., CRESSMAN, E., NAGELKERKE, P., AND CHUA, R. 2005. Identifying visual–vestibular contributions during target-directed locomotion. *Neuroscience letters 384,* 3, 217–221. 7

CHOI, M., LEE, J., AND SHIN, S. 2003. Planning biped locomotion using motion capture data and probabilistic roadmaps. *ACM Transactions on Graphics (TOG) 22,* 2, 203. 20

CINELLI, M. AND WARREN, W. 2009. Eyes or head: Which has the greatest effect on steering control? *Journal of Vision 9,* 8, 1122–1122. 8

COURTINE, G. AND SCHIEPPATI, M. 2003a. Human walking along a curved path. i. body trajectory, segment orientation and the effect of vision. *The European journal of neuroscience 18*, 177–90. 53

COURTINE, G. AND SCHIEPPATI, M. 2003b. Human walking along a curved path. ii. gait features and emg patterns. *The European journal of neuroscience 18*, 191–205. 53

DIETZ, V. 2002. Do human bipeds use quadrupedal coordination? *Trends in Neurosciences 25,* 9, 462–467. 9, 10

EARHART, G. AND HONG, M. 2006. Kinematics of podokinetic after-rotation: Similarities to voluntary turning and potential clinical implications. *Brain research bulletin 70,* 1, 15–21. 53

ESTEVES, C. 2007. Motion planning: from digital actors to humanoid robots. Ph.D. thesis, Institut National Polytechnique, Toulouse. Doctorat. 68

FAJEN, B. AND WARREN, W. 2003. Behavioral dynamics of steering, obstacle avoidance, and route selection. *Journal of Experimental Psychology Human Perception and Performance 29,* 2, 343–362. 15, 16

FINK, P., FOO, P., AND WARREN, W. 2007. Obstacle avoidance during walking in real and virtual environments. *ACM Transactions on Applied Perception (TAP) 4,* 1, 2. 15

FITTS, P.-M. 1954. Journal exp. psychol. *The information capacity of the human motor system in controlling the amplitude of movements 47*, 381–391. 9

FITZPATRICK, R., WARDMAN, D., AND TAYLOR, J. 1999. Effects of galvanic vestibular stimulation during human walking. *The Journal of Physiology 517,* 3, 931–939. 7, 8

FLASH, T. AND HOGAN, N. 1985. The coordination of arm movements: an experimentally confirmed mathematical model. *Journal of Neuroscience 5*, 1688–1703. 9, 13

GORDON, C., FLETCHER, W., MELVILL JONES, G., AND BLOCK, E. 1995. Adaptive plasticity in the control of locomotor trajectory. *Experimental Brain Research 102,* 3, 540–545. 53

GRASSO, R., GLASAUER, S., TAKEI, Y., AND BERTHOZ, A. 1996. The predictive brain: anticipatory control of head direction for the steering of locomotion. *Neuroreport 7(6)*, 1170–1174. 53

GRILLNER, S. 1975. Locomotion in vertebrates: central mechanisms and reflex interaction. *Physiol Rev 55,* 2, 247–304. 5

GUIGON, E., BARADUC, P., AND DESMURGET, M. 2007. Computational motor control: Redundancy and invariance. *Journal of Neurophysiology 97*, 331–347. 13

HARRIS, C.-M. AND WOLPERT, D.-M. 1998. Signal-dependent noise determines motor planning. *Nature 394*, 780–784. 14

HASE, K. AND STEIN, R. 1999. Turning strategies during human walking. *Journal of Neurophisiology 81*, 2914–2922. 8, 9

HATZE, H. AND BUYS, J. 1977. Energy-optimal controls in the mammalian neuromuscular system. *Biological Cybernetics 27,* 1, 9–20. 12

HICHEUR, H. AND BERTHOZ, A. 2005. How do humans turn? head and body movements for the steering of locomotion. In *IEEE / RAS Int. Conf. on Humanoid Robots*. Tsukuba, Japan. 8

HICHEUR, H., GLASAUER, S., VIEILLEDENT, S., AND BERTHOZ, A. 2005. *Head direction control during active locomotion in humans*. MIT Pres, Cambridge. 7

HICHEUR, H., PHAM, Q.-C., ARECHAVALETA, G., LAUMOND, J.-P., AND BERTHOZ, A. 2007. The formation of trajectories during goal-oriented locomotion in humans. i. a stereotyped behaviour. *In European Journal of Neuroscience 26*. 24, 52, 55

HICHEUR, H., VIEILLEDENT, S., RICHARDSON, M.-J.-E., FLASH, T., AND BERTHOZ, A. 2005. Velocity and curvature in human locomotion along complex curved paths : A comparison with hand movements. *Experimental Brain Research 162(2)*, 145–154. 9

HODGINS, J., WOOTEN, W., BROGAN, D., AND O'BRIEN, J. 1995. Animating human athletics. In *Proceedings of the 22nd annual conference on Computer graphics and interactive techniques*. ACM, 78. 19, 20

HOLLANDS, M., ZIAVRA, N., AND BRONSTEIN, A. 2004. A new paradigm to investigate the roles of head and eye movements in the coordination of whole-body movements. *Experimental brain research 154,* 2, 261–266. 7

IJSPEERT, A. 1995. Locomotion, vertebrate. *The Handbook of Brain and Neural Networks*. 6

IMAI, T., MOORE, S.-T., AND RAPHAN, T. 2000. Interation of the body, head, and eyes during walking and turning. *Experimental Brain Reseach 136*, 1–18. 7

JAIN, S., YE, Y., AND LIU, C. 2009. Optimization-based interactive motion synthesis. 66

JORDAN, M.-I. AND WOLPERT, D.-M. 1999. *Computational motor control*. Gazzaniga, (Ed.), MIT Press, Cambridge, MA. 11

KAJITA, S., KANEHIRO, F., KANEKO, K., FUJIWARA, K., YOKOI, K., AND HIRUKAWA, H. 2002. A realtime pattern generator for biped walking. In *Proceedings- IEEE International Conference on Robotics and Automation*. Vol. 1. Citeseer, 31–37. 17, 19

KAJITA, S., KANEHIRO, F., KANEKO, K., YOKOI, K., AND HIRUKAWA, H. 2001. The 3D Linear Inverted Pendulum Mode: A simple modeling for a biped walking pattern generation. In *Proceedings of the IEEE/RSJ International Conference on Intelligent Robots and Systems*. 239–246. 17

KANOUN, O., YOSHIDA, E., AND LAUMOND, J. 2009. An optimization formulation for footsteps planning. In *9th IEEE-RAS International Conference on Humanoid Robots, 2009. Humanoids 2009*. 202–207. 17, 19

KAWATO, M. 1999. Internal models for motor control and trajectory planning. *Current opinion in neurobiology 9,* 6, 718–727. 11

KENNEDY, P.-M., CARLSEN, A.-N., INGLIS, J.-T., CHOW, R., FRANKS, I.-M., AND CHUA, R. 2003. Relative contributions of visual and vestibular information on the trajectory of human gait. *Experimental Brain Research 153*, 113–117. 7

KHATIB, O., SENTIS, L., PARK, J., AND WARREN, J. 2004. Whole body dynamic behavior and control of human-like robots. *International Journal of Humanoid Robotics 1,* 1, 29–43. 17

KIRK, D. 2004. *Optimal control theory: an introduction*. Dover Pubns. 12

KLAPP, S. T. 1975. Feedback versus motor programming in the control of aimed movements. *Journal of Experimental Psychology: Human Perception and Performance 104*, 147–153. 55

KOVAR, L., GLEICHER, M., AND PIGHIN, F. 2008. Motion graphs. In *ACM SIGGRAPH 2008 classes*. ACM, 51. 66

LATOMBE, J. C. 1991. *Robot Motion Planning*. Kluwer Academic Publishers. 1

LAUMOND, J. 2001. La robotique mobile. *Hermes Science, Paris*. 25

LAUMOND, J. 2006. Kineo CAM: a success story of motion planning algorithms. *IEEE Robotics & Automation Magazine 13,* 2, 90–93. 68

LAUMOND, J.-P., ARECHAVALETA, G., TRUONG, T.-V.-A., HICHEUR, H., PHAM, Q.-C., AND BERTHOZ, A. 2007. The words of the human locomotion. *Robotic Research: The 13th Symposium (ISRR-2007). Springer STAR Series*. 26, 29

LAUMOND, J.-P., SEKHAVAT, S., AND LAMIRAUX, F. 1998. *Robot Motion Planning and Control*. J.-P. Laumond (Ed.), Lectures Notes in Control and Information Sciences 229, Springer, Chapter Guidelines in Nonholonomic Motion Planning for Mobile Robots. 1, 25

MAGNENAT-THALMANN, N. AND THALMANN, D. 1991. Complex models for animating synthetic actors. *IEEE Computer Graphics and applications 11,* 5, 32–44. 20

MCGEER, T. 1990. Passive dynamic walking. *The International Journal of Robotics Research 9,* 2, 62. 17

MERGNER, T., HLAVACKA, F., AND SCHWEIGART, G. 1993. Interaction of vestibular and proprioceptive inputs. *Journal of vestibular research: equilibrium & orientation 3,* 1, 41. 53

MOMBAUR, K., LAUMOND, J.-P., AND YOSHIDA, I. 2008. An optimal control model unifying holonomic and nonholonomic walking. In *IEEE / RAS Int. Conf. on Humanoid Robots*. Daejeon, Korea. 55

MOMBAUR, K., LAUMOND, J.-P., AND YOSHIDA, I. 2010. An optimal control based formulation to determine natural locomotor paths for humanoid robots. *Advanced Robotics 24,* 4. 59

MOMBAUR, K., TRUONG, A., AND LAUMOND, J.-P. 2010. From human to humanoid locomotion–an inverse optimal control approach. *Autonomous Robots 28,* 3, 369–383. 57, 59, 62, 65, 86, 88

PARK, S., SHIN, H., AND SHIN, S. 2002. On-line locomotion generation based on motion blending. In *Proceedings of the 2002 ACM SIGGRAPH/Eurographics symposium on Computer animation*. ACM, 111. 66

PETTRE, J. AND LAUMOND, J.-P. 2006. A motion capture-based control-space approach for walking mannequins. *Computer Animation Virtual Worlds 17,* 2, 109–126. 65, 79

PETTRÉ, J., LAUMOND, J.-P., AND SIMÉON, T. 2003. A 2-stages locomotion planner for digital actors. In *SCA '03: Proceedings of the 2003 ACM SIGGRAPH/Eurographics symposium on Computer animation*. Eurographics Association, Aire-la-Ville, Switzerland, Switzerland, 258–264. 20

PHAM, Q. AND HICHEUR, H. 2009. On the open-loop and feedback processes that underlie the formation of trajectories during visual and nonvisual locomotion in humans. *Journal of neurophysiology 102,* 5, 2800. 11

PHAM, Q.-C., HICHEUR, H., ARECHAVALETA, G., LAUMOND, J.-P., AND BERTHOZ, A. 2007. The formation of trajectories during goal-oriented locomotion in humans. ii. a maximum smoothness model. *In European Journal of Neuroscience 26*. 11, 13

POZZO, T., BERTHOZ, A., AND LEFORT, L. 1990. Head stabilization during various tasks in humans. *Experimental Brain Reseach 82*, 97–106. 8, 53

PRATT, J. AND PRATT, G. 1998. Intuitive control of a planar bipedal walking robot. In *1998 IEEE International Conference on Robotics and Automation, 1998. Proceedings*. Vol. 3. 17

RAIBERT, M., BLANKESPOOR, K., NELSON, G., AND PLAYTER, R. BigDog, the Rough-Terrain Quadruped Robot. *Proceedings of the 17th International Federation of Automation Control.(April 2008)*. 17

RAIBERT, M.-H. 1986. *Legged Robots That Balance*. MIT Press, Cambridge. 17

REYNOLDS, C. 1987. Flocks, herds and schools: A distributed behavioral model. In *Proceedings of the 14th annual conference on Computer graphics and interactive techniques*. ACM, 25–34. 20

ROSE, C., COHEN, M., AND BODENHEIMER, B. 1998. Verbs and adverbs: Multidimensional motion interpolation. *IEEE Computer Graphics and Applications 18,* 5, 32–40. 20, 21

ROSENBAUM, D. 2009. *Human motor control*. Academic Press. 14

ROSSIGNOL, S. 1996. Visuomotor regulation of locomotion. *Canadian journal of physiology and pharmacology 74,* 4, 418–425. 7

SABES, P. 2000. The planning and control of reaching movements. *Current opinion in neurobiology 10,* 6, 740–746. 12, 13

SARANLI, U., BUEHLER, M., AND KODITSCHEK, D. 2001. Rhex: A simple and highly mobile hexapod robot. *The International Journal of Robotics Research 20,* 7, 616. 17

SAUNDERS, INMAN, V. T., AND EBERHART, H. D. 1953. The major determinants in normal and pathological gait. *Journal of Bone Joint Surgery 35,* 3, 543–558. 14

SCHAAL, S. AND SCHWEIGHOFER, N. 2005. Computational motor control in humans and robots. *Current Opinion in Neurobiology 15*, 675–682. 11, 12

SOECHTING, J.-F. AND FLANDERS, M. 1994. Moving in three-dimensional space: frames of reference, vectors and coordinate systems. *Annu. Rev. Neurosci. 15*, 167–191. 7

TODOROV, E. 2004. Optimality principles in sensorimotor control. *Nature Neuroscience 7(9)*, 907–915. 12, 14

TODOROV, E. AND JORDAN, M.-I. 2002. Optimal feedback control as a theory of motor coordination. *Nature Neuroscience 5*, 1226–1235. 12

TRUONG, T. 2007. Modélisation de la locomotion humaine par techniques de commande optimale. M.S. thesis, Institut National Polytechnique de Grenoble. 26

TUAN, T., SOUERES, P., TAIX, M., AND GUIGON, E. 2008. A principled approach to biological motor control for generating humanoid robot reaching movements. In *2st IEEE/RAS-EMBS Int. Conf. on Biomedical Robotics and Biomechatronics*. Scottsdale, Arizona, USA. 13

UNO, Y., KAWATO, M., AND SUZUKI, R. 1989. Formation and control of optimal trajectory in human multijoint arm movement: Minimum torque-change model. *Biological Cybernetics 61*, 89–101. 13

UNUMA, M., ANJYO, K., AND TAKEUCHI, R. 1995. Fourier principles for emotion-based human figure animation. In *SIGGRAPH '95: Proceedings of the 22nd annual conference on Computer graphics and interactive techniques*. ACM, New York, NY, USA, 91–96. 66

VIEILLEDENT, S., KERLIRZIN, Y., DALBERA, S., AND BERTHOZ, A. 2001. Relationship between velocity and curvature of a locomotor trajectory in human. *Neuroscience Letters 305*, 65–69. 9

VUKOBRATOVIC, M. AND BOROVAC, B. 2004. Zero-moment point-thirty five years of its life. *International Journal of Humanoid Robotics 1,* 1, 157–173. 17

WEBER, K., FLETCHER, W., GORDON, C., JONES, G., AND BLOCK, E. 1998. Motor learning in the podokinetic system and its role in spatial orientation during locomotion. *Experimental Brain Research 120,* 3, 377–385. 53

WHITING, H. AND BERNSTEIN, N. 1984. *Human motor actions: Bernstein reassessed.* Elsevier. 7

WILEY, D. AND HAHN, J. 1997. Interpolation synthesis of articulated figure motion. *IEEE Computer Graphics and Applications*, 39–45. 66

WINTER, D. 2009. *Biomechanics and motor control of human movement*. Wiley. 14, 15

WITKIN, A. AND POPOVIC, Z. 1995. Motion warping. In *Proceedings of the 22nd annual conference on Computer graphics and interactive techniques*. ACM, 105–108. 20

WOLPERT, D.-M. 1995. An internal model for sensorimotor integration. *Sciences 269*, 1880–1882. 11

WWW.CGAL.ORG. 2008. Cgal, computational geometry algorithms library. 75

YIN, K., LOKEN, K., AND VAN DE PANNE, M. 2007. Simbicon: Simple biped locomotion control. In *ACM SIGGRAPH 2007 papers*. ACM, 105. 66

ZAJAC, F. E., NEPTUNE, R. R., AND KAUTZ, S. A. 2002. Biomechanics and muscle coordination of human walking. part i: introduction to concepts, power transfer, dynamics and simulations. *Gait & Posture 16,* 3, 215–32. 15

ZAJAC, F. E., NEPTUNE, R. R., AND KAUTZ, S. A. February 2003. Biomechanics and muscle coordination of human walking. part ii: Lessons from dynamical simulations and clinical implications. *Gait & Posture 17*, 1–17(17). 15

ZEHR, E. AND DUYSENS, J. 2004. Regulation of arm and leg movement during human locomotion. *The Neuroscientist 10,* 4, 347. 8, 10

ZELTZER, D. 1982. Motor control techniques for figure animation. *IEEE Computer Graphics and Applications 2,* 9, 53–59. 20